

Titre: Interprétation of Victor Borehole resistivity and IP data
Title:

Auteur: Ji Ma
Author:

Date: 1994

Type: Mémoire ou thèse / Dissertation or Thesis

Référence: Ma, J. (1994). Interprétation of Victor Borehole resistivity and IP data [Master's
Citation: thesis, Polytechnique Montréal]. PolyPublie. <https://publications.polymtl.ca/57023/>

 **Document en libre accès dans PolyPublie**
Open Access document in PolyPublie

URL de PolyPublie: <https://publications.polymtl.ca/57023/>
PolyPublie URL:

**Directeurs de
recherche:** Peter Fullagar
Advisors:

Programme: Génie minéral
Program:

UNIVERSITÉ DE MONTRÉAL

Interpretation of Victor Borehole

Resistivity and IP Data

par

Ji MA

DÉPARTEMENT DE GÉNIE MINÉRAL

ÉCOLE POLYTECHNIQUE

MÉMOIRE PRÉSENTÉ EN VUE DE L'OBTENTION
DU GRADE DE MAÎTRE ÈS SCIENCES APPLIQUÉES (M.Sc.A)

Juillet 1994

@ droits réservés de Ji MA 1994.



National Library
of Canada

Acquisitions and
Bibliographic Services Branch

395 Wellington Street
Ottawa, Ontario
K1A 0N4

Bibliothèque nationale
du Canada

Direction des acquisitions et
des services bibliographiques

395, rue Wellington
Ottawa (Ontario)
K1A 0N4

Your file *Votre référence*

Our file *Notre référence*

THE AUTHOR HAS GRANTED AN IRREVOCABLE NON-EXCLUSIVE LICENCE ALLOWING THE NATIONAL LIBRARY OF CANADA TO REPRODUCE, LOAN, DISTRIBUTE OR SELL COPIES OF HIS/HER THESIS BY ANY MEANS AND IN ANY FORM OR FORMAT, MAKING THIS THESIS AVAILABLE TO INTERESTED PERSONS.

L'AUTEUR A ACCORDE UNE LICENCE IRREVOCABLE ET NON EXCLUSIVE PERMETTANT A LA BIBLIOTHEQUE NATIONALE DU CANADA DE REPRODUIRE, PRETER, DISTRIBUER OU VENDRE DES COPIES DE SA THESE DE QUELQUE MANIERE ET SOUS QUELQUE FORME QUE CE SOIT POUR METTRE DES EXEMPLAIRES DE CETTE THESE A LA DISPOSITION DES PERSONNE INTERESSEES.

THE AUTHOR RETAINS OWNERSHIP OF THE COPYRIGHT IN HIS/HER THESIS. NEITHER THE THESIS NOR SUBSTANTIAL EXTRACTS FROM IT MAY BE PRINTED OR OTHERWISE REPRODUCED WITHOUT HIS/HER PERMISSION.

L'AUTEUR CONSERVE LA PROPRIETE DU DROIT D'AUTEUR QUI PROTEGE SA THESE. NI LA THESE NI DES EXTRAITS SUBSTANTIELS DE CELLE-CI NE DOIVENT ETRE IMPRIMES OU AUTREMENT REPRODUITS SANS SON AUTORISATION.

ISBN 0-315-97116-9

UNIVERSITÉ DE MONTRÉAL
ÉCOLE POLYTECHNIQUE

Ce mémoire intitulé:

Interpretation of Victor Borehole

Resistivity and IP Data

présenté par: Ji MA

en vue de l'obtention du grade de: Maître ès sciences appliquées (M.Sc.A)

a été dûment accepté par le jury d'examen constitué de:

M. CHOUTEAU, Michel, Ph.D., président

M. FULLAGAR, Peter, Ph.D., membre et directeur de recherche

M. BAILEY, Richard C., Ph.D., membre

SOMMAIRE

Inco possède une grande quantité de données de résistivité et de polarisation provoquée (PP) de forage préexistantes, la plupart d'entre elles n'ont pas été interprétées quantitativement. Cependant il était nécessaire de développer une méthode capable d'interpréter cette sorte de données.

Les données de résistivité et de PP en provenance de Victor à Sudbury East Range étaient interprétées. A partir des résultats de modélisation avec les programmes NEWROID et U.B.C 2D DCR/IP, on remarque que leurs modèles sont différents, mais les deux résultats révèlent que les "gisements de sulfures" interceptés par le forage 60003-2 sont responsables des anomalies produites dans les profiles de résistivité apparente et de chargeabilité apparente mesurée. La possibilité d'existence d'un objet "off-hole" n'est pas supportée par les données.

Comme les corps de sulfure massif à Sudbury sont souvent inclus dans un halo de minéralisation disséminée, est-il possible de détecter le noyau de minéralisation massive en utilisant les données de résistivité et de PP de forage ?

Pour répondre à cette question et interpréter les données de Victor, le programme NEWROID de Fullagar a été testé et utilisé dans cette étude. NEWROID calcule la

résistivité DC et la réponse PP pour une sphéroïde avec le noyau, dans un demi-espace excité par une source de courant dipôle ou monopole.

D'après l'étude de modélisation, nous voyons qu'il est difficile de détecter le noyau, avec une configuration de Schlumberger modifié, si le contraste de résistivité entre le fond et la coque sphéroïdale est large (> 10), ceci à cause de la concentration du courant à la surface de la sphéroïde.

Durant l'étude, la méthode des images électriques conventionnelle s'est avérée inadaptée pour la mesure de résistivité en forage; une nouvelle méthode d'image modifié a été proposée. En comparant les résultats de ces deux méthodes, on peut voir que le résultat avec la méthode d'image modifiée est beaucoup plus proche de la vraie solution que la méthode des images conventionnelle.

Le programme de modélisation deux dimensionnelle de U.B.C 2D DCR/IP a également été utilisé dans cette étude, permettant de calculer la réponse de résistivité et PP pour un modèle à couches multiples.

ABSTRACT

Inco has a large quantity of pre-existing borehole resistivity and IP data, most of it has not been quantitatively interpreted. Therefore, it was necessary to find a method to be able to interpret this kind of data.

Resistivity and IP data from the Victor, in Sudbury East Range, were interpreted. From the results of modelling with NEWROID and U.B.C 2D DCR/IP programs, we see that their models are different, but both results reveal that the "stringers of sulphide" intercepted by borehole 60003-2 are responsible for the anomalies occurred in the measured apparent resistivity and apparent chargeability profiles. The possibility of the existence of an "off-hole" target is not supported by the data.

Since the orebodies in Sudbury are often included in a halo of disseminated mineralization, is it possible to detect the core of massive mineralization using the borehole resistivity and IP data ?

To answer this question and interpret the field data, program NEWROID of Fullagar was tested and used in this study. NEWROID calculates the DC resistivity and IP response for a spheroid with a core, in a half-space excited by a pole or dipole current source.

From the study of modelling, we see that with a modified Schlumberger configuration, if the contrast of resistivity between the host and the spheroidal shell is large (> 10), due to concentration of the current on the surface of the spheroid, it is difficult to detect the core.

During the study, the conventional image method was found to be inappropriate for the borehole resistivity measurements; a new modified image method was proposed. By comparing the results with these two methods, we can see that the result with the modified image method is much closer to the true solution than that with conventional image method.

The U.B.C 2D DCR/IP modelling program was used also in this study, which can compute the resistivity and IP response for a model with multi-layers.

RÉSUMÉ

La prospection minière s'est maintenant tournée vers la détection de gisements profonds parce que les gisements superficiels importants ont presque tous été exploités. A cet effet, l'application de la méthode de résistivité en surface, très longtemps utilisée avec succès pour la détection de zones conductrices, s'est avérée en général inefficace pour les cibles profondes à cause de la faible résolution causée par les effets parasites (topographie, mort-terrain, effets d'écran des structures superficielles et des hétérogénéités locales).

Pour résoudre le problème des structures profondes, une nouvelle technique en forage (borehole technique) a été introduite. Celle-ci possède une bonne résolution pour mettre en évidence les signatures des corps profonds.

Les objectifs principaux de cette étude consistent en deux parties: (i) Inco possède une grande quantité de données de résistivité et de polarisation provoquée (PP) de forage, la plupart d'entre elles n'ont pas été interprétées quantitativement. Donc, on aimerait, pour interpréter les données mesurées dans la région de Victor, développer une méthode capable d'interpréter ce type de données; (ii) comme les gisements de sulfures massifs à Sudbury sont souvent inclus dans un halo de minéralisation disséminée, on aimerait aussi savoir s'il est possible de détecter le noyau de minéralisation massive en utilisant

les données de résistivité et de PP de forage.

Il y a peu de programmes appropriés disponibles pour cette étude. On a utilisé deux programmes de modélisation, DSSPHIP et NEWROID, développés par Fullagar (Fullagar, 1993 a,b). Ils permettent de calculer les réponses de résistivité et de PP pour une sphère avec un noyau et une sphéroïde avec un noyau dans un demi-espace homogène. Le programme de modélisation bi-dimensionnelle de U.B.C a également été utilisé dans cette étude. Il permet de calculer les réponses de résistivité et de PP.

Dans cette étude, la configuration de Schlumberger modifiée a été utilisée, dans laquelle on fixe deux électrodes d'émission à la surface et déplace simultanément deux électrodes de mesure dans deux forages. Cette configuration est presque pareille à la géométrie du levé de Victor, pour laquelle seulement une électrode de mesure est déplacée, l'autre demeurant fixe (Fig. 1.1).

Pour la configuration de Schlumberger modifié, la formule de résistivité peut être écrite comme:

$$\rho_a = \frac{2\pi}{\frac{1}{R_{AM}} - \frac{1}{R_{AN}} - \frac{1}{R_{BM}} + \frac{1}{R_{BN}}} \frac{\Delta V}{I}$$

où R_{AM} , R_{AN} , R_{BM} et R_{BN} sont des distances entre électrodes A, M, N et B, respectivement; I est le courant injecté; et ΔV est le voltage entre deux électrodes de mesure M et N.

Quant à la chargeabilité apparente, on détecte un corps polarisable dans le sous-sol lorsque, le courant étant coupé, le voltage ne tombe pas à zéro immédiatement. Les charges induites sur la surface du corps produisent une différence de voltage, même lorsque le courant est interrompu, qui est mesuré par le récepteur. On appelle ce phénomène l'effet de polarisation provoquée (PP), qui est équivalent à augmenter la résistivité effective du corps. Le voltage secondaire V_s est causé par cette résistivité effective (Fig. 2.1). D'après Seigel (1959), la chargeabilité apparente est définie par

$$M_a = \frac{V(\rho') - V(\rho)}{V(\rho')} = \frac{V_s}{V_p}$$

et

$$\rho' = \frac{\rho}{1-m}$$

où m est la chargeabilité du corps.

D'après cette définition, pour calculer la chargeabilité apparente, il faut calculer

le voltage deux fois par modélisation directe, avec les résistivités ρ et $\rho/(1-m)$.

Avant de faire la modélisation, on compare les programme DSSPHIP, NEWROID et IP3DDH (le programme de Daniels). D'après les résultats, on peut voir que les résultats de DSSPHIP et NEWROID sont presque identiques, mais il y a un peu de différence entre ceux de DSSPHIP et IP3DDH. Considérant les différentes méthodes utilisées dans ces programmes, solution analytique pour DSSPHIP et NEWROID et intégrale de surface pour IP3DDH, on pense que cette différence est d'ordre numérique.

Généralement, avec la méthode des images électriques, on peut utiliser les formules pour un espace homogène pour approcher des réponses en demi-espace. Cependant, durant cette étude, on a trouvé que cette méthode est inadaptée pour la mesure de résistivité en forage, parce qu'elle viole le "principe de réciprocité". Une nouvelle méthode d'image (Appendix B) utilisée dans DSSPHIP et NEWROID approche mieux la vraie solution que la méthode des images conventionnelle.

A cause des deux raisons suivantes: (i) IP3DDH ne peut pas calculer les réponses d'une sphère ou d'une sphéroïde avec un noyau; (ii) IP3DDH utilise la méthode d'image conventionnelle qui produit une grande erreur quand la ou les source(s) ou le ou les récepteur(s) sont dans le sol; on n'a pas utilisé le programme de Daniels (IP3DDH) dans cette étude. Des deux constats précédents, on peut conclure que DSSPHIP et NEWROID

sont supérieurs à IP3DDH. Considérant qu'une sphéroïde peut simuler beaucoup de formes des corps, on a choisi NEWROID pour faire la modélisation.

Avec NEWROID, on a calculé des réponses d'une sphéroïde uniforme et d'une sphéroïde avec un noyau conducteur pour cinq modèles différents. Après comparaison, on a vu qu'il est difficile de détecter le noyau avec la configuration de Schlumberger modifiée, si le contraste de résistivité entre le milieu encaissant et la coque sphéroïdale est élevé (> 10), ceci à cause de la concentration du courant à la surface de la sphéroïde. Cependant, si le contraste de résistivité est plus faible (< 10), et les deux électrodes de mesure sont placées dans la coque, il est alors possible de détecter le noyau conducteur.

Durant la modélisation, on a remarqué un changement de la polarité des réponses. Quand la sphéroïde est entre deux forages, la polarité de la résistivité apparente est négative, et celle de la chargeabilité apparente est positive. Quand la sphéroïde est à l'extérieur de la zone entre les deux forages, la polarité est inversée, celle de la résistivité est positive, celle de la chargeabilité est négative. Ces phénomènes peuvent être expliqués par la distribution des charges induites sur la surface de la sphéroïde.

Par modélisation théorique, on a obtenu plusieurs réponses correspondantes à différentes sphéroïdes. D'après la position du sommet de la réponse, on peut facilement savoir la profondeur du centre de la sphéroïde. D'après la forme de la réponse

(symétrique ou asymétrique), on peut savoir si la sphéroïde est horizontale ou inclinée. La polarité des réponses nous donnent des information de la position horizontale de la sphéroïde. Mais, si la sphéroïde se trouve à l'extérieur de la zone entre les forages, on ne peut pas exactement déterminer de quel côté se situe la sphéroïde par rapport à ces forages.

-
La région de Victor se situe à l'extrémité Est du Bassin de Sudbury (Fig. 4.1). La structure dans cette région est complexe. Deux gisements minières sont connus. Un se trouve au nord entre 1,524 et 1,676 m de profondeur, l'autre est environ 500 m au sud de celui-ci, entre 2,133 et 2,682 m de profondeur (Fig. 4.2).

Inco a fait beaucoup de levés de résistivité et de PP en forage dans les années 70 et au début des années 80. Les mesures à Victor nous ont intéressé car on veut savoir quelle est la géométrie des corps responsables des anomalies mesurées, et s'il y a un troisième gisement inconnu jusqu'à présent.

Avec les données mesurées, on a calculé la chargeabilité apparente (Fig. 4.6). D'après les polarités de la résistivité apparente et de la chargeabilité apparente, on sait que les anomalies sont produites par un conducteur entre deux forages. D'après la position du sommet de l'anomalie de la chargeabilité apparente, on suppose que la profondeur du centre de conducteur se trouve à 1,600 m. Avec ces suppositions, on

construisait un modèle initial, à partir duquel, on a trouvé un modèle d'une sphéroïde avec un noyau conducteur. Il y a une assez bonne correspondance entre les réponses du voltage et de la résistivité théoriques et les données mesurées. Malheureusement, la chargeabilité apparente théorique ne s'accorde pas bien avec les données mesurées. En réalité, il y a plusieurs gisements minces interceptés par le forage 60003-2. On a utilisé une sphéroïde avec un noyau pour simuler ces gisements, ce qui n'est pas approprié. Cependant, ce résultat indique qu'il n'y a pas d'évidence pour un grand corps minier existant entre les deux forages, et l'anomalie de PP est produite par les gisements de sulfures interceptés par le forage 60003-2.

Le programme de U.B.C nous permet de simuler ces gisements avec des couches minces. Après calculs, on a trouvé un modèle de quatre-couches. Les réponses de ce modèle s'accordent très bien avec les données mesurées.

On a remarqué que les modèles trouvés par NEWROID et le programme de U.B.C sont différents, mais les deux résultats révèlent que les gisements de sulfure interceptés par le forage 60003-2, qui se prolongent au moins jusqu'au forage 60060, sont responsables pour les anomalies des profils mesurés, et qu'il n'y a pas d'évidence pour un troisième grand cible minière entre les deux forages.

Une méthode d'interprétation des données de résistivité et de PP en forage dans

la région de Victor a été présentée. Le processus est d'abord de construire un modèle initial par comparaison des résultats théoriques avec les données mesurées, ensuite, avec l'aide des programmes NEWROID et de U.B.C, modifier ce modèle jusqu'à ce qu'un modèle acceptable soit trouvé. Cette méthode s'est avérée applicable pour cette étude. On peut l'utiliser pour interpréter toute les données de résistivité et de PP en forage de Inco.

Pour optimiser effectivement les paramètres d'un modèle sphéroïdal, on recommande de développer la capacité d'inversion pour le programme NEWROID.

ACKNOWLEDGEMENTS

I would like to take this opportunity to thank all the persons, who have given direct or indirect help to my study at the Ecole Polytechnique.

My greatest appreciation belongs to my supervisor, Professor Fullagar, who spent a large amount of time examining and constructively criticizing my thesis. Without his patience, knowledge and experience, this investigation could not have been completed.

I am grateful to Inco Limited for providing the Victor borehole resistivity data, and to Alain King, Ebe Berrer, and Gord Morrison for their technical assistance in the course of the project.

Also, I would like to thank Dr. P. Zhang for his help in modifying the program of Daniels.

I would also like to thank Professors Chouteau and Bailey for their reading and very useful comments to the manuscript of my thesis.

I am grateful to NSERC, TVX Gold, and Golden Knight Resources who have provided the financial support to me for accomplish this study.

TABLE OF CONTENTS

	<u>PAGE</u>
SOMMAIRE	iv
ABSTRACT	vi
RÉSUMÉ	viii
ACKNOWLEDGEMENTS	xvi
TABLE OF CONTENTS	xvii
LIST OF FIGURES	xx
LIST OF TABLE	xxiii
LIST OF APPENDIX	xxiv
 CHAPTER 1 - INTRODUCTION	
1.1 Borehole Resistivity and IP in Deep Exploration	1
1.2 Objective of This Study	2
1.3 Review of Previous Work	3
1.4 Methodology	5
1.5 Outline of Thesis	7
 CHAPTER 2 - BASIC THEORY OF RESISTIVITY AND IP	
2.1 Introduction	11
2.2 Apparent Resistivity	12
2.3 Induced Polarization	14

CHAPTER 3 - THEORETICAL MODELLING STUDY

3.1 Introduction	19
3.2 Formulation of DC Resistivity Response of Spheroid with a Core	19
3.2.1 Potential Due to a Spheroid with a Core in a Whole-Space	20
3.2.2 Approximate Potential of a Spheroid with a Core in a Half-Space Using a Modified Image Method	20
3.3 Verification of DSSPHIP and NEWROID	23
3.4 Precision of The Modified Image Method	26
3.5 Resolution Studies For a Conductive Core	34
3.6 Change of Polarity of Responses	44
3.7 Conclusion	55

CHAPTER 4 - INTERPRETATION OF VICTOR BOREHOLE RESISTIVITY AND IP

DATA

4.1 General Geology of the Victor Area	56
4.2 Data Acquisition	60
4.3 Data Reduction	61
4.4 Resistivity and IP Modelling	67
4.4.1 Modelling with NEWROID Program	71
4.4.2 Modelling with U.B.C 2D DCR/IP Program	79

CHAPTER 5 - CONCLUSION AND RECOMMENDATION

REFERENCES	86
------------------	----

APPENDIX A	90
APPENDIX B	95

LIST OF FIGURES

	<u>PAGE</u>
<u>Chapter One</u>	
FIGURE 1.1	8
<u>Chapter Two</u>	
FIGURE 2.1	17
<u>Chapter Three</u>	
FIGURE 3.1	21
FIGURE 3.2	24
FIGURE 3.3	27
FIGURE 3.4	28
FIGURE 3.5	29
FIGURE 3.6	30
FIGURE 3.7	32
FIGURE 3.8	33
FIGURE 3.9	36
FIGURE 3.10	37
FIGURE 3.11	39
FIGURE 3.12	40
FIGURE 3.13	41

FIGURE 3.14	42
FIGURE 3.15	43
FIGURE 3.16	45
FIGURE 3.17	46
FIGURE 3.18	48
FIGURE 3.19	50
FIGURE 3.20	52
FIGURE 3.21	53
FIGURE 3.22	54

Chapter Four

FIGURE 4.1	57
FIGURE 4.2	59
FIGURE 4.3	62
FIGURE 4.4	64
FIGURE 4.5	68
FIGURE 4.6	69
FIGURE 4.7	73
FIGURE 4.8	74
FIGURE 4.9	75
FIGURE 4.10	77
FIGURE 4.11	78

FIGURE 4.12 80
FIGURE 4.13 81

Appendix B

FIGURE B.1 96
FIGURE B.2 97
FIGURE B.3 99

LIST OF TABLE

PAGE

TABLE 1 - Legend for the host geology in Figure 4.6. 70

LIST OF APPENDIX

PAGE

APPENDIX A - DC RESISTIVITY RESPONSE OF A STRATIFIED SPHEROID	
.....	90
APPENDIX B - A MODIFIED METHOD OF IMAGE FOR BOREHOLE	
RESISTIVITY	95

CHAPTER 1

INTRODUCTION

1.1 Borehole Resistivity and IP in Deep Exploration

With continuing exploitation of known base metal deposits, the need for new mineral discoveries will increase greatly in Canada. However, mineral discoveries at the surface and within reach of conventional exploration technologies (e.g. field mapping, surface and airborne geophysical methods) are not expected to satisfy future demands for new reserves. To cope with this situation, we must now research and develop new geophysical methods and geological models which permit us to detect mineralization at depths of 300 to 3,000 meters, approximately one order of magnitude deeper than is possible with present methods. Thus, there is a strong case for research in borehole geophysics, to extend the range of investigation of conventional surface geophysical methods.

Of all the geophysical techniques, the electrical (especially electromagnetic) methods have had the most widespread use in ground mineral investigations because they respond to good electrical conductors underground. However, the problem with this conventional surface method is that measurements are insensitive to ore bodies if they are too deeply buried or if their mineral concentration (conductivity contrast) is low. Further, such surveys are usually strongly influenced by the inhomogeneities near

surface.

These problems can be reduced if the resistivity measurements are made downhole and with combinations of downhole and surface current sources. In these cases, the sensitivity of measurements improves significantly. This kind of technique is called "borehole resistivity".

Due to its sensitivity to disseminated mineralization, the induced polarization method (IP) has proved itself to be an effective tool for mineral exploration. The IP technique can also be applied down hole to meet the need for deeper exploration for disseminated mineral deposits.

1.2 Objective of This Study

Inco (International Nickel Company) has a large quantity of borehole resistivity and IP data, most of which has not been quantitatively interpreted. In particular a set of borehole resistivity and IP data was measured by Inco in the Victor area near Sudbury in 1978. Originally, this set of data was of interest because we thought maybe there was an "off-hole" nickel-copper sulphide target which was responsible for the anomaly in the observed IP data. In this study we aimed, by interpreting the Victor data set, to develop a methodology to be used for interpreting all this kind of borehole data.

The orebodies in the Sudbury Basin are often surrounded by a halo of disseminated mineralization. A secondary objective of this study was to investigate if it is possible to detect a core of massive mineralization from outside the halo of disseminated mineralization using borehole resistivity and IP data.

1.3 Review of Previous Work

In the past 20 years, there were many papers published in the field of borehole resistivity (e.g. Daniels, 1977, 1983, 1984; Dey and Morrison, 1979; Dobecki, 1980; Yang and Ward, 1985 a, 1985 b; Bevc and Morrison, 1991;). Daniels (1977), with the help of Barnett's surface-integral technique, presented theoretical studies of a sphere and an ellipsoid in the presence of buried current sources. In his study, Daniels discussed in detail the anomalies due to a sphere and an ellipsoid in a half-space, for six different hole-to-hole, hole-to-surface and surface-to-hole configurations. Dey and Morrison (1979) compared downhole and surface current electrode configurations using a general 3-D numerical modelling algorithm. Theoretical solutions for apparent resistivity anomalies due to sphere and oblate and prolate spheroids were discussed in Dobecki (1980). Yang and Ward (1985 a, 1985 b), using integral-equation technique, presented the results of sensitivity analyses for thin oblate spheroids and ellipsoids with arbitrary attitude. From the results, we can see that hole-to-hole resistivity measurements are more effective than single hole measurements for delineating resistivity anomalies. However,

there is no "best" method for all situation encountered in the field. The choice of method depends upon depth of the body, spacing of the boreholes, and electrical properties of the body.

Although most of the cited papers dealt primarily with theoretical model responses, some presented field applications of borehole resistivity techniques, e.g. Daniels (1983, 1984), Bevc and Morrison (1991). Daniels (1983) presented a study of hole-to-surface resistivity measurements for defining geoelectric inhomogeneities; and Daniels (1984) described the successful tests of hole-to-hole resistivity measurements for detecting old mine workings in a coal seam. The paper of Bevc and Morrison showed the sensitivity of borehole-to-surface resistivity measurements in ground-water investigations, to delineate aquifers, locate fresh and saline water-bearing zones. They identified a ground-water flow pattern not detected by hydrological measurements.

For borehole IP, few papers have been published (e.g. Snyder and Merkel, 1973; Daniels, 1977). With a hole-to-surface configuration, we can have a good resolution to a deeply buried target. Snyder and Merkel found, after a careful study of IP response, that for good resolution, the current source must be buried deeper than half the depth to the top of the sphere target. In Daniels' paper, he presented some IP modelling results with different configurations (hole-to-hole, hole-to-surface, surface-to-hole, etc.), and pointed out that for hole-to-hole IP measurements a major concern is the effect of EM

coupling.

1.4 Methodology

Since there were few appropriate programs available for this interpretation, we have used two modelling programs, DSSPHIP and NEWROID, developed by Fullagar. They calculate the resistivity and IP responses of a sphere with a core and a spheroid with a core, respectively, in a homogeneous host (Fullagar, 1993 a, 1993 b). A 2D borehole resistivity and IP modelling program from U.B.C (University of British Columbia) was also used in this study.

Before programs DSSPHIP and NEWROID were used for modelling, we compared them with Daniels IP3DDH program (Daniels, 1977) for two models in order to verify them. From the comparison, we see that the responses from DSSPHIP and NEWROID are identical for both models, but there are slight differences between them and IP3DDH. Considering different methods used in these programs, analytic solutions are used in DSSPHIP and NEWROID, and IP3DDH uses surface-integral technique (Barnett, 1972), we think that these differences are numerical. There are two reasons we did not use IP3DDH in our study: (I) IP3DDH can not compute the responses of a sphere or a spheroid with a core; (II) IP3DDH used the conventional image method which has a large error when current source(s) or receiver electrode(s) are in subsurface. At least,

from these two standpoints DSSPHIP and NEWROID are superior to Daniels IP3DDH program.

With NEWROID, we calculated responses of a uniform spheroid and a spheroid with a conductive core for five different models. From their comparison, we reach the conclusion that it is difficult to detect a conductive core if the resistivity contrast between the spheroidal shell and the host is large. However, if the resistivity contrast is modest (< 10) and two voltage electrodes are located in the spheroidal shell, it is still possible to detect a conductive core.

With the help of the modelling programs from Ecole and U.B.C, we have found subsurface models which can explain the Victor data. Figure 1.1 illustrates the "modified Schlumberger" configuration which Inco used at Victor. This is a surface-to-hole dipole-dipole measurement. As shown in the figure, two current sources are separately placed on the surface of earth and nearly 4,000 meters apart; two receive electrodes are put in two boreholes, which are about 600 meters apart; one is moving between depths of 915 to 1,890 m (3,000 to 6,200 ft) and the other is fixed at depth 1,731 m (5,680 ft). In the survey, potentials differences between these two electrodes were measured.

Construction of a subsurface model from the observed geophysical responses is a geophysical inversion problem. Without an appropriate inversion program, we could

not find a model automatically by computer. Our procedure consisted of three steps: firstly, with the help of modelling program, performing a theoretical study by calculating different model responses for a modified Schlumberger configuration to find their characteristics; then, comparing these characteristics with the real responses to design a good initial model; finally, modifying this initial model by trial and error until a final satisfactory interpretation was found.

1.5 Outline of Thesis

This thesis consists of five chapters. The following four chapters are:

Chapter Two --- sketches basic theory of resistivity and IP;

Chapter Three --- Results from DSSPHP and NEWROID are compared with Daniels IP3DDH program for two models, to verify DSSPHP and NEWROID, NEWROID was then used for modelling. During the modelling, we found that the conventional image method violates the "Principle of Reciprocity" and brings a large error when current source(s) or receive electrode(s) are in the subsurface. A "modified image method" proposed by Fullagar is used in DSSPHP and NEWROID. By comparing the result of this method and that of the conventional image method, we can see that the modified image method is superior to the conventional image method in the borehole

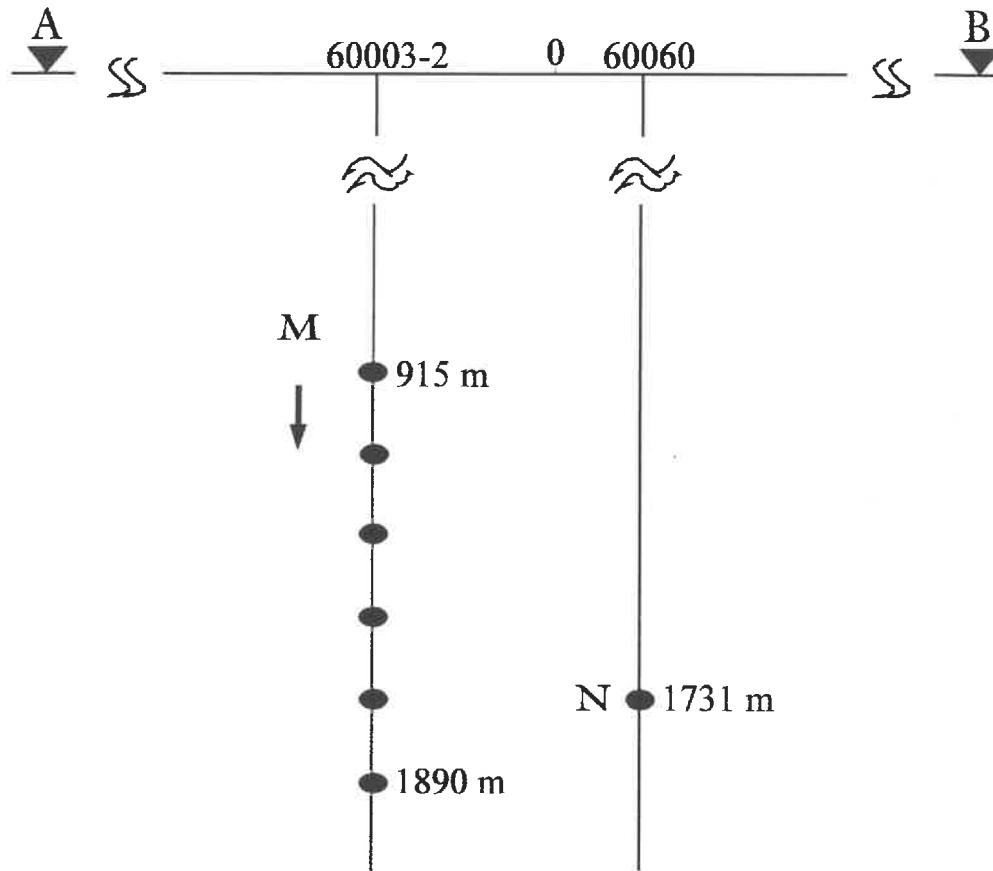


Figure 1.1: A configuration Inco used in Victor survey. The distance between two surface current source A and B is about 4,000 m, and two boreholes separation is about 600 m. Potential electrode M is moving between depths of 915 to 1,890 m (3,000 and 6,200 ft), and potential electrode N is fixed at a depth of 1,731 m (5,680 ft).

application. From modelling for five different models, we found that, due to distortion of current flow at the interface of spheroidal shell, it is difficult to detect a conductive core from a homogeneous spheroidal shell if the resistivity contrast between the shell and the host is large.

Chapter Four --- outlines the geological situation of the Victor area and the data collecting; apparent chargeability is calculated with the observed IP data. Then, the resistivity and IP modelling with NEWROID and U.B.C 2D DCR/IP programs is described. The models found with these two programs are different, one is a spheroid with a conductive core and the other is four conductive layers. Since, the responses of voltage from these two different models fitted the observed data well, this is an example of "non-uniqueness" in geophysical prospecting. Even though these two models are different, both reveal that the "stringers of sulphide" intercepted by borehole 60003-2, which probably extend continuously south as far as the Deep Footwall Body, are responsible for the anomaly in observed data. The possibility of the existence of an "off-hole" target is not supported by the data.

Chapter Five --- concludes that our purpose of this study is realized. Through this study, we have understood better the anomaly in observed data at Victor measured with a modified Schlumberger configuration, and obtained the experience for further interpretation of borehole resistivity and IP data. We have also known that it is difficult

to detect a conductive core enclosed within a disseminated "halo" if the resistivity contrast between the host and the "halo" is large (> 10). At the end, considering the efficiency of interpretation, a new version of NEWROID with an inversion capability is recommended.

CHAPTER 2

BASIC THEORY OF RESISTIVITY AND IP

2.1 Introduction

The resistivity method employs an artificial source of current, which is introduced into the ground through point electrodes. The procedure is to measure potentials at other electrodes in the vicinity of the current flow. Because the current is known, it is possible to draw inferences about the distribution of resistivity of the subsurface.

Consider a continuous current flowing in an isotropic homogeneous earth of conductivity σ . Then Ohm's law takes the form

$$\mathbf{J} = \sigma \mathbf{E} \quad , \quad (1)$$

where \mathbf{J} is the vector current density in amperes per square metre and \mathbf{E} is the vector electric field in volts per metre.

The electric field can be derived from the gradient of a scalar potential V :

$$\mathbf{E} = -\nabla V \quad . \quad (2)$$

By the continuity of current;

$$\nabla \cdot \mathcal{J} = 0 \quad , \quad (3)$$

which holds everywhere except at the source itself. It follows from Equations (1), (2), and (3) if σ is constant throughout, that the potential is harmonic:

$$\nabla^2 V = 0 \quad . \quad (4)$$

There are two boundary conditions that must hold at any contact between two regions of different conductivity namely that the potential and the normal current density are continuous. In general, we can solve the Laplace equation (4) and boundary conditions for various shaped bodies in a half-space.

2.2 Apparent Resistivity

From Ohm's law, equation (1), and from (2) it follows that the distribution of the potential caused by a single current source at the surface of a homogenous half-space has the form

$$V = \left(\frac{I\rho}{2\pi} \right) \frac{1}{r} \quad , \quad (5)$$

where I is the input current in amperes, r is the distance between the current source and the potential point, and ρ is the resistivity of the ground.

It is useful to connect the potential with some "geological" parameters. Therefore, we can define an apparent resistivity for the pole-pole configuration ρ_a by inverting equation (5),

$$\rho_a = 2\pi r \frac{V}{I} \quad (6)$$

If the ground is inhomogeneous, ρ_a provides some indication of the variation in subsurface resistivity. In general, apparent resistivity has the form:

$$\rho_a = K \frac{V}{I} \quad (7)$$

where K is a geometric factor. Geometric factors for some common electrode arrays are given by Sumnes (1976, p26).

For the modified Schlumberger configuration used by Inco at Victor, two current electrodes (A and B) are located at the surface and two potential electrodes (M and N) are underground (Fig. 1.1). We can use the principle of superposition to calculate the voltage difference between two receiver electrodes. We can measure the difference ΔV in potential between M and N, and express it in terms of apparent resistivity using (5)

and (7):

$$\Delta V = \frac{I\rho_a}{2\pi} \left(\frac{1}{R_{AM}} - \frac{1}{R_{AN}} - \frac{1}{R_{BM}} + \frac{1}{R_{BN}} \right) \quad (8)$$

where R_{AM} , R_{AN} , R_{BM} and R_{BN} are the distances between electrodes A, M, N and B respectively, and I is the input current in amperes. Therefore, we can define the apparent resistivity of the modified Schlumberger configuration as:

$$\rho_a = \frac{2\pi}{\frac{1}{R_{AM}} - \frac{1}{R_{AN}} - \frac{1}{R_{BM}} + \frac{1}{R_{BN}}} \frac{\Delta V}{I} \quad (9)$$

2.3 Induced Polarization

Induced polarization (IP) is a branch of electrical methods, and is employed mainly in base-metal exploration. The IP phenomenon can be observed with a four-electrode DC resistivity spread by interrupting the current abruptly. The voltage across the potential electrodes generally does not drop to zero instantaneously, but decays rather slowly with time, after an initial large decrease from the original steady-state value. The rate of voltage decay is finite for the following two reasons:

I. *Electromagnetic Induction*: the flow of current around the transmitter circuit gives rise to a magnetic field, and each time the current is switched off by the transmitter, the change in magnetic field induces voltages in the ground which can be detected by the receiver;

II. *Induced Polarization*: when there is a polarizable body underground, under the effect of electrical field, the charges will accumulate at the surface of the body; when the current is shut-off, the voltage produced by these charges can be measured by the receiver, too.

The IP effect can be divided into two parts. The first is known as *membrane* or *electrolytic polarization* and constitutes the background or so-called *normal IP effect* . It may occur in rocks that do not contain metallic minerals. The second is known as *electrode polarization* or *overvoltage*. It is generally larger in magnitude than the background IP and depends on the presence of metallic minerals in the rock (Telford, Geldart and Sheriff, 1990).

The IP response is measured by passing a controlled current through the ground and observing resultant voltage changes with time. If there is a polarizable body underground, we will find that the voltage increases with time after the inducing current is switched on. According to Ohm's Law, we can assume that the IP effect is equivalent

to increasing the effective resistivity of the polarized body, or reducing its effective conductivity. In consequence, the effective reduction of the conductivity will produce a secondary voltage when the inducing current is turned off. Accordingly, the chargeability M of a medium with conductivity σ can be defined by (Seigel, 1959),

$$M = \frac{V(\sigma') - V(\sigma)}{V(\sigma')} = \frac{V_s}{V_p} \quad (10)$$

where σ' is the reduced conductivity, and V_p is the (primary) voltage immediately prior to current shut-off. V_s is the peak secondary voltage (Fig. 2.1). For a homogeneous medium, this is equivalent to

$$M = -\Delta\sigma/\sigma = -(\sigma' - \sigma)/\sigma \quad (11a)$$

or, in terms of resistivity,

$$M = \frac{\Delta\rho}{\rho'} = \frac{\rho' - \rho}{\rho'} \quad (11b)$$

where ρ and ρ' denote the original and perturbed resistivities respectively. The chargeability defined in (10)-(11) relates to peak secondary voltage only, and does not, in any way, characterise the time decay or spectral character of the induced polarization voltage.

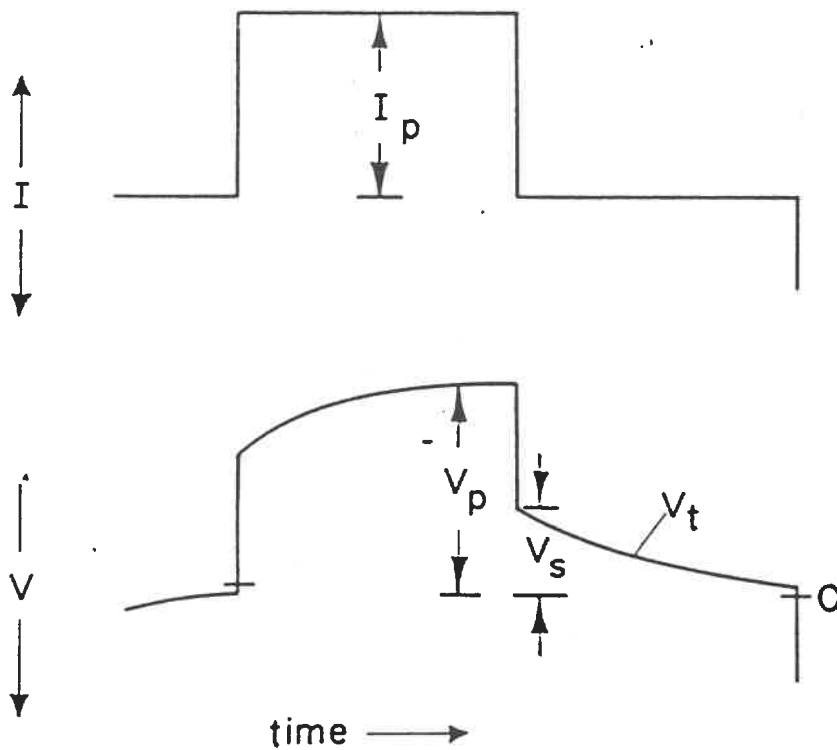


Figure 2.1: The IP pulse or time-method waveforms, ideally due to a long period pulse, showing the induced primary current I_p being detected as a maximum primary voltage V_p . When current is turned off, voltage drops to a secondary level V_s and transient voltage V_t decays with time. A theoretical measure of chargeability, M , is $M=V_s/V_p$. (After Sumner, 1976, p.5)

For an earth model composed of J materials, with resistivities $\{\rho_j\}$ and chargeabilities $\{M_j\}$, the general expression for apparent chargeability, M_a , can be induced from (11b),

$$M_a = \frac{V(\vec{\rho}') - V(\vec{\rho})}{V(\vec{\rho}')} \quad (12)$$

where $V(\rho)$ denotes the DC voltage for a model with resistivities $\rho = \{\rho_j; j=1,2,\dots,J\}$ and where

$$\rho_j' = \rho_j / (1 - M_j) \quad . \quad (13)$$

From the discussion above, we see that in order to carry out forward modelling to compute apparent chargeability, we need to carry out two DC resistivity forward modelling with conductivities σ and $\sigma(1-M)$.

CHAPTER 3

THEORETICAL MODELLING STUDY

3.1 Introduction

Several computer programs were available to us for calculating numerically the borehole resistivity response of a model of the Earth when excited by a point current source. Specifically, we have U.B.C 2D DCR/IP modelling program and modelling programs for a single simple body in a uniform host: Daniels IP3DDH (1977), DSSPHIP (Fullagar, 1993 a), and NEWROID (Fullagar, 1993 b). The various programs have been developed quite independently and have been based on several different methods --- analytic, finite difference, and surface-integral, for example. Therefore, it is desirable to compare and as far as possible verify these programs.

In this chapter, we will compare these three programs and see if DSSPHIP and NEWROID are reliable; then compute the responses for different models to see if we can distinguish a spheroid with a conductive core from a homogeneous spheroid.

3.2 Formulation of DC Resistivity Response of Spheroid with a Core

3.2.1 Potential Due to a Spheroid with a Core in a Whole-Space

The geometry of the problem we wish to consider is illustrated in Figure 3.1 (a,b). A prolate spheroid (or an oblate spheroid) encased with a shell, lies in a homogeneous whole-space of resistivity ρ . A point source C is outside the spheroid. P is an arbitrary point in the space either outside or inside the spheroid (can be either in the shell or in the core), at which we wish to determine the electrical potential.

The solution for a uniform spheroid in a whole space has been discussed before (Bibby and Risk, 1973; Dobecki, 1980; Wait, 1982). However, the solution for a stratified spheroid was first given by Fullagar (1993 b), and is included in Appendix A.

3.2.2 Approximate Potential of a Spheroid with a Core in a Half-Space Using a Modified Method of Image

Webb (1931) published an exact solution for a spheroid in a half-space. Because this solution is very complicated mathematically, it has not yet been used in reality. In the past, a spheroid in a half-space has been computed approximately by the image method. However, in our interpretation of borehole resistivity data, this image method (we call "conventional image method") gave us too large an error to be accepted, due to the potential electrodes in the subsurface.

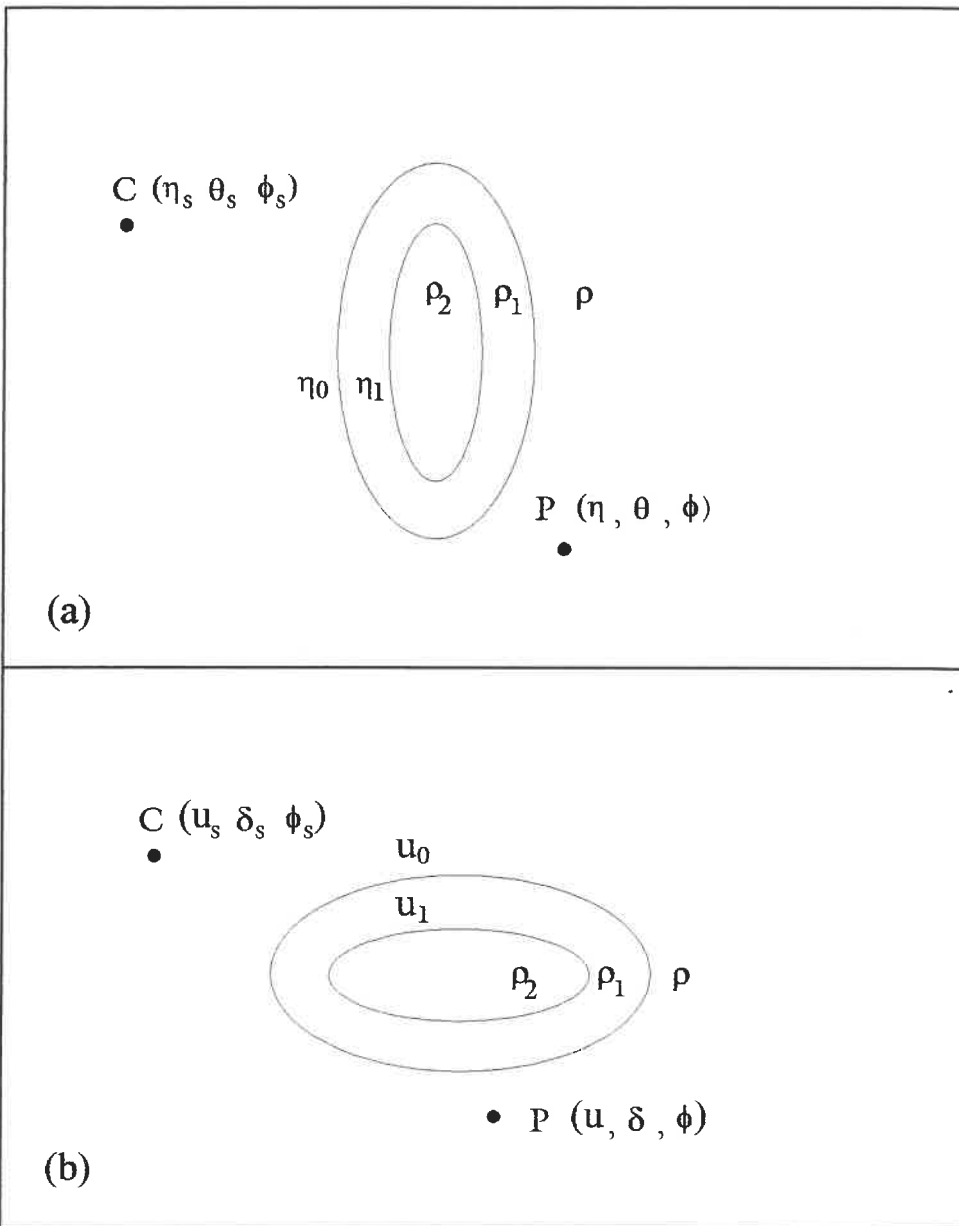


Figure 3.1: A stratified spheroid is in a whole-space. A point current source C is outside the spheroid; a potential electrode P is in the space either inside or outside the stratified spheroid; (a) a prolate spheroid with a core; (b) an oblate spheroid with a core.

In general, by means of the image method we can use the formulae derived in whole-space to approximate the response in a half-space. The image solution technique involves superposing two "spheroid with a core in a whole space" solutions in their correct geometrical relation. For the case of sphere, the image technique yields an acceptably accurate solution if the ratio of centre depth-to-radius (of sphere) exceeds 1.3 (Grant and West, 1965; Telford, Geldart and Sheriff, 1990). In fact, this is correct only when both current source(s) and receive electrode(s) are on the surface. If one of them or both of them are in the subsurface and near the spheroid (body), even though the spheroid is in a great depth, the image method still sometimes produces a "large" error, because this "conventional" image method violates the Principle of Reciprocity in these cases. For better approximating DC response of a spheroid in a half-space, Fullagar (1993 a) proposed a new approach, described in Appendix B.

All the formulae described in Appendix A and Appendix B have been implemented in Program NEWROID, which can be used to calculate the voltage, apparent resistivity and apparent chargeability (or the peak secondary voltage) for a spheroid with a core (either prolate or oblate) in a half-space for hole-to-hole, hole-to-surface, or surface-to-hole different configurations. A separate program DSSPHIP is used to calculate the response for a sphere with a core in a half-space. These two programs were written by Fullagar and both of them are run on PC. Generally, for a model with 100 receive points, NEWROID takes only about one or two minutes on

PC486 DX2-66, and less time is taken for DSSPHIP. We will show and discuss some modelling results in the following sections.

3.3 Verification of DSSPHIP and NEWROID

Before we use DSSPHIP and NEWROID to do modelling study, we have to prove them to be reliable and correct. We compare these two programs with Daniels IP3DDH program for two different models, as shown in Figure 3.2.

DSSPHIP can calculate the responses of a single sphere or a stratified sphere in a whole space, and NEWROID can compute the responses of a uniform spheroid or a spheroid with a core (prolate or oblate) in a whole space. Daniels IP3DDH program can compute the electrical responses of sphere, spheroid and ellipsoid in a whole space. All these three programs employ image method to approximate the response in half-space. The difference is: in Daniels IP3DDH program the conventional image method is used, but in DSSPHIP and NEWROID the modified image method described in Appendix B is normally used. However, in order to compare with Daniels IP3DDH program, the conventional image method is temporarily used in DSSPHIP and NEWROID. As for computing methods used in three programs, they are based on two different methods. Daniels IP3DDH program is based on surface-integral technique (Barnett, 1972). DSSPHIP and NEWROID are based on analytic solutions.

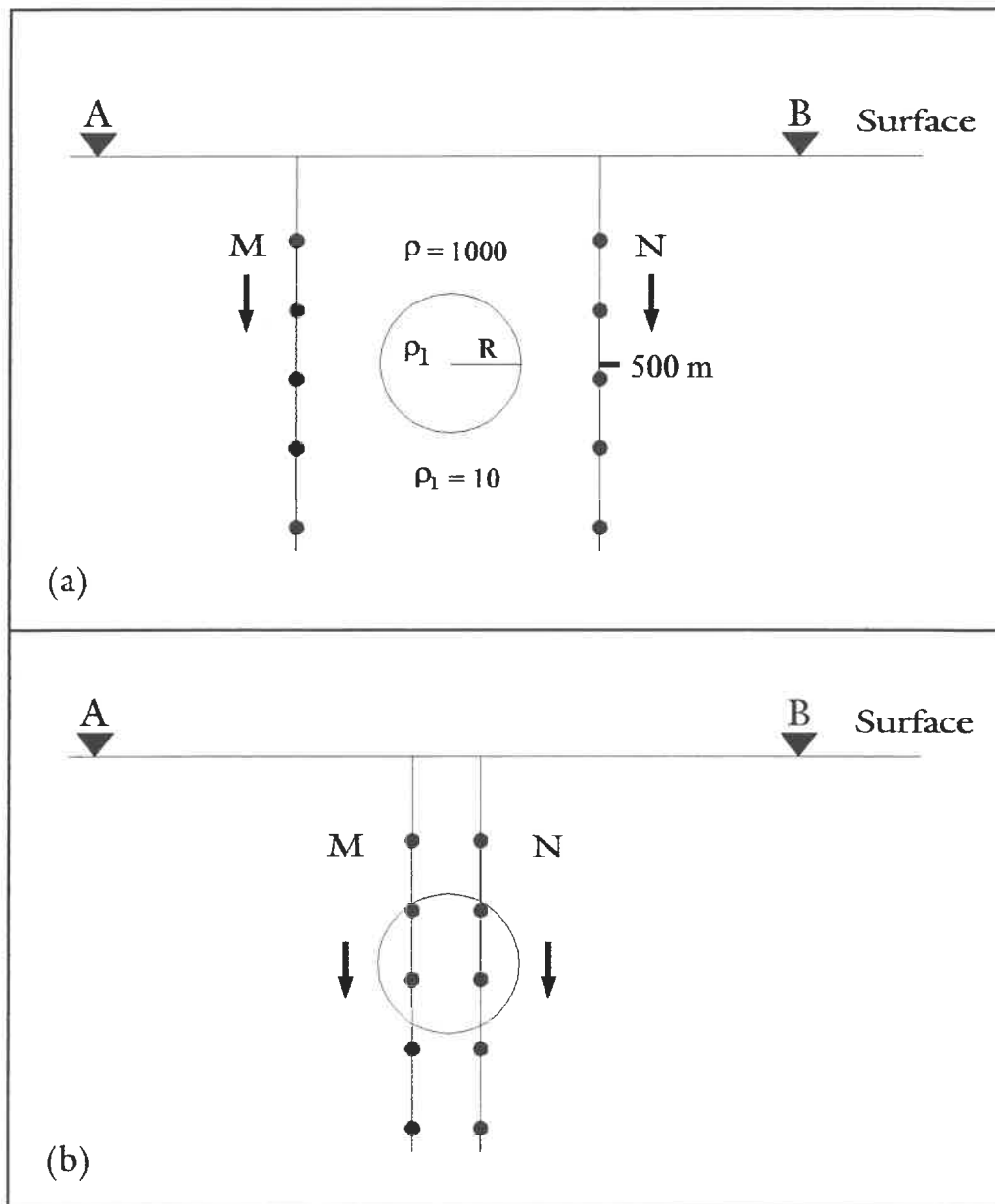


Figure 3.2: A sphere of radius R ($=100$ m) is in a half-space with a modified Schlumberger configuration. The distance between two surface current sources is 1000 m. Resistivities of the half-space and the sphere are 1000 and 10 ohm-m, respectively; (a) the sphere is between two boreholes which are 400 m apart; (b) two boreholes 100 m apart traverse the sphere.

To compare them, we use these three programs in computing the electrical response for two simple models with the modified Schlumberger configuration, in which two current sources are on the surface and the receiver electrodes are put in two boreholes. For the first model, a single sphere of radius of 100 m with a resistivity of 10 ohm-m is located between two boreholes in a half-space of resistivity of 1000 ohm-m; the centre depth of the sphere is 500 m, and the chargeability of the sphere is 100 mV/V (Fig. 3.2 a). For the second model, all the parameters are the same as for the first, except that the distance between two boreholes is 100 m instead of 400 m, with the result that the two boreholes traverse the sphere (Fig. 3.2 b).

With these programs, we calculate total voltage, residual potential (the difference between total voltage and the half-space voltage), apparent resistivity and peak secondary voltage, V_s (Fig. 2.1).

Before comparing DSSPHIP and NEWROID with Daniels IP3DDH program, we first compare these two programs for the models (Fig. 3.2 a,b). There is a tiny difference in the models used for these two programs. For DSSPHIP the model is exactly as shown in Figure 3.2 (a,b); for NEWROID a prolate spheroid (major and minor semi-axes $a=101$ m and $b=100$ m) instead of a sphere is used. Because these two models are nearly the same, and both programs are all based on the analytic solution, even though different formulations used in them, we still have reason to expect their responses to be

basically identical. From the results shown in Figures 3.3 and 3.4, we see that the responses of these two programs are in good agreement as we expected.

Then, DSSPHIP and Daniels IP3DDH were used to calculate the responses for the same models as above. From Figures 3.5 and 3.6, we see that there are differences in the responses between two programs. However, these differences are small and they are thought to be caused by different computing methods used in the programs. For example, in the program of Daniels the sphere is approximated by 72 triangular facets, this variation of sphere's dimension will certainly produce an error. Considering an analytic solution was used in DSSPHIP, it is reasonable to think DSSPHIP is more correct. For this and the following two reasons, we did not use Daniels IP3DDH program for interpretation of Victor borehole resistivity and IP data: (I) it can not compute the response for a spheroid with a core; (II) it uses the conventional image method which is not always appropriate for borehole measurements.

On the basis of this comparison, we can say that DSSPHIP and NEWROID are reliable and can be used in our future study.

3.4 Precision of The Modified Image Method

In Appendix B, we discussed a shortcoming of the conventional image method for

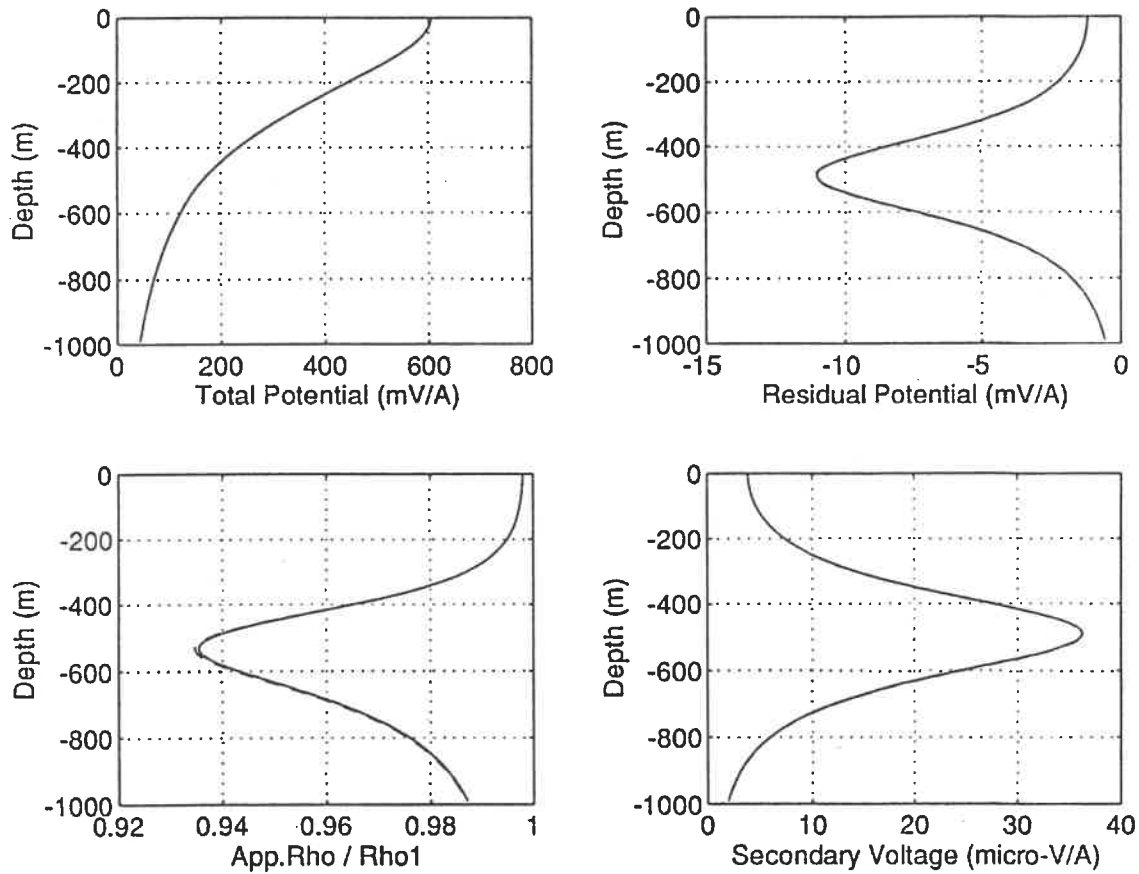


Figure 3.3: Comparison of the results of DSSPHIP and NEWROID for the model (a) in Fig. 3.2. A prolate spheroid (major and minor semi-axes are 101 m and 100 m) is calculated by NEWROID. Solid line represents result of DSSPHIP; and dashed line represents that of NEWROID.

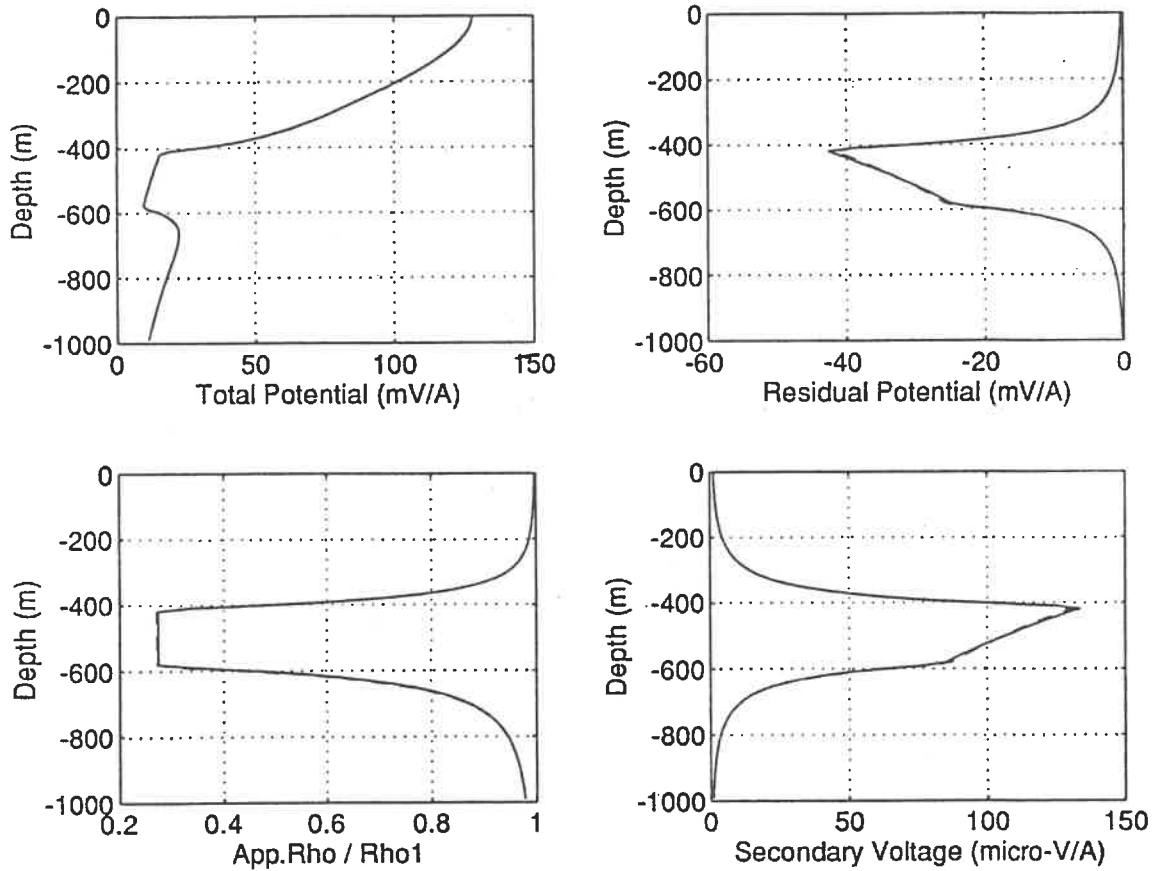


Figure 3.4: Comparison of the results of DSSPHIP and NEWROID for the model (b) in Fig. 3.2. A prolate spheroid (major and minor semi-axes are 101 m and 100 m) is calculated by NEWROID. Solid line represents result of DSSPHIP; and dashed line represents that of NEWROID.

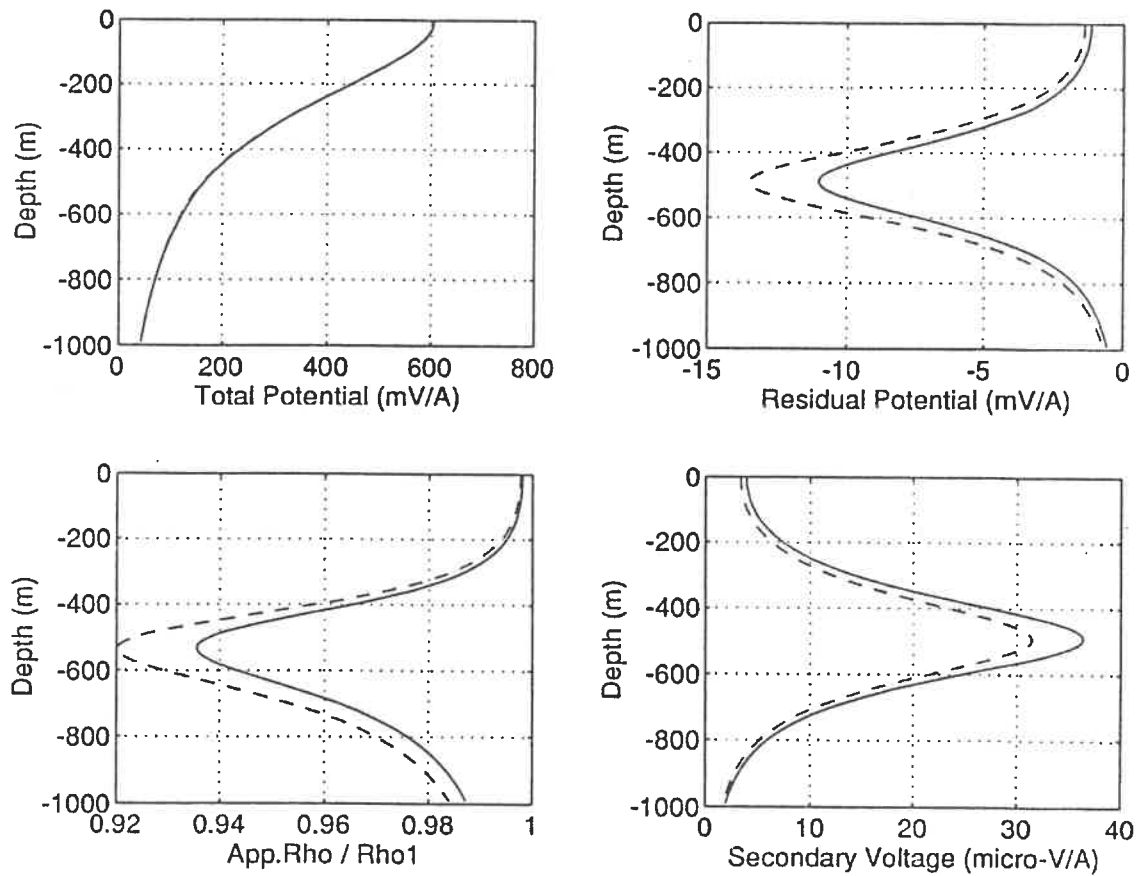


Figure 3.5: Comparison of the results of Daniels' program and DSSPHIP for the model (a) in Fig. 3.2. Solid line represents result of DSSPHIP; and dashed line represents that of Daniels.

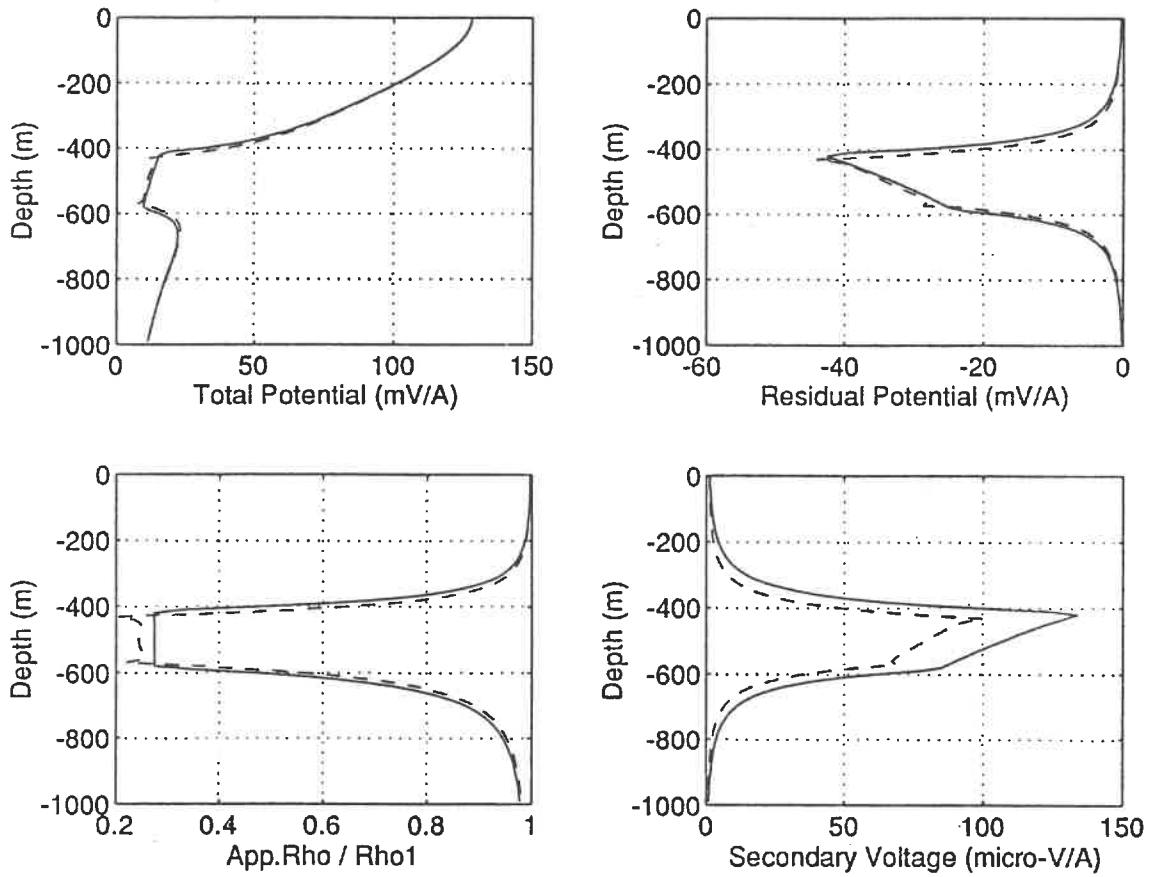


Figure 3.6: Comparison of the results of Daniels' program and DSSPHIP for the model (b) in Fig. 3.2. Solid line represents result of DSSPHIP; and dashed line represents that of Daniels.

borehole resistivity technique. In this section, we compare the modelling results using the conventional method with those obtained with the modified image method described in Appendix B. The modified image method consists of four different approaches according to whether both, neither, or, only one current source and receiver is inside the body. Through the comparison of the results, we see that the result of modified image method is closer to the true solution than that of the conventional image method.

For the model shown in Figure 3.2 (b), the sphere is intersected by two boreholes, through which the receiver electrodes pass. According to the Ohm's Law, for two electrodes inside the sphere, the more conductive the sphere, the smaller the voltage difference between two electrodes; if the sphere is a perfect conductor, the voltage difference is zero. We compute total voltage and apparent resistivity using two versions of DSSPHIP, one with the modified image method and the other with the conventional image method. The results are given in Figure 3.7. From the figure, we can see that the amplitudes of responses with the modified image method are smaller than those for the conventional image method. The apparent resistivity values with the modified image method, when the receivers are inside the sphere, are about 32 ohm-m, and they are near to the true resistivity of the sphere 10 ohm-m. If we change the resistivity of the sphere to 0 ohm-m, we know that inside the sphere the voltage difference should be zero. With the modified image method we obtain this result, as shown in Figure 3.8. From these two examples, we see when the receiver is inside the sphere, it is preferable to always

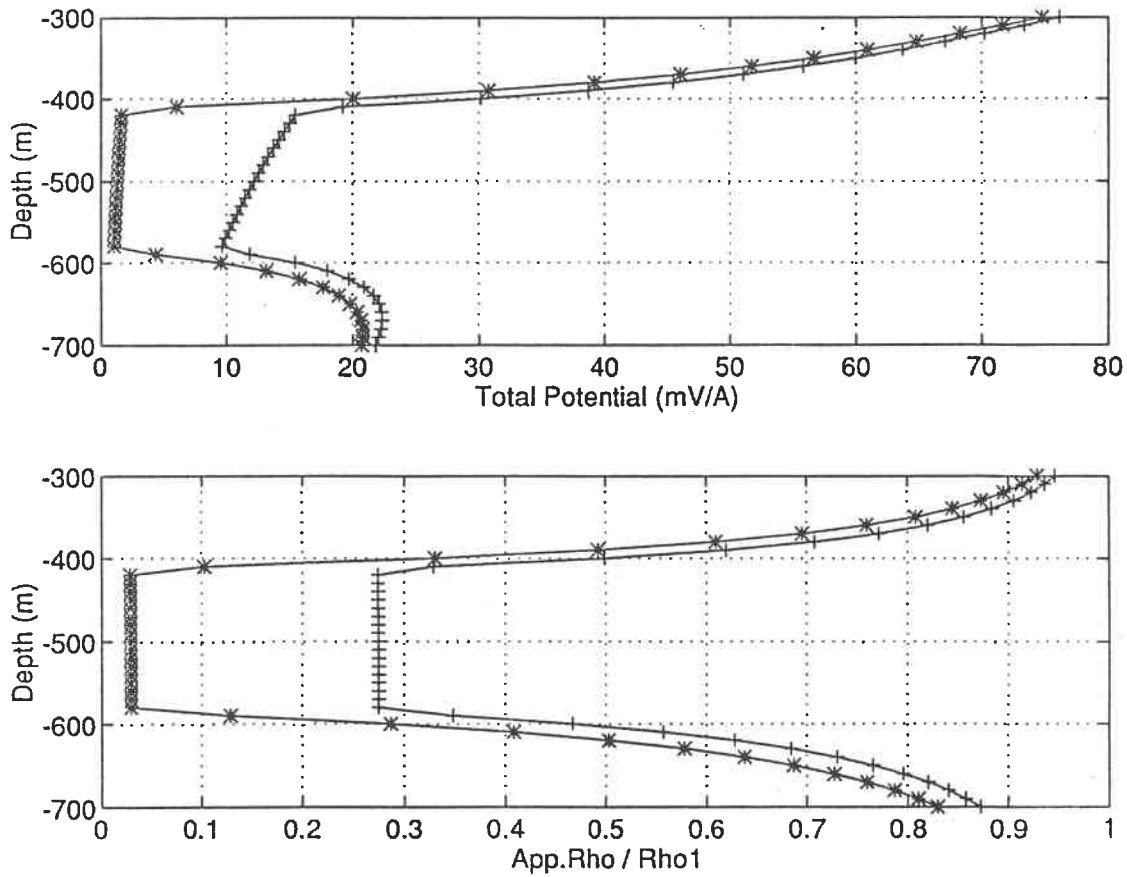


Figure 3.7: Comparison of the modified image method and the conventional image method for the model (b) in Fig. 3.2. *** represents modified image method and +++ represents conventional image method. Resistivities of host and sphere are 1,000 and 10 ohm-m.

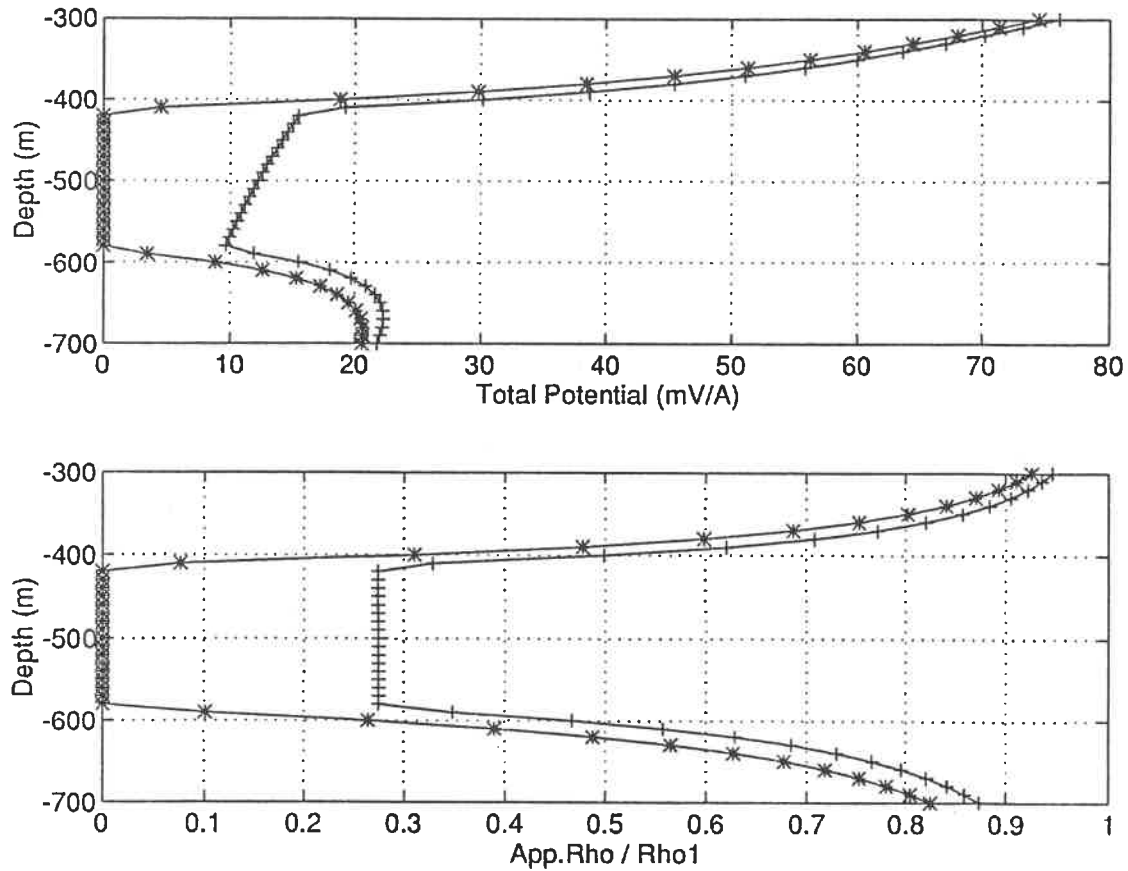


Figure 3.8: Comparison of the modified image method and the conventional image method for the model (b) in Fig. 3.2. *** represents modified image method and +++ represents conventional image method. Resistivities of host and sphere are 1,000 and 0 ohm-m.

treat the internal receiver as a current source when computing the image contribution.

As we mentioned in the last section, in Daniels IP3DDH program the conventional image method is used, which is not appropriate for the borehole resistivity measurement.

3.5 Resolution Studies For A Conductive Core

Massive sulphide orebodies at Sudbury are sometimes encased within a "shell" of relatively weak mineralization. It is therefore of practical interest to investigate whether bodies with a highly conductive core can be distinguished from relatively homogeneous bodies of disseminated mineralization. Considering again the variety of shapes of mineral bodies, we say that a spheroid with a core possesses more practical significance than a sphere. Therefore, we use the program NEWROID to carry out our modelling.

Figure 3.9 (a,b) depicts a spheroid with a core in a half-space surveyed with a modified Schlumberger configuration. The major and minor semi-axes of the spheroidal shell are 150 m and 100 m, and the major and minor semi-axes of the core are 120 m and 44 m. The resistivities of the host, the spheroidal shell and the core are 1000, 100 and 10 ohm-m, respectively. The chargeabilities of the spheroidal shell and the core are

both 100 mV/V. In model (a) the spheroid is between two boreholes, in model (b) the spheroidal shell is traversed by two boreholes. We calculate the responses of this spheroid with a core and a homogeneous spheroid of resistivity 100 ohm-m for models (a) and (b).

The comparison of the responses of a spheroid with a core and a homogeneous spheroid for model (a) is given in Figure 3.10. From the residual voltage and apparent resistivity results, we can see the differences between the two spheroids, but they are small, about 15% for residual potential and about 5% for apparent resistivity. In fact, from these differences we can hardly see the existence of a conductive core. This is because the resistivity contrast between the host and the spheroidal shell is large ($\rho/\rho_1 = 10$), so the current flows at the surface of the spheroid, and very little current can penetrate to the conductive core (Ma, 1993). However, for apparent chargeability, the difference between these two spheroids is marked and about 25%. This is because IP parameter is sensitive to a small change of resistivity and this is why IP measurement are often used for detecting disseminated mineralization.

In Figure 3.11, when two boreholes cross the spheroidal shell, there are big differences between two spheroids. For apparent resistivity, the difference between two spheroids is as large as 50%, by which we can see the existence of a conductive core. From total potential, we can also see the difference. As for apparent chargeability, when

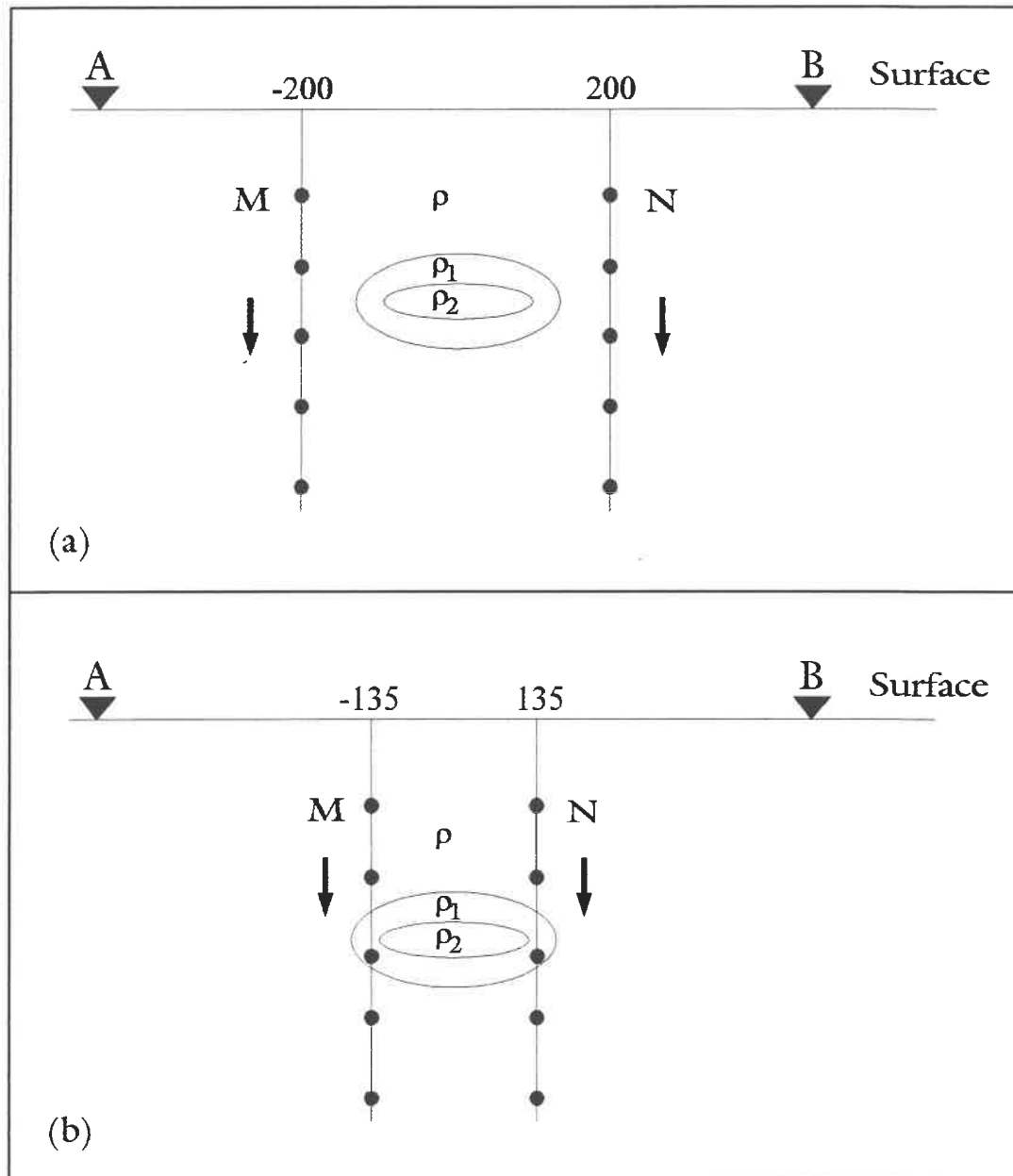


Figure 3.9: A spheroid with a core is in a half-space. The distance between A and B is 1000 m. Resistivities of the half-space, the shell and the core are 1000, 100 and 10 ohm-m, respectively. The dimension of the spheroid with a core is $a=150$, $b=100$, $aa=120$ and $bb=44$ m. (a) the spheroid is between two boreholes which are 400 m apart; (b) two boreholes of 270 m apart traverse the spheroidal shell.

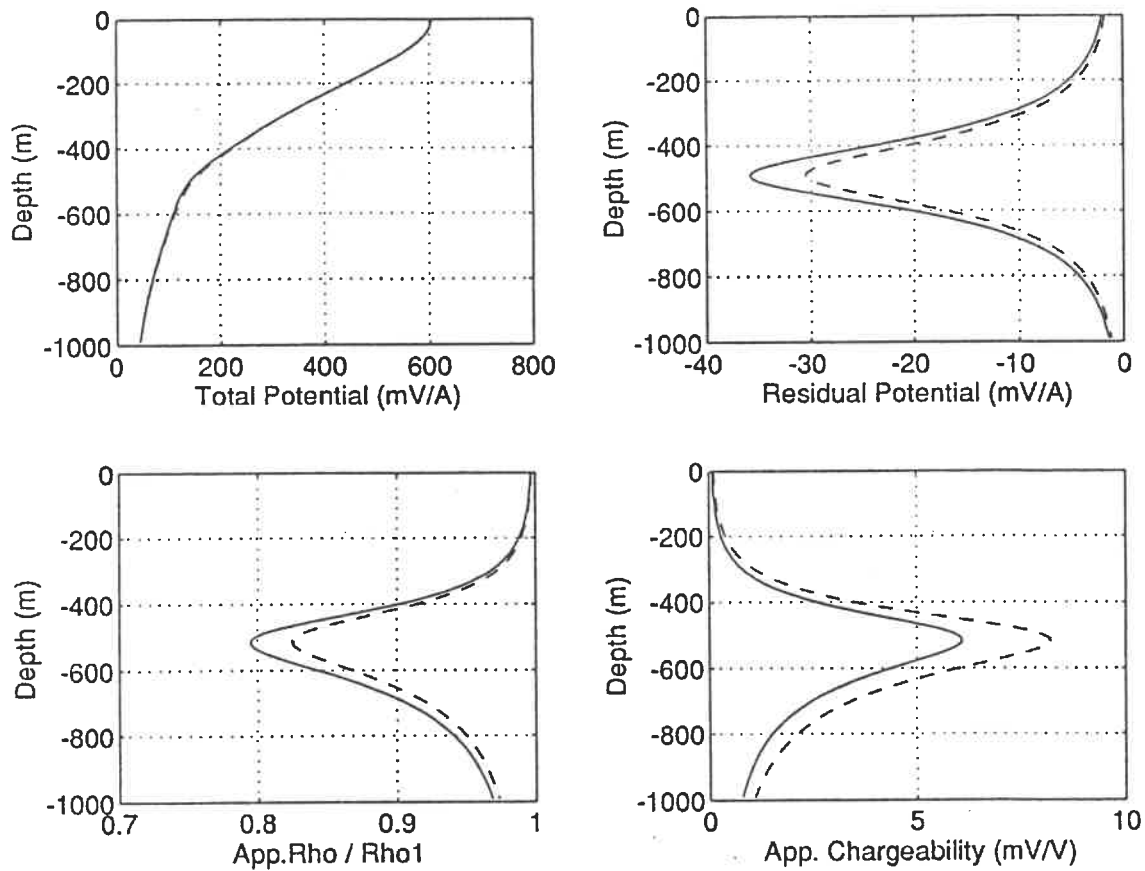


Figure 3.10: Comparison of the results of NEWROID for a spheroid with a core and a simple spheroid for the model (a) in Fig. 3.9. Solid line represents responses of spheroid with a core; and dashed line represents that of spheroid without a core.

both electrodes are near the core, the apparent chargeability of spheroid with a core is larger than that of uniform spheroid. This is as we mentioned above, it is sensitive to a small change of resistivity. If we increase the resistivity contrast between host and spheroidal shell, the situation will totally change. To confirm the influence of the resistivity contrast to detect ability of a conductive core, we changed the resistivities of spheroidal shell and core to 10 ohm-m and 0.1 ohm-m, respectively. From the results (Fig. 3.12), we can not see any indication of existence of the core, due to concentration of current near the surface of the spheroid.

Figure 3.13 (a,b) depicts two models: for model (a) the left borehole moved to $X_m = -200$ m and the right borehole moved to $X_n = 135$ m, with the result only the right borehole passes the spheroidal shell; and for model (b) the spheroid in Figure 3.9 has moved toward right side, the centre of spheroid is at $X_c = 180$ m and most of the spheroid is to the right of the two boreholes. The separation of two boreholes is still 100 as in Figure 3.9, and the right borehole crosses the spheroid shell. From the results (Figs. 3.14 and 3.15), we see that when the spheroid is moved toward to one side of two boreholes, the amplitude of responses decrease, then it becomes more difficult to see the conductive core. We have also noticed that the polarities of responses were reversed in these two figures. We will talk about this phenomenon in the next section. If we move the spheroid further, as far as to one side of two boreholes (Fig. 3.16), the amplitude becomes much smaller, we can not see the existence of a conductive core.

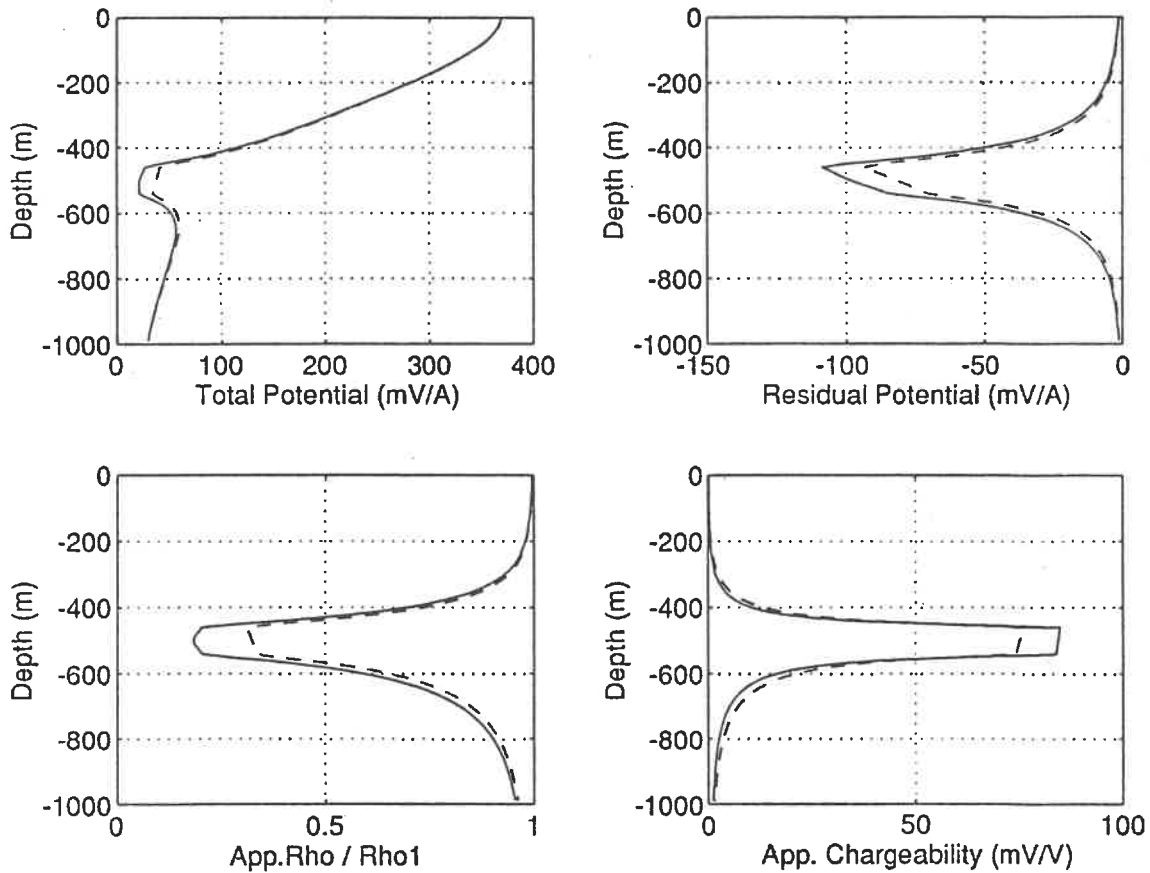


Figure 3.11: Comparison of the results of NEWROID for a spheroid with a core and a simple spheroid for the model (b) in Fig. 3.9. Solid line represents responses of spheroid with a core; and dashed line represents that of spheroid without a core.

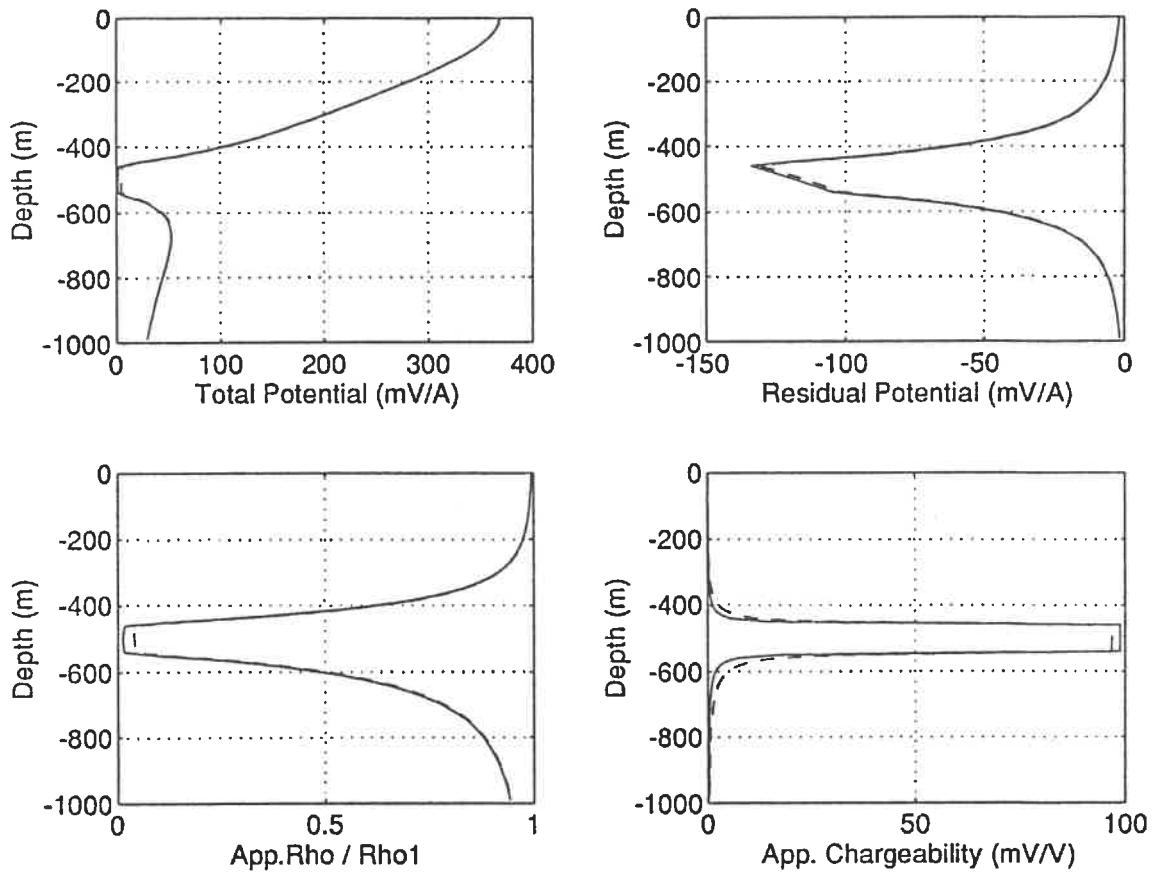


Figure 3.12: Comparison of the results of NEWROID for a spheroid with a core and a simple spheroid for the model (b) in Fig. 3.9. Resistivities for the spheroidal shell and core are changed to 10 ohm-m and 0.1 ohm-m. Solid line represents responses of spheroid with a core; and dashed line represents that of spheroid without a core. Figure

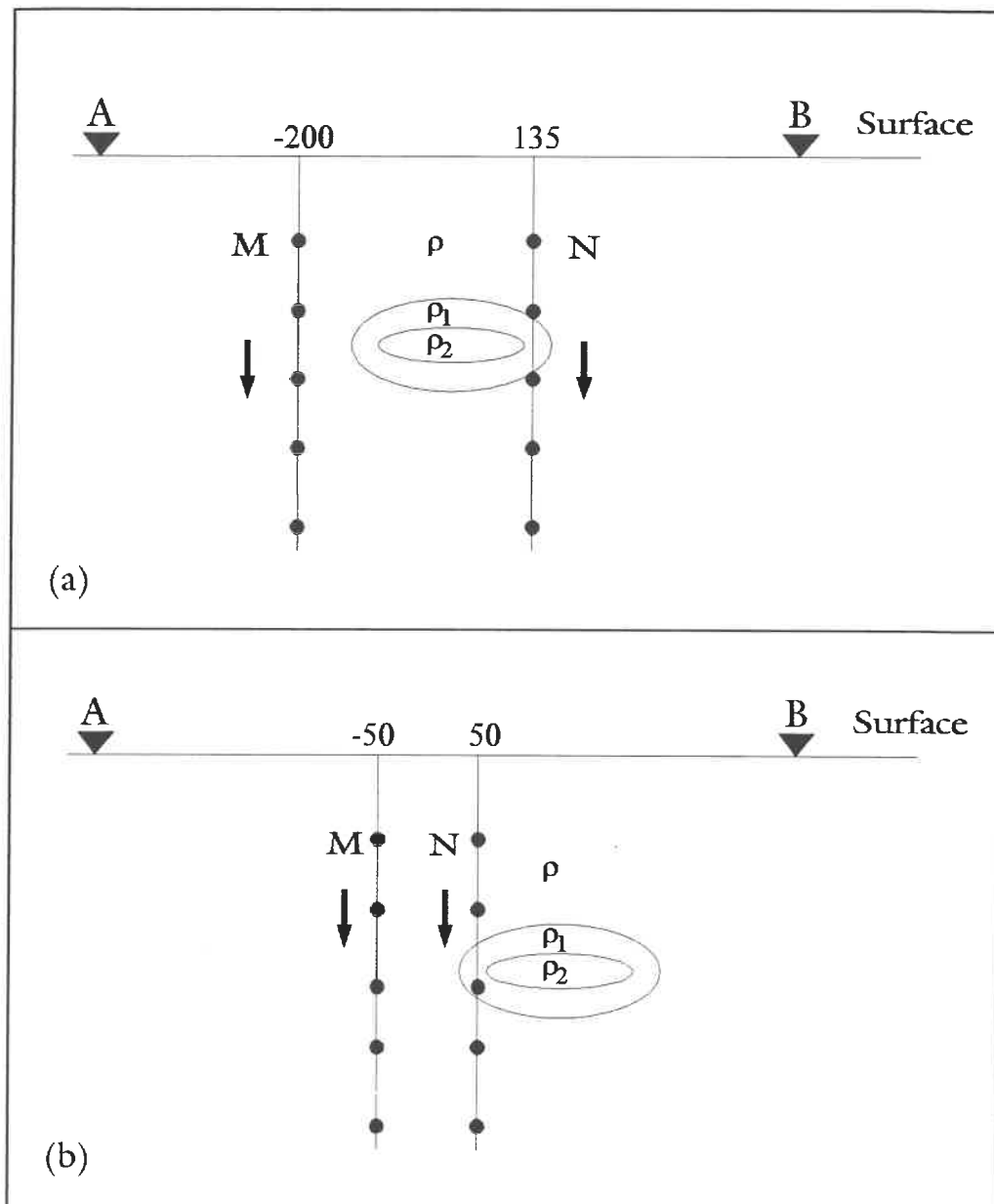
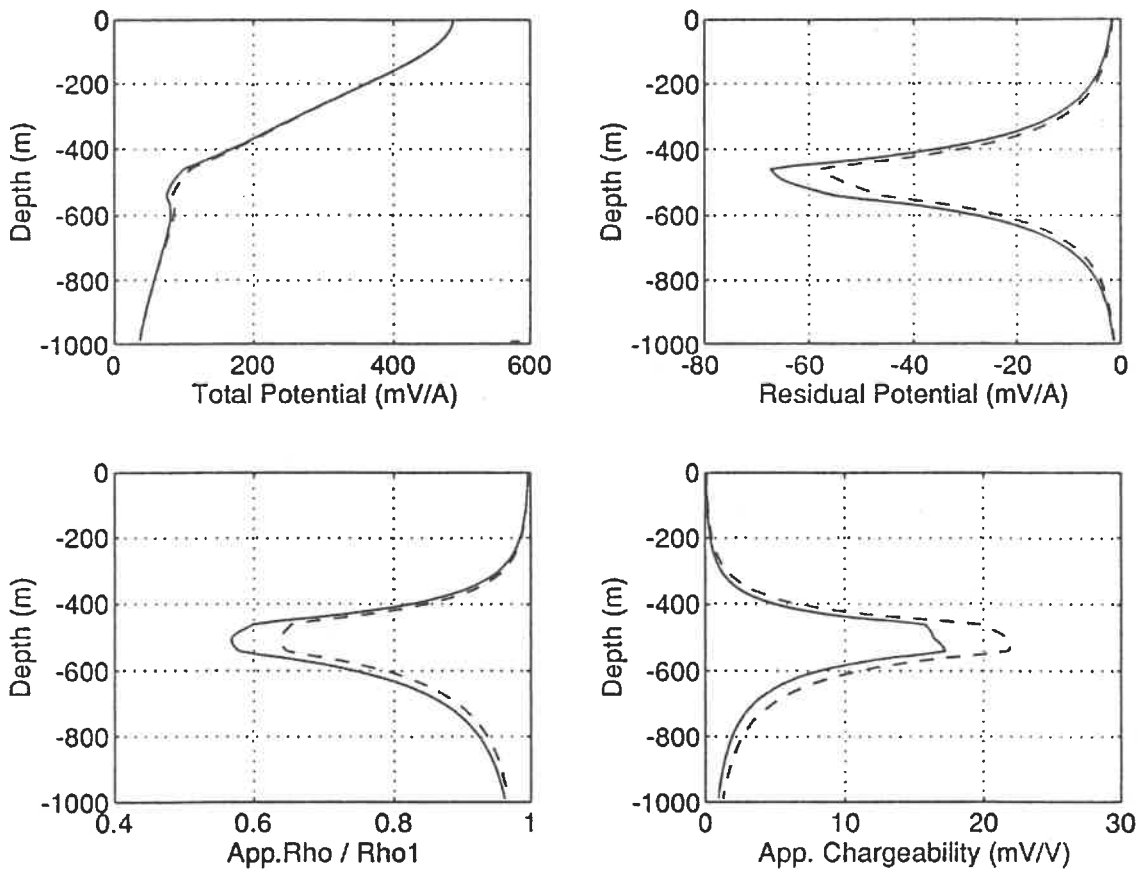
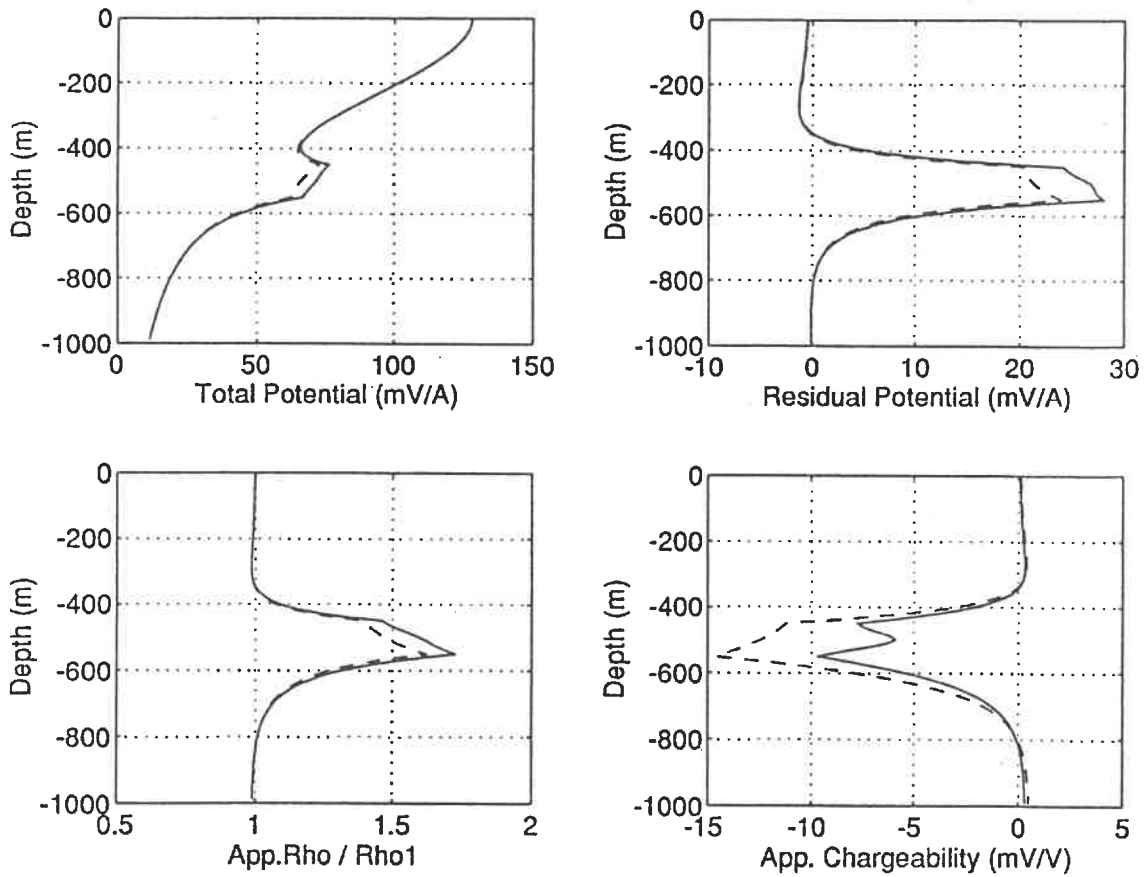


Figure 3.13: The same spheroid with a core, as in Fig. 3.9, (a) the right borehole passed spheroidal shell; (b) spheroid displaced horizontally, $X_c=180$ m, and two boreholes are 270 m apart.



3.14: Comparison of the results of NEWROID for a spheroid with a core and a simple spheroid for the model (a) in Fig. 3.13. Solid line represents responses of spheroid with a core; and dashed line represents that of spheroid without a core.



3.15: Comparison of the results of NEWROID for a spheroid with a core and a simple spheroid for the model (b) in Fig. 3.13. Solid line represents responses of spheroid with a core; and dashed line represents that of spheroid without a core.

From this study, we have seen that the detectability of a conductive core depends on two factors: one is the resistivity contrast between the host and the homogeneous environment, the other is the position of receiver electrodes. If the resistivity contrast is not very large ($\rho/\rho_1 < 10$) and two boreholes traverse the spheroidal shell, it is quite possible to detect a conductive core from an homogenous environment. Even though these conditions are restrictive, this conclusion is still useful in some surveys.

3.6 Change of Polarity of Responses

From Figures 3.10 - 3.12, 3.14, 3.15 and 3.17 in the last section, we have seen when the spheroid is moved horizontally, the polarities of the responses are changed. When the spheroid is between two boreholes, the residual potential and apparent resistivity are negative, and the apparent chargeability is positive; when most of the spheroid or all spheroid is to one side of two boreholes (Fig. 3.13 b and Fig. 3.16), the polarities of responses are reversed. In this section we will explain this phenomenon in terms of the distribution of induced charge at surface of the spheroid.

From Figure 3.18 (a,b,c), we can see, under the effect of electrical field between A and B, there are negative and positive induced charges occurred at surface of a conductive sphere (Ma, 1993). The residual potential depends on the secondary electrical field caused by these induced surface charges. When the sphere is between two boreholes

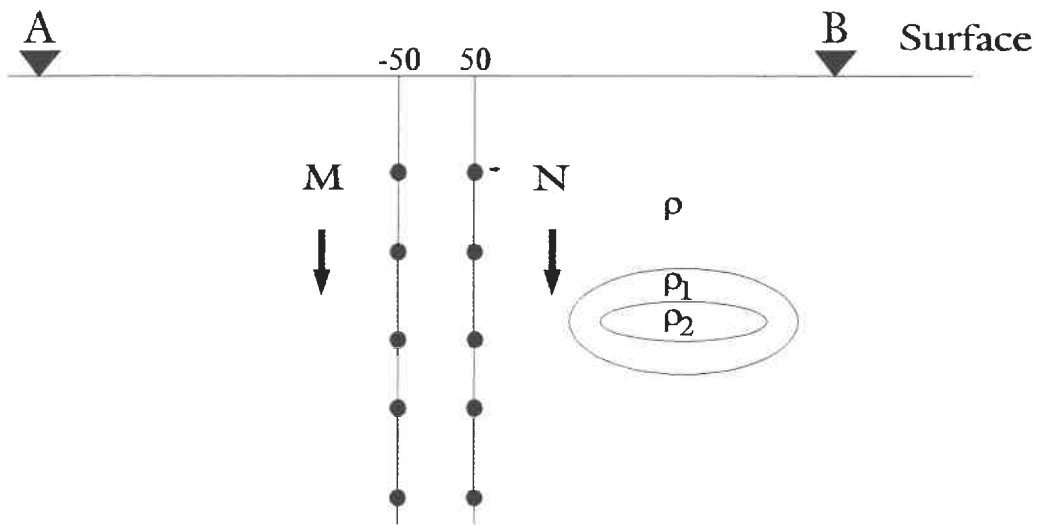


Figure 3.16: The same spheroid with a core, as in Fig. 3.9, displaced horizontally; the center of spheroid is $X_c=250$ m, and two boreholes are 100 m apart.

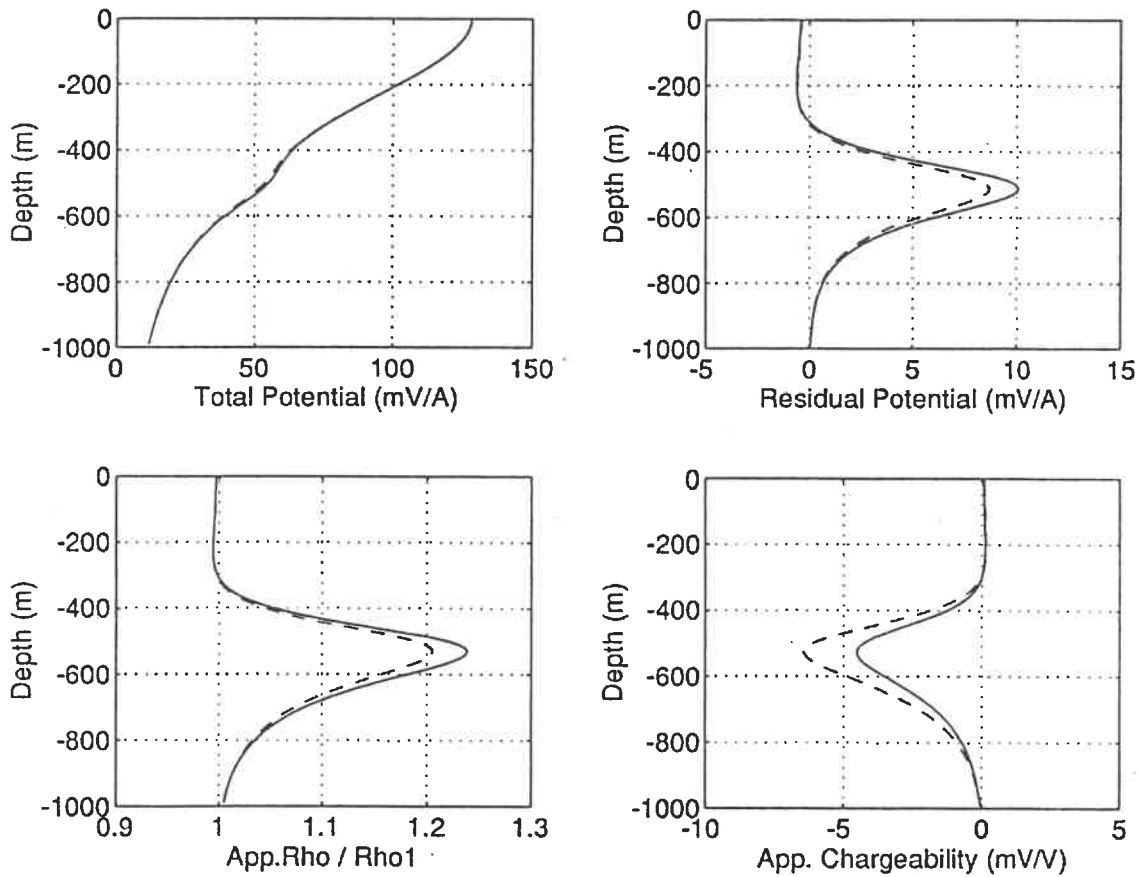


Figure 3.17: Comparison of the results of NEWROID for a spheroid with a core and a simple spheroid for the model in Fig. 3.16, Solid line represents responses of spheroid with a core; and dashed line represents that of spheroid without a core.

(Fig. 3.18 a), the secondary potential at point M is always negative, because it is close to the negative charges which build up on the left side of the sphere; the secondary potential at point N is always positive due to its proximity to the positive charges. So the difference between M and N is negative. When the sphere is to the left or right of both boreholes (Fig. 3.18 b,c), the difference between the secondary voltages M and N is always positive.

To understand the polarity of the IP response (or peak secondary voltage), we know that IP effect makes the resistivity of the sphere increase (Seigel, 1959). This leads to a reduction of the number of induced charges at the surface of the sphere. Due to the proportional relation between potential and induced charge, when the sphere is between two boreholes, we have

$$| V_m(p) | < | V_m | \quad \text{and} \quad | V_n(p) | < | V_n |$$

where $V_m(p)$ and $V_n(p)$ are peak secondary potentials at point M and N with IP effect; V_m and V_n are peak secondary potentials at M and N without IP effect. Because $V_m(p)$ and V_m are negative, and $V_n(p)$ and V_n are positive, we have

$$[V_m(p) - V_n(p)] > [V_m - V_n] \quad .$$

Recalling the definition of V_s in equation (9), this is why the polarity of apparent chargeability (or peak secondary voltage) is positive in Figures 3.10 - 3.12. When the sphere is to one side or the other of the boreholes, the secondary electrical field with IP

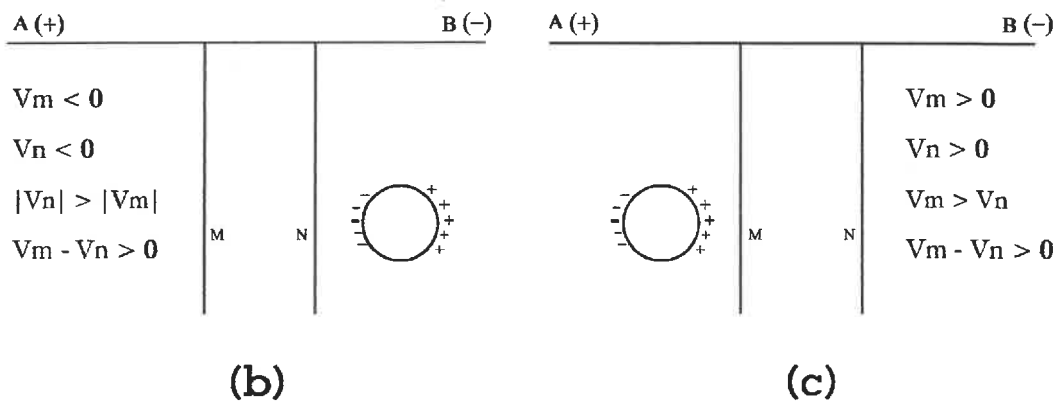
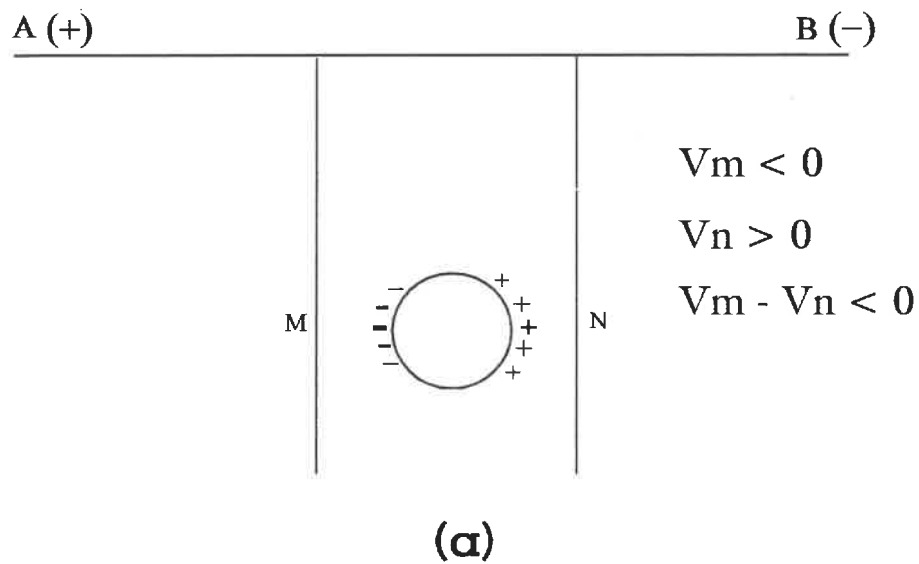


Figure 3.18: Distribution of induced charges at surface of a conductive sphere when the sphere is in the electric field caused by current sources A and B; (a) the sphere is between two boreholes; (b) and (c) the sphere is out of two boreholes.

effect is weaker than that without IP effect, given the lower charge density. Hence

$$[V_m(p) - V_n(p)] < [V_m - V_n] ,$$

and the polarity of V_s is negative.

Similar analysis of charge distribution can be used to explain why we can not distinguish a body with a conductive core from homogeneous body if the resistivity contrast between the host and the environment is large. For the case of a stratified sphere, the distribution of induced charge at surfaces of the shell and the core is illustrated schematically in Figure 3.19. Due to the distortion of the current, the larger the resistivity contrast between the host and the shell, the fewer the number of induced charges at the surface of the core (for a given geometry). For example, in Figure 3.12, there is nearly no difference in the residual potential between a spheroid with a core and that without a core. This is because the resistivity contrast between the host and the spheroidal shell is very large ($=100$), the current can not penetrate the shell to reach the core, so there are very few charges induced at the surface of the core; then the potentials at M and N depend mainly on the induced charges at the surface of the shell as the case of a uniform spheroid. For the apparent chargeability, due to the large resistivity contrast, the change of the resistivity of the core with IP effect has very little influence to the number of induced charges at surface of the core, therefore the difference between the potential with IP effect and that without IP effect is very small too, as shown in the figure.

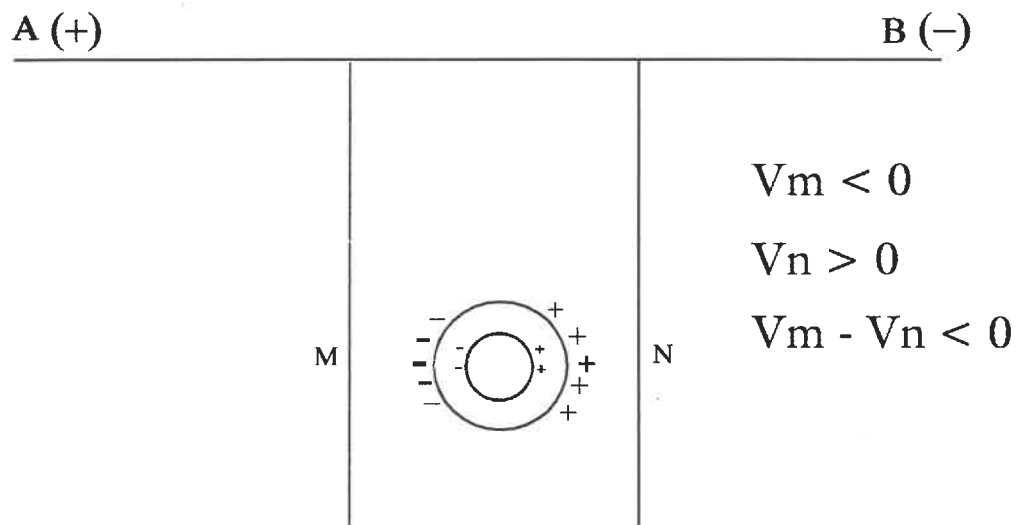


Figure 3.19: Distribution of induced charges at surfaces of the shell and the core when the stratified sphere is in the electric field caused by the sources A and B.

When there is a resistive spheroid in between two boreholes, that is, the resistivity of spheroid is larger than that of the host (Fig. 3.20), its responses are shown in Figure 3.21. From the polarities of residual potential and apparent resistivity, it is easy to confuse with the case of a conductive spheroid being to one side of two boreholes (see Fig. 3.17). However, we can distinguish these two cases with the polarity of apparent chargeability. This is because when a resistive spheroid is in the electric field caused by current sources A and B, the distribution of induced charge at the surface of spheroid is opposite with that of a conductive spheroid (Fig. 3.22). With IP effect, the number of induced charges at surface of spheroid is increased, so the polarity of apparent chargeability is positive.

From these discussion, we see that the polarity of responses is related to the distribution of induced charge, and the positions of current and voltage electrode. Therefore, according to the polarity of responses, we can deduce the position of sphere (or spheroid), because the position of receiver is known. However, from the discussion above we have already seen that when the body is to one side or other of both boreholes (Fig. 3.19 b,c), the polarities of responses are the same. This means in this situation if we want to locate exactly the horizontal position of an orebody, we have to have other information, e.g. surface geophysical data, or geological information. In spite of this limitation, the polarity of responses can still bring us some useful information about the position and general dimension of an orebody in reality.

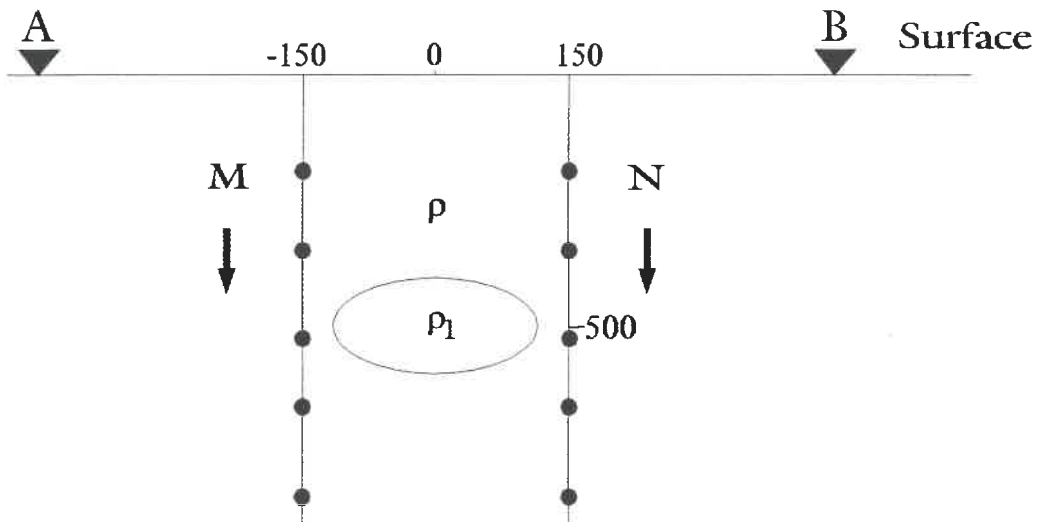


Figure 3.20: A resistive spheroid is between two boreholes, which are 300 m apart; resistivities of the host and the spheroid are 100 and 1,000 ohm-m, respectively. The semi-axes of the spheroid are 100 and 50 m, and chargeability of the spheroid is 100 mV/V. The distance between current sources A and B is 1,000 m.

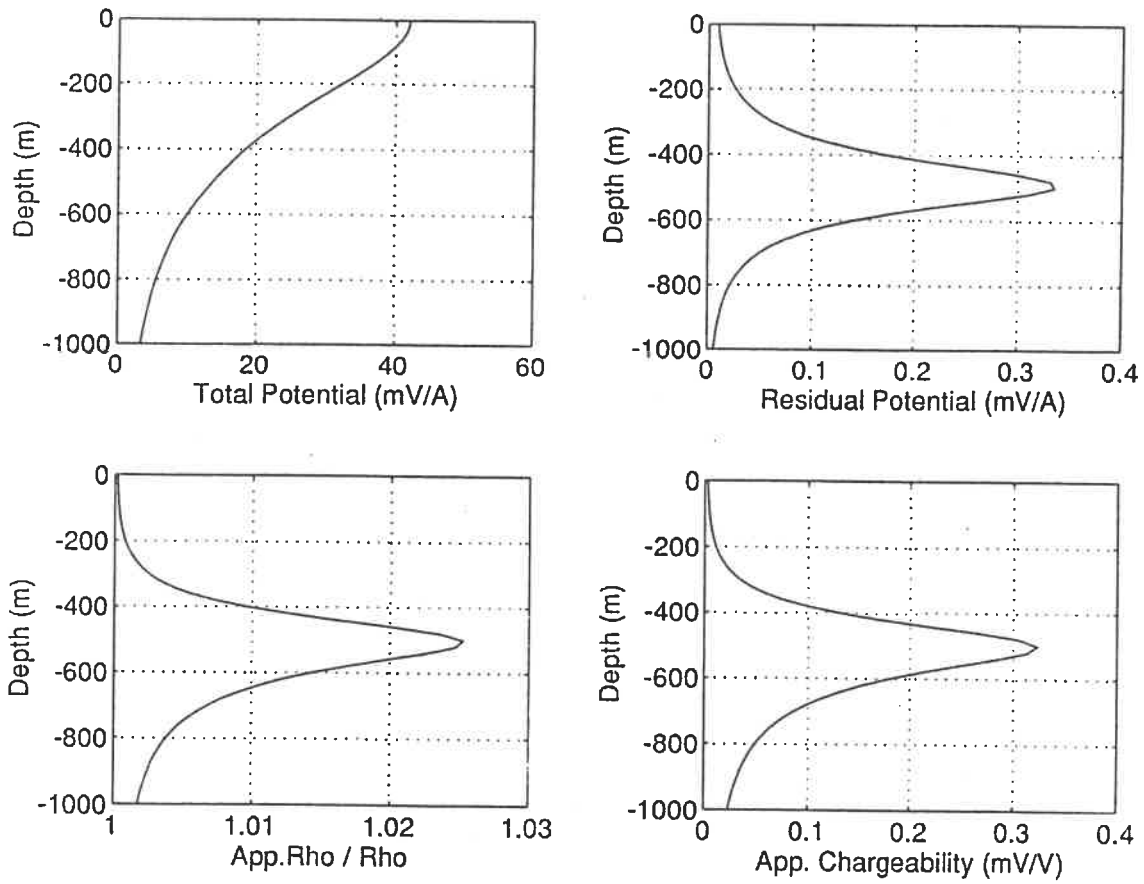


Figure 3.21: Results of NEWROID for a resistive spheroid in the model of Fig. 3.20.

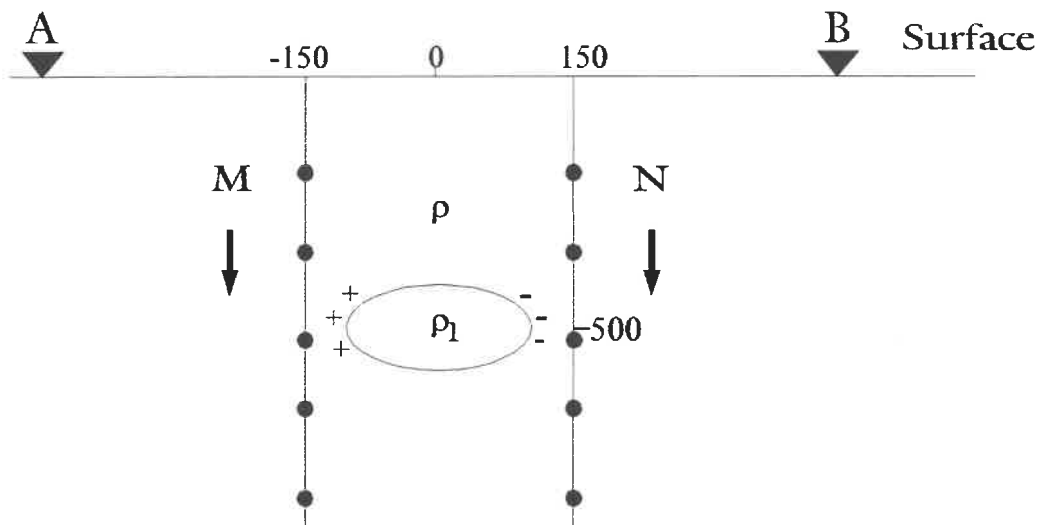


Figure 3.22: Distribution of induced charge on the surface of the resistive spheroid. All the parameters are the same as Figure 3.20.

3.7 Conclusion

From our modelling study, we see that the responses of spheroid model with modified Schlumberger configuration (surface to hole) has some characteristics, which aid interpretation.

According to the position of the peak of amplitude for the responses, we can easily find the depth of the centre of the anomalous body. From the form of responses (symmetric or assymmetric), we know that the spheroid is horizontal or inclined.

From the polarity of the responses, we will have immediately a preliminary idea where the anomalous body probably occurs (between or to one side of the holes).

Unfortunately, to distinguish a conductive core from a homogeneous conductive body, is not easy due to the concentration of the current near the exterior surface of the body if the resistivity contrast between the host and the homogenous environment is large. However, if the position of voltage electrodes are located in the surrounding of the core, and the resistivity contrast is not too large, it is still possible to detect a conductive core enclosed within a less conductive "halo".





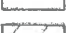
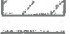


CHAPTER 4
INTERPRETATION OF VICTOR BOREHOLE
DC RESISTIVITY AND IP DATA

4.1 General Geology of The Victor Area

The Sudbury Structure is considered by many geologists to be a highly eroded and modified impact crater, which is at the "junction" of three major geological subdivisions of the Canadian Shield: these are the Superior, Southern, and Grenville Provinces. All bedrock in the area is Precambrian in age (Pye, 1984).








The Sudbury Igneous Complex has an elliptical outline, is approximately 60 km long and 25 km wide, and has the shape of an asymmetric funnel (Fig. 4.1). The ore deposits of the Sudbury area are found in the Sublayer, the Footwall, and the Footwall Breccia along the lower contact of the Sudbury Igneous Complex and in the so-called offsets (Pye, 1984).

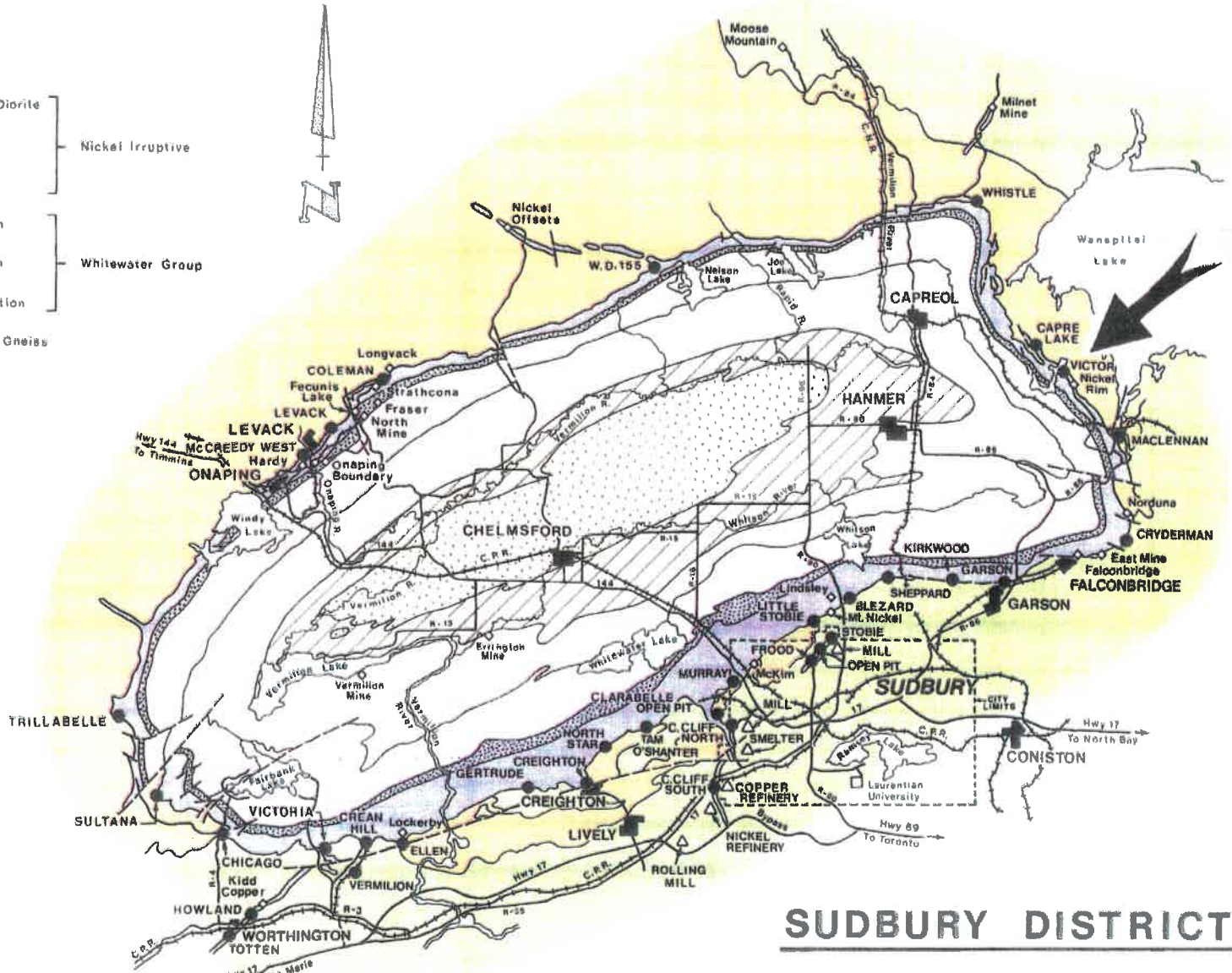
Victor area is located at the north-eastern end of the Sudbury Basin (Fig. 4.1). The structural history of the East Range is complex and there are many steep, north-striking faults with major strike-slip displacements. The surface contact of this area is marked with numerous sublayer and Footwall Breccia-related gossans. The footwall rocks

-  Norite and Quartz Diorite
-  Quartz Gabbro
-  Micropegmatite
-  Onaping Formation
-  Onwatin Formation
-  Chelmsford Formation
-  Granite and Granite Gneiss
-  Greenstones and Sedimentary Rocks

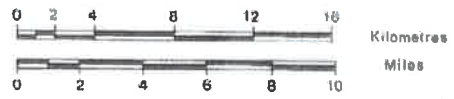
Nickel Intrusive

Whitewater Group

-  INCO Properties
-  INCO Reduction Plants
-  Mines of other Companies
-  Faulting
-  Highways
-  Regional Roads
-  Railways



SUDBURY DISTRICT



INCO LIMITED

June 1987

Figure 4.1: Map of Sudbury district.

are generally granitoid in nature, with common basic xenoliths along with some larger gabbroic dykes and sills. Sudbury Breccia is common throughout these rocks (Morrison, Jago and Little, 1994).

The Victor mineralisation is massive nickel-copper sulphide. There are two separate deposits (Fig. 4.2): a contact sulphide body in the north is located between 1,524 to 1,676 m (5,000 to 5,500 ft) below surface and a "deep footwall" deposit is indicated 2,133 to 2,682 m (7,000 to 8,800 ft) below surface.

The contact sulphide body (Main Lode) in the north contains a minimum of 7.9 million tons of 0.50% copper and 2.17% nickel. This deposit is associated with the base of "terrace" structure which is part of a larger "trough" structure with which much of the Victor environment is associated (Morrison, Jago and Little, 1994). This orebody is hosted in meta-breccia between the Sublayer Norite and the Footwall Gneisses. The mineralization is overlain by basic footwall lithologies as well as hybrid contact zone rocks (mafic norite, Sublayer Norite, and Footwall Breccia). Below the mineralization lies the footwall granitoid complex containing variable amounts of Sudbury Breccia.

This contact mineralization is disseminated to massive with a Cu/Ni ratio ranging from 0.25 to 0.50. Predominant sulphide minerals include pyrrhotite, chalcopyrite, pentlandite and pyrite.

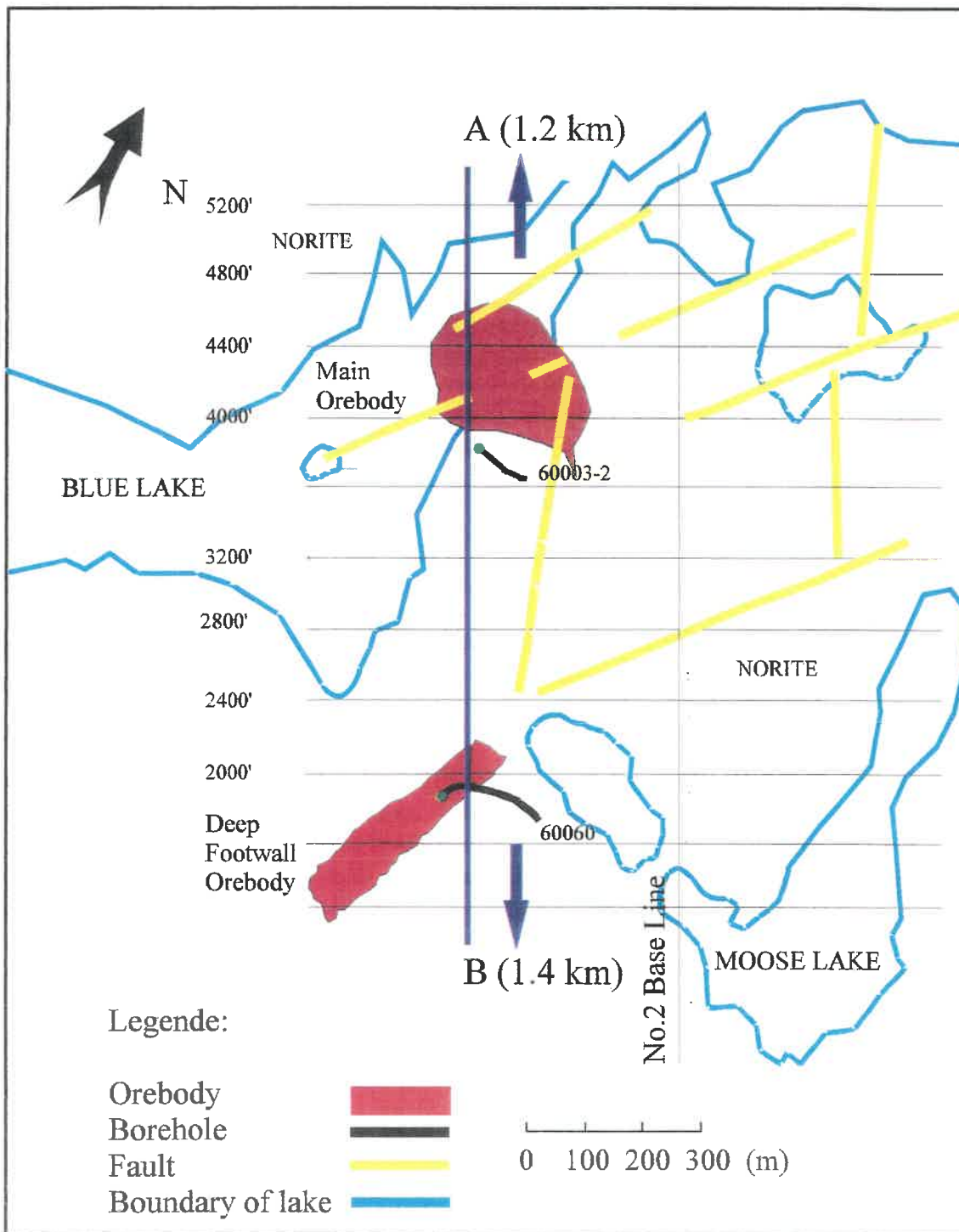


Figure 4.2: Orebody and borehole location plan, Victor, Sudbury, East Range.

The Victor "deep footwall" deposit is located about 488 m (1,600 ft) south of the Main Lode and has been described by Morrison, Jago and Little (1994). The mineralization occurs at depths of 2,133 to 2,682 m (7,000 to 8,800 ft) below surface and consists of two zones (South Lode and Footwall Lode) containing stringers and veins of massive sulphide: a major chalcopyrite-pentlandite zone underlain by a less extensive bornite-millerite zone. The South Lode lies on the contact between the Sublayer Norite and the Footwall Gneisses. The Footwall Lode is, as the name suggests, hosted within the Footwall Gneisses, and its morphology is structurally controlled. Insufficient data exist for a resource calculation. However, borehole intersections through the major zone range in width from 32 to 77 m (103.9 to 253.4 ft) with copper grades from 4.37% to 7.37% and nickel grades from 1.49% to 2.61%. Significant quantities of Platinum (Pt), Palladium (Pd), Gold (Au) and Silver (Ag) are found in the two zones. Host for the mineralization is variably metamorphosed Sudbury Breccia. Footwall rocks above and below the zones are metamorphosed granitoids.

4.2 Data Acquisition

Time-domain borehole IP and resistivity surveys were carried out annually in Sudbury by Inco Limited during the late 1970s and early 1980s (Krause, 1986). The aim of this kind of survey was to confirm the geologist's interpretation, detect blind targets or provide new ideas about the likely extent of intersected mineralization.

The Victor borehole resistivity and IP survey was carried out in 1978. Inco measured resistivity and IP data in drilled holes in the gap between the Victor Main and South Lodes. The configuration used in the survey was the modified Schlumberger array. Two current sources were located at the surface, on the NW ore trend, about 4 km apart; the two receiver electrodes were located in holes 60003-2 and 60060 (Fig. 4.2). The distance between these two holes is about 600 m. The resistivity and IP data were measured by fixing one receiver electrode in hole 60060 at a depth of 1,731 m (5,680 ft) and moving another electrode in hole 60003-2 between depths of 915 to 1,890 m (3,000 and 6,200 ft), as shown in Figure 4.3. Station spacing was 61 m above 1219 m (200 ft above 4,000 ft) and 15 m between 1,219 to 1,890 m (50 ft between 4,000 and 6,200 ft) down-hole.

All the data were recorded with a Hunttec M-3 time domain IP receiver, which measures the amplitude of the decay voltage at four preselected times after current shut-off. For the Victor data in question the voltage windows were centred at 505, 580, 730, and 1,030 ms (Fig. 4.4). The period of the transmitter waveform was 8 s and duty ratio (on/off ratio) was 1.0.

4.3 Data Reduction

The decay curve amplitudes are automatically normalized with respect to the

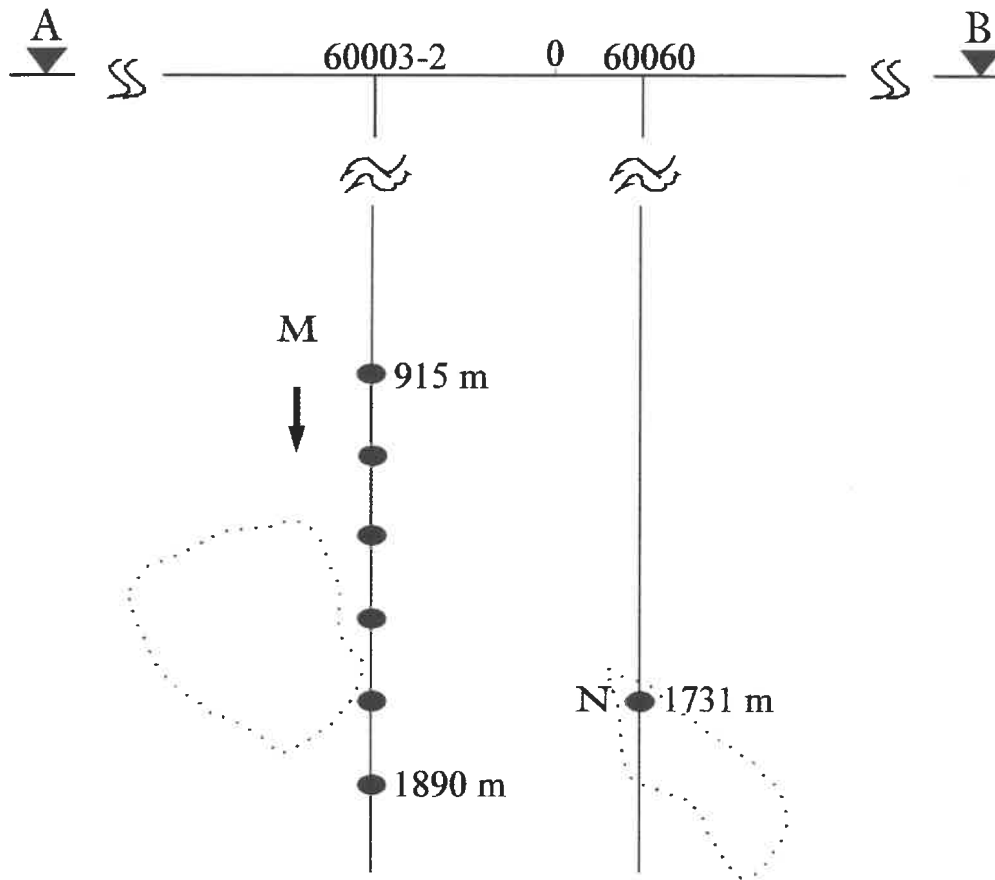


Figure 4.3: A simplified grid N-S sectional view of the Victor survey; the distance between A and B is about 4 km; the distance between two boreholes is about 600 m. The dotted lines delineate the projection of the orebodies.

reading V_p , the primary voltage immediately prior to current shut-off (Fig. 4.4). Thus the four readings of the receiver can be regarded as "instantaneous chargeability" defined as:

$$M_n = \frac{V_n}{V_p}, \quad n=1, 2, 3, 4 \quad (14)$$

where V_1, V_2, V_3 and V_4 are average voltage values over the four sampling windows, as shown in Figure 4.4 (a). The apparent chargeability computed by the modelling program is given by

$$M_a = \frac{V_s}{V_p}, \quad (15)$$

where V_s is the peak secondary voltage, i.e. the voltage at time $t = 0+$, as shown in Figure 4.4 (b).

The decay voltage should consist of two parts: a transient EM component, and a polarization (IP) component. The rate of decay of EM coupling effects is normally much faster than that of IP effect, so if we chose the first sample time late enough after the current is shut-off ($t_d=480$ msec) we can usually assume our readings on the decay curve are IP voltages. However, conditions at Sudbury are not "normal", and in particular the Victor orebodies are extremely conductive. The assumption of negligible

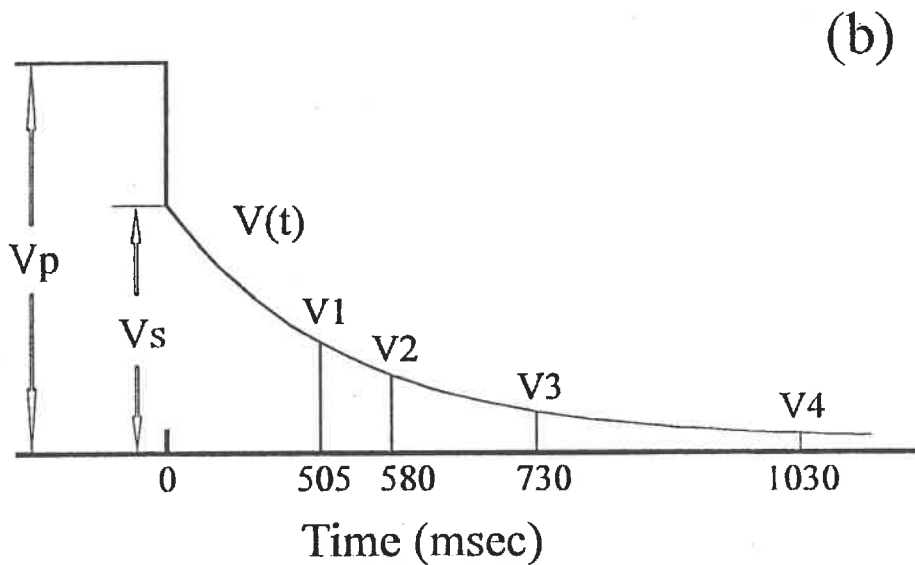
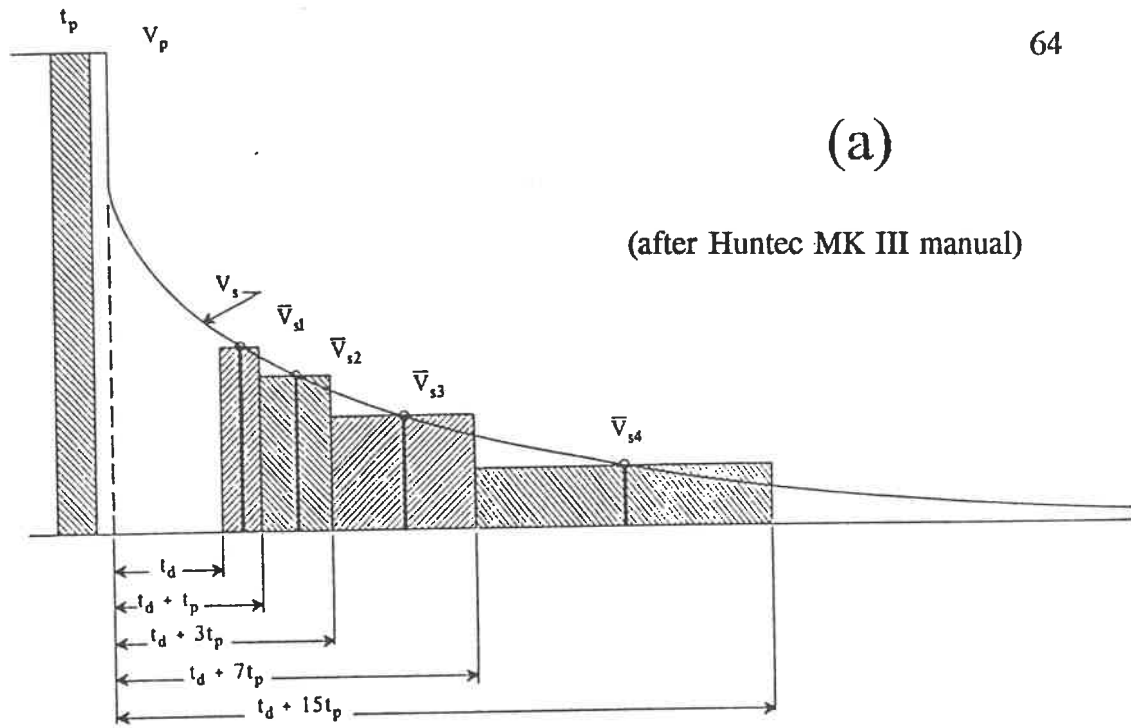


Figure 4.4: Illustration of the signal which is measured by the M-3 receiver. (a) the receiver parameters t_d delay time and t_p integration time define completely the measurements M_1 , M_2 , M_3 and M_4 ; (b) in Victor survey, $t_d = 480$ msec and $t_p = 50$ msec.

EM coupling will be further justified after presentation of the DC resistivity modelling result.

It is necessary to determine the apparent chargeability from the four measurements $\{ M_n \}$. Assuming an exponential IP decay (Sumner, 1976), we may write the decay curve in the form

$$M(t) = Ae^{-Bt} . \quad (16)$$

where A is apparent chargeability which we want to calculate, and B is the decay rate.

For the readings M_1, M_2, M_3 and M_4 on the decay curve, we have

$$M_i = Ae^{-Bt_i}, \quad i=1, 2, 3, 4 \quad (17)$$

where t_1, t_2, t_3 and t_4 are the sample times.

To solve for A and B in equation (17), we first take the logarithm of both sides, whence

$$\ln M_i = \ln A - Bt_i \quad (18)$$

let $Y_i = \ln M_i$, $Z = \ln A$, and $W = -B$. Then substituting Y_i , Z , and W into equation

(18), we have

$$Y_i = Z + Wt_i \quad (19)$$

Now, the problem becomes a "linear regression". We will fit four data points (t_i , Y_i) to the straight-line model.

We construct a chi-square merit function:

$$\chi^2(Z, W) = \sum_{i=1}^4 (Y_i - Z - Wt_i)^2 \quad (20)$$

To determine Z and W , we have to minimize the merit function χ^2 . At its minimum, derivatives of χ^2 with respect to Z and W vanish. Therefore,

$$\begin{aligned} \frac{\partial \chi^2}{\partial Z} &= -2 \sum_{i=1}^4 (Y_i - Z - Wt_i) = 0 \\ \frac{\partial \chi^2}{\partial W} &= -2 \sum_{i=1}^4 (Y_i - Z - Wt_i) t_i = 0 \end{aligned} \quad (21)$$

A program CHAR was written to solve these two equations, in which a subroutine FIT from Numerical Recipes (Press, 1986) is used. With the program CHAR, we can easily solve equations (21) to find Z and W , and at the same time we calculate the variances in the estimates Z and W . With the variance, we can calculate a coefficient of variation; then according to this value, we can judge if the model agrees well with the data. The coefficient is defined as

$$\text{coefficient of variation} = \frac{\text{standard deviation of estimate}}{\text{estimate}} \times 100\% .$$

From this definition, we see the smaller the coefficient, the smaller the uncertainty of the estimate. The coefficient of variation for Z is shown in Figure 4.5. From the figure, we can see that there are only five points where the coefficient of variation are greater than 10%, and four of them occurred below the depth of 1,830 m (6,000 ft). So we can say that the estimate of Z is reliable. We accepted the estimates Z, then calculated apparent chargeability as

$$A = e^Z \quad (22)$$

Figure 4.6 shows the calculated apparent chargeability and the measured resistivity in Victor survey as well as sulphide occurrence and host geology in borehole 60003-2. Table 1 defines the legend for the host geology.

4.4 Resistivity and IP Modelling

Before our modelling, we were aware that several thin bands (< 3") of massive sulphide were intersected by borehole 60003-2, and we thought that they were responsible for the peaks in the apparent chargeability profile. However, we were not sure if this was entirely right or whether there was an off-hole target contribution to the

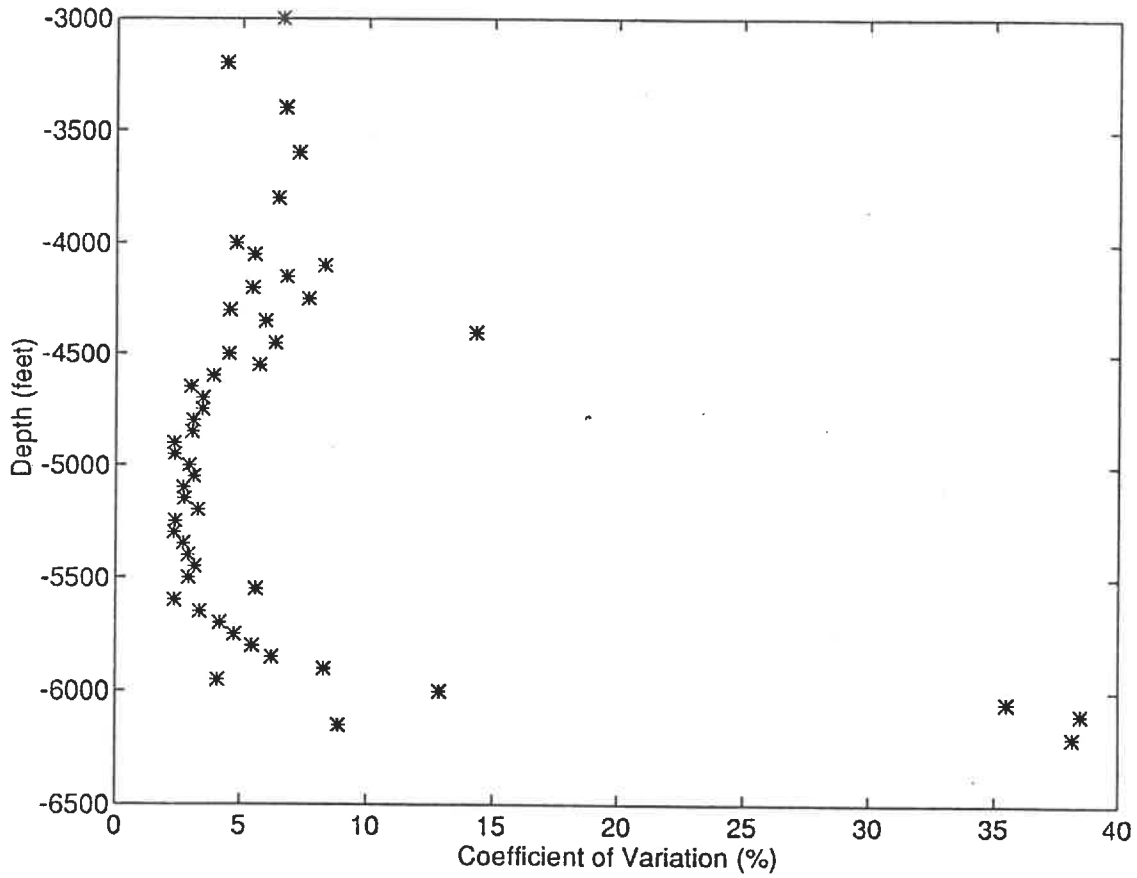


Figure 4.5: Coefficient of variation of estimate Z on 50 measured points between 3,000 and 6,200 ft in borehole 60003-2.

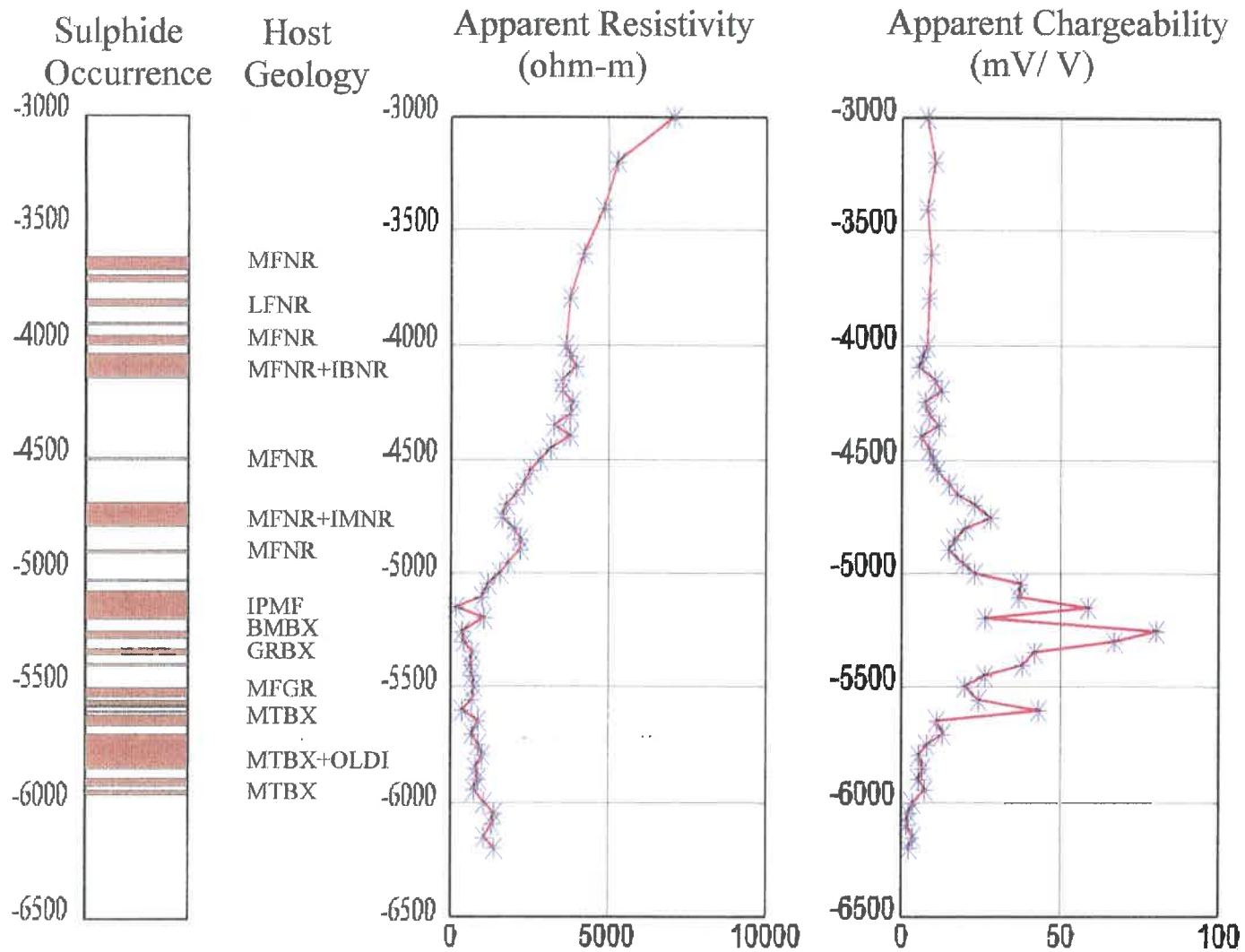


Figure 4.6: Borehole resistivity and chargeability logs, hole 60003-2, Victor. (Data per favour Inco Limited).

Table 1: Legend for the host geology in Figure 4.6.

Abbreviation	Explication
MFNR	mafic norite
LFNR	lower felsic norite
MFNR+IBNR	mafic norite+inclusion basic norite
MFNR+IMNR	mafic norite+inclusion mafic norite
IPMF	irruptive permeated mafic footwall
BMBX	basic meta-breccia
GRBX	granite breccia
MFGR	mafic gneiss
MTBX	meta-breccia
MTBX+OLDI	meta breccia + olivine diabase

IP response.

For a start, we had to construct an initial model. At first, from the position of the peak of apparent chargeability in field data (Fig. 4.6), we can suppose that the main sulphide zone should be at a depth of about 1,615 m (5,300 ft); then from the polarity of the field data, negative for apparent resistivity and positive for apparent chargeability, we assume that the main sulphide zone should be in between two boreholes (c.f. Fig. 3.10); finally, from the small values of apparent resistivity, we know that there is electrical connection between these two boreholes. Considering the fact that the typical ore target (in Sudbury) was a massive, conductive, magnetic sulphide zone with, usually, a halo of similar but disseminated sulphide (Krause, 1986), we selected NEWROID for the modelling.

4.4.1 Modelling with NEWROID program

According to the information mentioned above, and from the profile of apparent chargeability (Fig. 4.6) we see the curve is symmetric which is compatible with a spheroid, so we constructed a spheroid with a conductive core as our initial model. With NEWROID, we calculated the responses of the model. There are many parameters which can affect the responses, therefore, it is not easy to find an appropriate model. After many modifications, a final model was found, being a prolate spheroid with a conductive

core (Fig. 4.7). Its major semi-axis and minor semi-axis are 600 m and 180 m, respectively, while the major and minor semi-axes of the core are 580 m and 94 m, respectively. The spheroid lies in the mineralised trough (20° inclined downward from horizon), striking NNW-SSE (25° west of true North), and its centre is in midway between two boreholes and at a depth of 1,755 m (5,760 ft). The resistivities for the host, the shell and the core are 10,000 ohm-m, 170 ohm-m and 20 ohm-m. The host resistivity value was chosen on the basis of borehole resistivity logs made by The Geological Survey of Canada in Sudbury (Killeen et al, 1993).

The theoretical voltage profile and resistivity profile for this spheroid model replicate the overall forms of the corresponding observed curves quite well (Figs. 4.8 and 4.9). Now, we can calculate "time constant" for the model spheroid to estimate the influence of EM coupling to the observed IP readings. The formula for "time constant" of a spheroid is given by

$$\tau = \frac{\mu_0 ab\sigma}{\pi^2} \quad (23)$$

where μ_0 is permeability in air, a and b are major and minor semi-axes of the spheroid, and σ is conductivity of the spheroid. We regarded the model spheroid with a core as a uniform spheroid, with conductivity of the core ($\sigma=0.05$), to calculate the "time constant" with formula (23). Its "time constant" is about $0.68 \cdot 10^{-3}$ s much less than 0.5

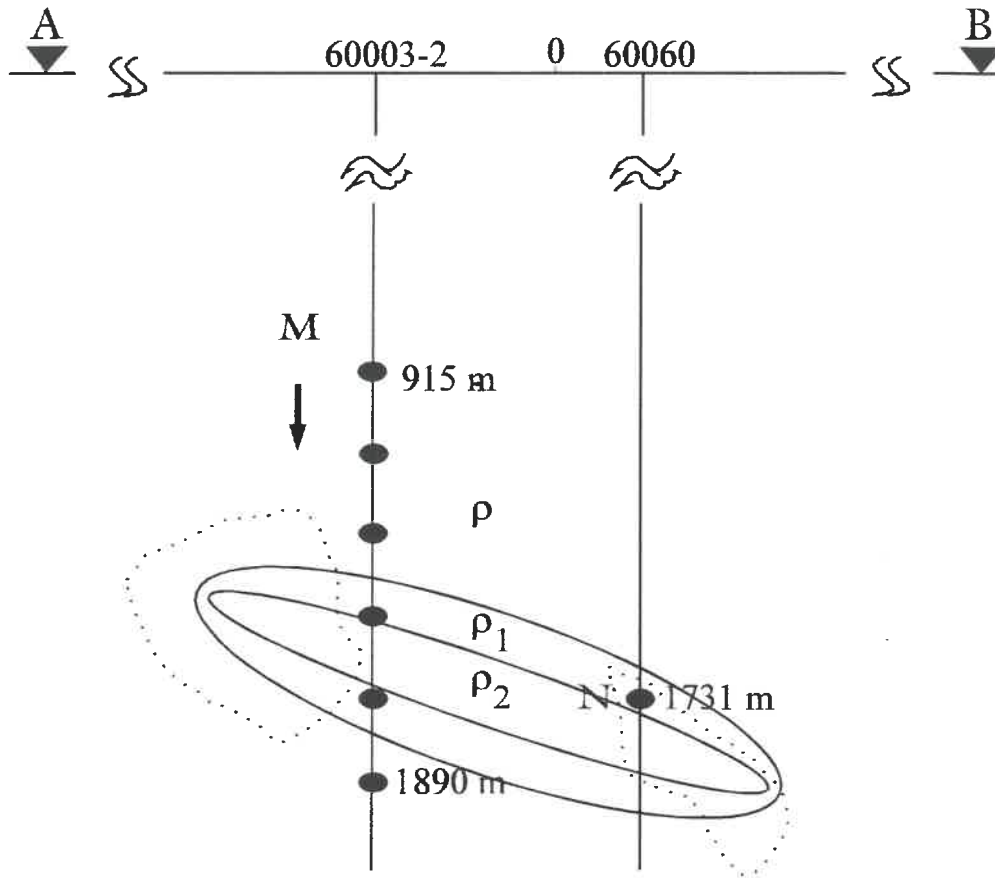


Figure 4.7: Comparison between the modelling result (a spheroid with a core) and a model constructed with Inco borehole logs; the spheroid's major and minor semi-axes are 600 m and 180 m, respectively; and major and minor semi-axes for the core are 580 m and 94 m, respectively. The resistivity for the host, the shell and the core are 10,000 ohm-m, 170 ohm-m and 20 ohm-m, respectively. The dotted lines delineate the projection of the orebodies.

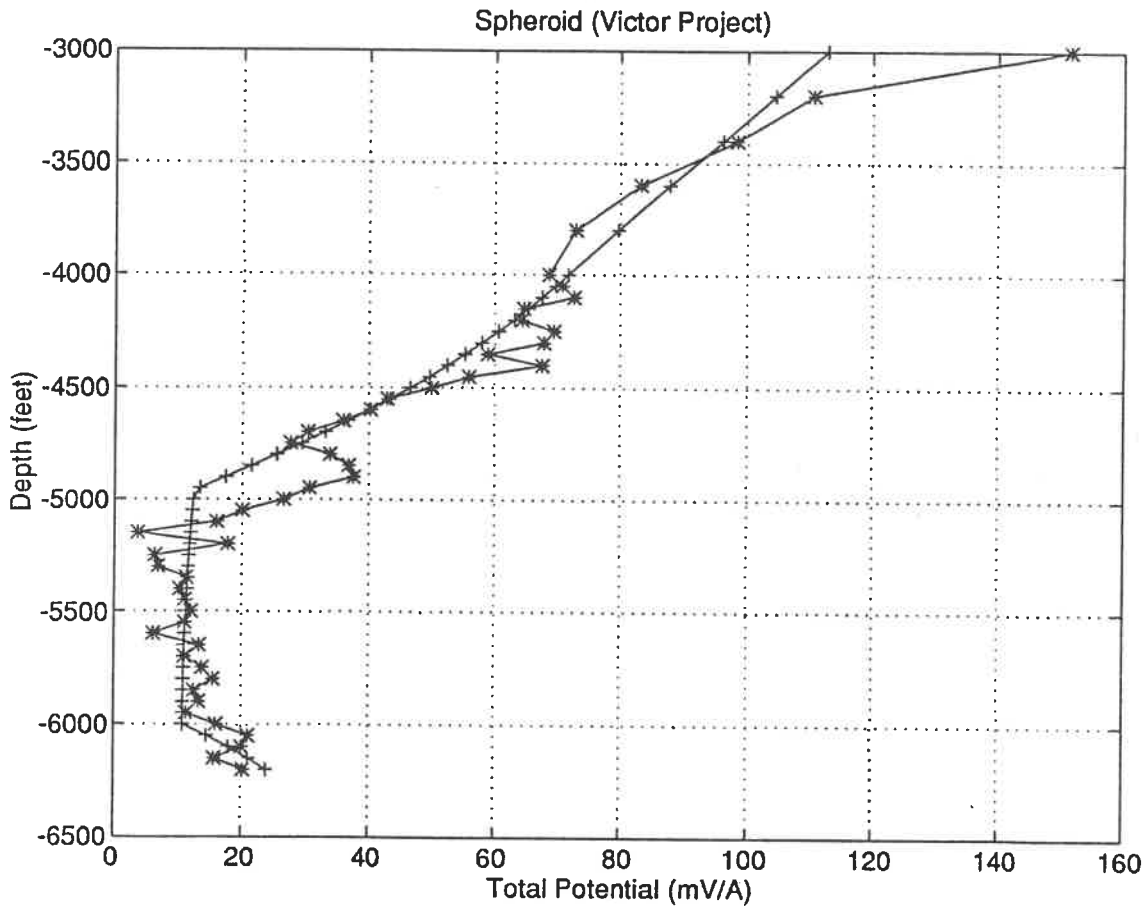


Figure 4.8: Observed (*) and calculated (+) total potential for borehole 60003-2 at Victor. Model is a prolate spheroid with a core, striking grid N-S, plunging 20°, and centred midway between two boreholes. The major and minor semi-axes for the spheroid and the core are 600 m, 180 m, 580 m and 94 m, respectively. The resistivities for the host, the shell and the core are 10,000 ohm-m, 170 ohm-m and 20 ohm-m, respectively.

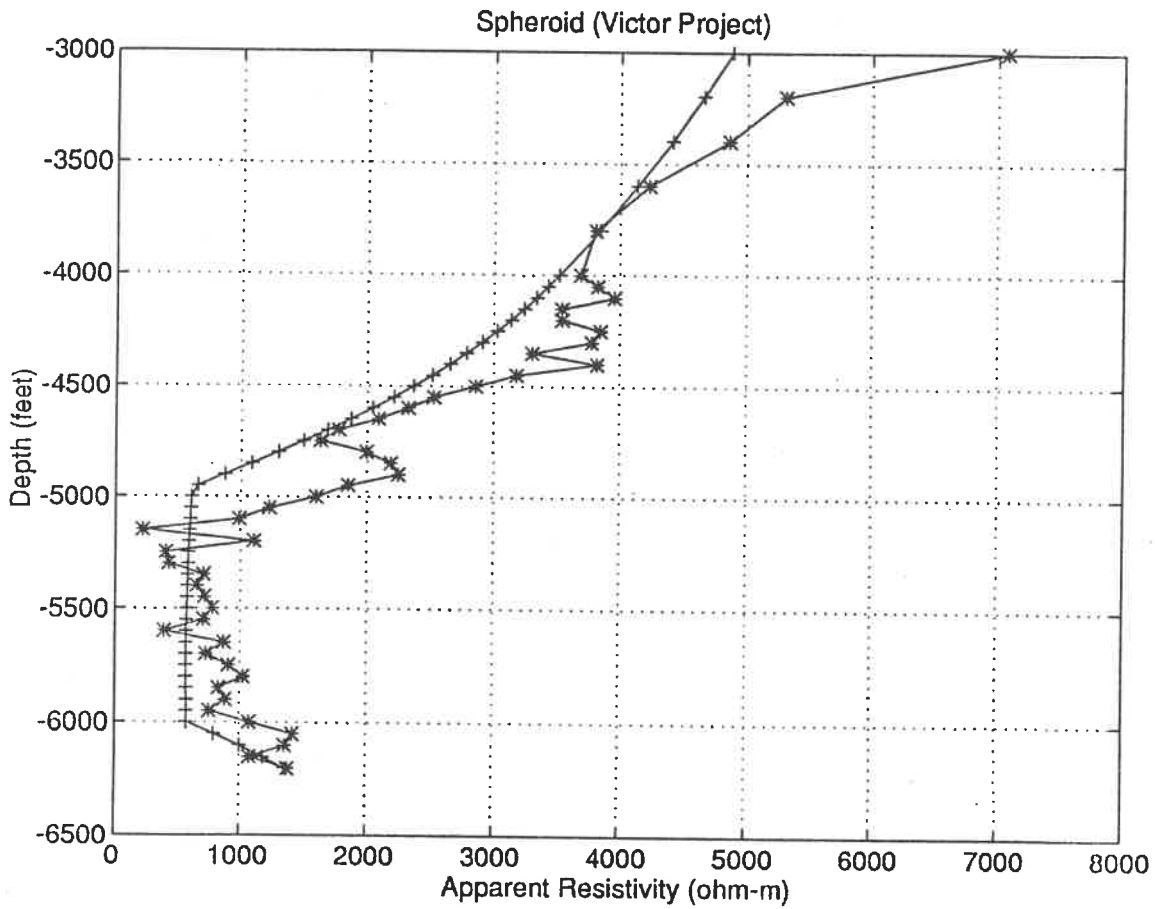


Figure 4.9: Observed (*) and calculated (+) apparent resistivity for borehole 60003-2 at Victor. Model is a prolate spheroid with a core, as per Figure 4.8.

s (500 ms), so the influence of EM coupling for observed IP readings is not important.

The theoretical chargeability, assuming the intrinsic chargeabilities for the shell and the core are 90 mV/V and 100 mV/V respectively is compared with the "observed" apparent chargeability in Figure 4.10. It is not as well fitted as the voltage and the apparent resistivity. The theoretical voltage is rather constant between 1,524 and 1,830 m (5,000 and 6,000 ft), as the measured voltage; but the "measured" apparent chargeability is variable, c.f. theoretical one rather constant. From the sulphide occurrences and host geology for borehole 60003-2 in Figure 4.6, we see that there were significant intervals with disseminated mineralization between 1,433 and 1,830 m (4,700 ft and 6,000 ft). Because the chargeability is more sensitive to these intervals with disseminated mineralization than the voltage and apparent resistivity, this is why in the borehole apparent chargeability profile is "spiky".

From this result of modelling, we see that the model of a spheroid with a core is not very appropriate for Victor area. However, we can infer that there is no evidence for a big off-hole target and that the IP response is due to the thin mineralization veins intersected by the borehole 60003-2.

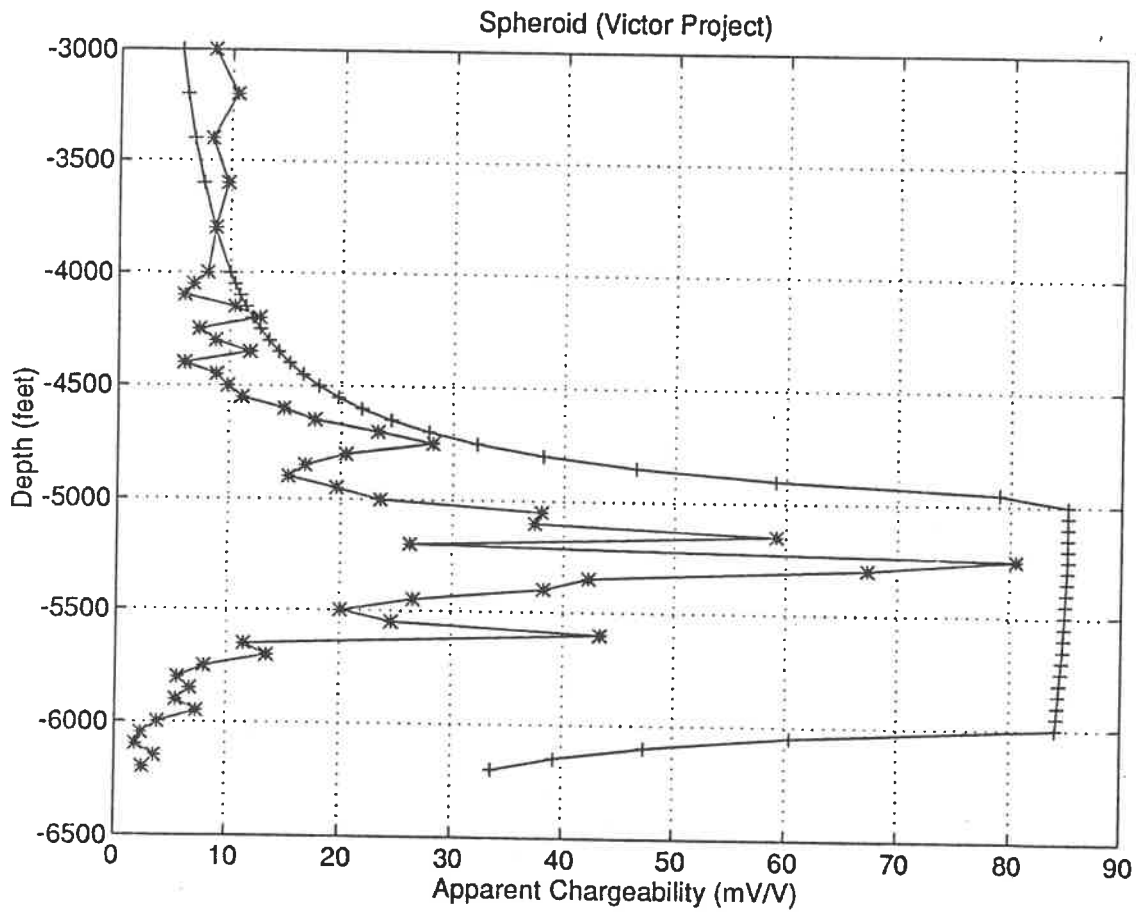


Figure 4.10: Observed (*) and calculated (+) apparent chargeability for borehole 60003-2 at Victor. Model is a prolate spheroid with a core, as per Figure 4.8; the intrinsic chargeabilities for the shell and the core are 90 mV/V and 100 mV/V, respectively.

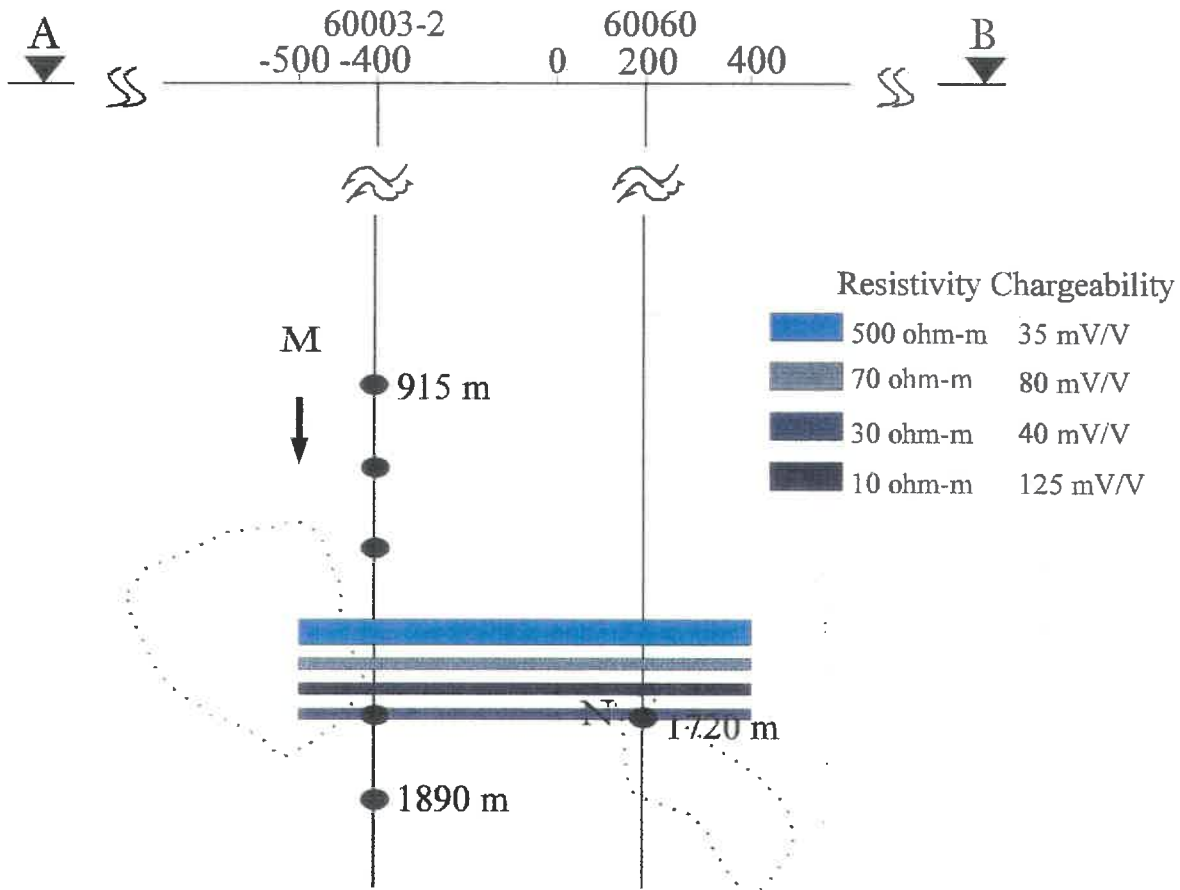


Figure 4.11: Comparison between the modelling result of U.B.C 2D program (four thin conductive layers) and a model constructed with Inco borehole logs. The thickness for four layers are 75, 20, 20 and 20 m, respectively. The dotted lines delineate the projection of the orebodies.

4.4.2 Modelling with U.B.C. 2D DCR/IP program

The University of British Columbia kindly provided us with a 2D borehole DCR/IP program. This was used to compute the response for a multi-layer model, representing zones of different resistivity intersected in hole 60003-2.

Because the responses of the model spheroid are basically corresponding to the field data, so we used the spheroid model to define a starting model with three separated thin conductive layers. By means of the U.B.C 2D DCR/IP program, after several iterations, we found a model whose responses fitted the observed data very well (Figs. 4.11). This model consists of four conductive layers. The resistivities for the four layers are 500, 70, 10 and 30 ohm-m, respectively; and considering the mineralization is different in these four layers (c.f. Table 1), we chose their intrinsic chargeabilities as 35, 80, and 125 and 40 mV/V. Their thicknesses are 75 m (277 ft), at depths from 1,425 to 1,500 m (4,675 to 4922 ft), 20 m (66 ft), from 1,560 to 1,580 m (5,118 to 5,184 ft), 20 m (66 ft), from 1,600 to 1,620 m (5,250 to 5,315 ft) and 20 m (66 ft) from 1,710 to 1,730 m (5,610 to 5,676 ft), respectively; and their horizontal dimension is 900 m (about 2950 ft). The voltage electrode N was located at depth of 1,720 m (5645 ft) in the conductive layer. The comparison between observed and calculated voltage and apparent chargeability profiles are shown in Figures 4.12 and 4.13.

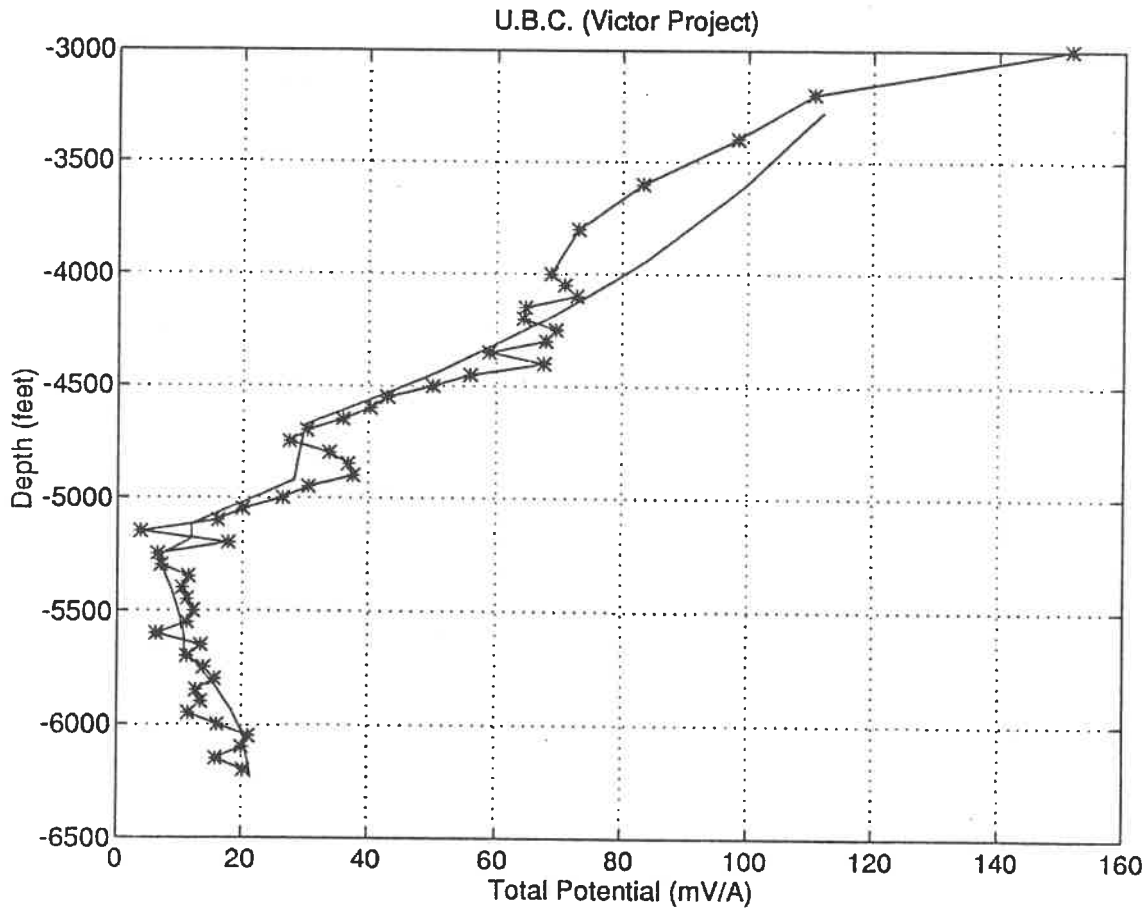


Figure 4.12: Observed (*) and calculated (- solid line) total potential for borehole 60003-2 at Victor. The model consists of four horizontal thin conductive layers. All the model parameters are shown in Figure 4.11.

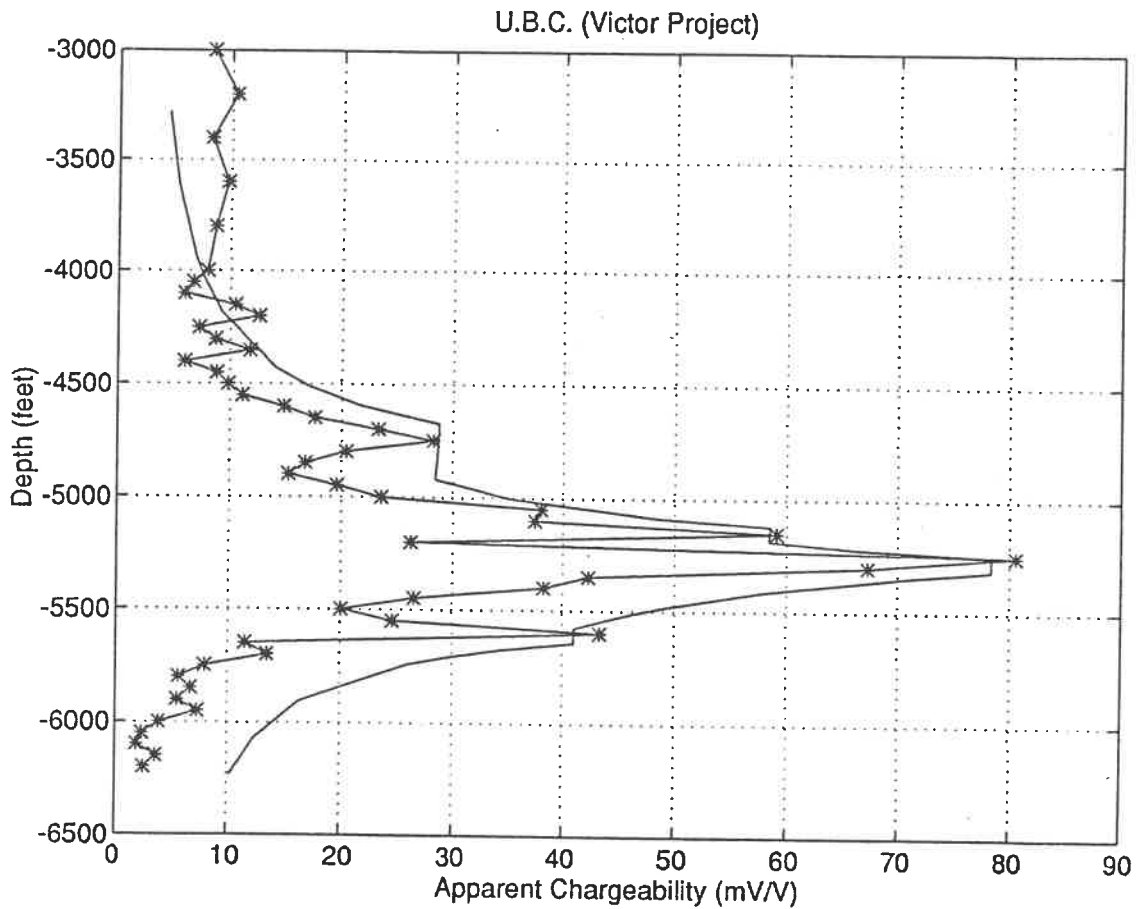


Figure 4.13: Observed (*) and calculated (- solid line) apparent chargeability for borehole 60003-2 at Victor. The model is four horizontal thin conductive layers. All the model parameters are shown in Figure 4.11.

From this model and its responses, we see that the chargeability is more sensitive to the thin layers (either conductive or resistive) than the voltage. From Figures 4.13 and 4.12 we see the zone of high chargeability is narrower than the zone of low voltage, consistent with the real data. From the total voltage profile, we can not easily distinguish the different layers, but from the chargeability profile we can. This is why IP survey is used very often in mining exploration, especially for disseminated mineralization, because it can bring us more information than the resistivity method alone.

This layered model verified our inference that the mineralized veins intersected in 60003-2 are responsible for the field data, and these veins are connected between the two boreholes.

CHAPTER 5

CONCLUSION AND RECOMMENDATION

A method of interpretation of Victor borehole resistivity and IP data was presented in this study and it consists of two main parts; the first is to construct an initial model by comparing theoretical modelling result with the field data; the second is, with the aid of program NEWROID and the U.B.C 2D DCR/IP program, to modify the initial model, until an acceptable model is found. This study illustrates the applicability of this method. We could interpret all of Inco's borehole resistivity and IP data in this manners.

With NEWROID, we found a conductive spheroid model whose response of voltage fitted well with the measured voltage, but whose apparent chargeability didn't. U.B.C 2D DCR/IP modelling program was also used in the interpretation. Both the voltage and IP data were well fitted by a model with four conductive layers separated by resistive host.

There are differences between the spheroid and layered models. The layered model replicates the IP response of the stringers much better than the spheroid model. This is because the current can flow directly into the layers, but in the spheroid model, the current can not penetrate the disseminated shell and reach the massive sulphide core.

Even though the models found by NEWROID and U.B.C 2D DCR/IP programs are different, both results indicate that the connectivity of sulphide between two boreholes is responsible for the anomaly occurred in observed data. We think, this connectivity of sulphide is stringers of sulphide which are probably connected with the Main Orebody and at least extend to the electrode N at a depth 5,680 ft in borehole 60060, or may extend continuously south as far as the Deep Footwall Body.

From the theoretical modelling study, we know that if the anomalies occurred in the observed profiles were produced by the two Victor orebodies (Fig. 4.3), the polarities of apparent resistivity and of apparent chargeability would be opposite to the observed data. From the agreement between the responses of two models and the observed data, we can say that the inference that the stringers of sulphide between the two boreholes are responsible for the anomalies is correct, and there is no evidence for another big "off-hole" target between the two boreholes.

For the detection of a massive sulphide core within a halo of disseminated mineralization, our theoretical modelling indicates that with a modified Schlumberger configuration it is difficult if the resistivity contrast between the host and the shell is large, due to the concentration of the current near the exterior surface of the shell.

Two programs DSSPHIP and NEWROID written by Fullagar (1993 a, 1993 b)

were tested and used in this study. A theoretical modelling study was undertaken with a modified Schlumberger configuration, (that is, two current source are fixed at the surface, two potential electrodes are located into two separated boreholes and moving down simultaneously). The qualitative aspects (resistivity) of anomalous body can be determined from voltage, resistivity and chargeability measurements. According to the position of the peak of the response for the modified Schlumberger configuration, we can locate the centre depth of a conductive sphere or spheroid between the boreholes. The polarity of the response can provide an indication of the horizontal position, but unfortunately, if the body is to one side of the two boreholes, we can not tell exactly on which side it is. These insights guided the choice of starting model at Victor.

In both programs DSSPHIP and NEWROID, a modified image method is used. This method is shown to be superior to the conventional image method which is found not to be appropriate for borehole resistivity measurements because it violates the Principle of Reciprocity.

We hope an inversion capability will be soon added to the program NEWROID in order to optimize the spheroid model parameters efficiently.

REFERENCES

- [1] BARNETT, C.T., 1972. Theoretical modeling of induced polarization effects due to arbitrarily shaped bodies. Ph.D. thesis, Colorado School of Mines.
- [2] BEVC, D. and MORRISON, H.F., 1991. Borehole-to-surface electrical resistivity monitoring of a salt water injection experiment. *Geophysics*, 56, p.769-777.
- [3] BIBBY, H.M. and RISK, G.F., 1973. Interpretation of dipole-dipole resistivity surveys using a hemispheroidal model. *Geophysics*, 38, p.719-736.
- [4] DANIELS, J.J., 1977. Three-dimensional resistivity and induced-polarization modeling using buried electrodes. *Geophysics*, 42, p.1006-1019.
- [5] DANIELS, J.J., 1983. Hole-to-surface resistivity measurements. *Geophysics*, 48, p.87-97.
- [6] DANIELS, J.J. and DYCK, A.V., 1984. Borehole resistivity and electromagnetic methods applied to mineral exploration. *IEEE, GE-22*, p.80-87.
- [7] DEY, A. and MORRISON, H.F., 1979. Resistivity modeling for arbitrarily shaped three-dimensional structures. *Geophysics*, 44, p.753-780.

[8] DOBECKI, T.L., 1980. Borehole resistivity curves near spheroidal masses. *Geophysics*, 45, p.1513-1522.

[9] FULLAGAR, P.K., 1993a, DC Resistivity/IP response of a "stratified" sphere: unpubl. Technical Note TN001/93, Ecole Polytechnique.

[10] FULLAGAR, P.K., 1993b, DC Resistivity/IP response of a uniform spheroid and a spheroid with core in a homogeneous half-space: unpubl. Technical Note TN005/93, Ecole Polytechnique.

[11] GRANT, F.S. and WEST, G.F., 1956. *Interpretation Theory in Applied Geophysics*. McGraw-Hill Book Co.

[12] KILLEEN, P.G., ELLIOTT, B.E. and MWENIFUMBO, C. J., 1993. Ore deposit signatures and borehole geophysics test sites in Ontario. The 5th International Symposium of the Minerals and Geotechnical Logging Society, Tulsa, p.24-28 October 1993.

[13] KRAUSE, B.R., 1986. Borehole Induced Polarization and Resistivity. *in* *Borehole Geophysics for Mining and Geotechnical Application*, P. G. KILLEEN (*ed.*), Geological Survey of Canada Paper p.85-27, p.375-378.

[14] MA, J., 1993. Comparaison de reponses DCR et IP entre la sphere avec un noyau: unpubl. Technical Note TN003/93, Ecole Polytechnique.

[15] MACROBERT, T.M., 1947. Spherical harmonics. Methuen & Co. Ltd., p.372.

[16] MORRISON, G., JAGO and LITTLE, 1994, Footwall mineralization of the Sudbury Igneous Complex. *in* Proc. of Sudbury - Noril'sk Symp. LIGHTFOOT, P.C. and NOLDRETT, A.J. *eds.*, Special Volume 5, Ontario Ministry of Northern Development & Mines.

[17] PRESS, W.H., FLANNERY, B.P., TEUKOLSKY, S.A. and VETTERLING, W.T., 1986. Numerical Recipes: the art of scientific computing. Cambridge University Press.

[18] PYE, E.G., NALDRETT, A.J. and GIBLIN, P.E., 1984. The Geology and Ore Deposits of the Sudbury Structure. Ontario Geological Survey Special Volume 1.

[19] SEIGEL, H.O., 1959. Mathematical formulation and type curves for induced polarization. *Geophysics*, 24, p.547-566.

[20] SNYDER, D.D. and MERKEL, R.M., 1973. Analytic models for the interpretation of electrical surveys using buried current electrodes. *Geophysics*, 38, p.513-529.

[21] SUMNER, J.S., 1976. *Principles of Induced Polarization for Geophysical Exploration*. Amsterdam: Elsevier.

[22] TELFORD, W.M., GELDART, L.P. and SERIFF, R.E., 1990. *Applied Geophysics*. Cambridge University Press.

[23] WAIT, J.R., 1982. *Geo-electromagnetism*. Academic Press, p.268.

[24] WEBB, J.H., 1931. The potential due to a buried spheroid. *Physical Review*, 38, p.2056-2067.

[25] YANG, F.W. and WARD, S.H., 1985. Single-borehole and cross-borehole resistivity anomalies of thin ellipsoids and spheroids. *Geophysics*, 50, p.637-655.

[26] YANG, F.W. and WARD, S.H., 1985. On sensitivity of surface-to-borehole resistivity measurements to the attitude and the depth to centre of a three-dimensional spheroid. *Geophysics*, 50, p.1173-1178.

APPENDIX A

DC RESISTIVITY RESPONSE OF A STRATIFIED SPHEROID

(after Fullagar, 1993 b)

As illustrated in Figure 3.1 (a), an elliptical coordinate system (η, θ, ϕ) is used. The surfaces of the spheroid and the core are defined by $\eta = \eta_0$ and $\eta = \eta_1$, respectively. A point source C is located at $(\eta_s, \theta_s, \phi_s)$ outside the spheroid ($\eta_s > \eta_0$) and P (η, θ, ϕ) is an arbitrary point in space either outside or inside spheroid (either in the shell or in the core). The potential expressions for point P in space, shell and core has been written as:

$$V = \sum_{n=0}^{\infty} \sum_{m=0}^n [A_{mn} P_n^m(\eta) + B_{mn} Q_n^m(\eta)] T_n^m(\delta) \cos m\phi \quad (\text{A1})$$

$$V_1 = \sum_{n=0}^{\infty} \sum_{m=0}^n [A'_{mn} P_n^m(\eta) + B'_{mn} Q_n^m(\eta)] T_n^m(\delta) \cos m\phi \quad (\text{A2})$$

$$V_2 = \sum_{n=0}^{\infty} \sum_{m=0}^n C_{mn} P_n^m(\eta) T_n^m(\delta) \cos m\phi \quad (\text{A3})$$

where (A_{mn}) represents the set of coefficients for a point source potential, given by

$$A_{mn} = \frac{I\rho\epsilon_m(2n+1)}{4\pi C} \left(\frac{(n-m)!}{(n+m)!} \right)^2 Q_n^m(\eta_s) T_n^m(\delta_s) \quad (\text{A4})$$

$$\delta = \cos \theta.$$

-

P_n^m and Q_n^m denote associated Legendre functions of the first and second kinds respectively, defined by MacRobert (1947, p. 122):

$$P_n^m(x) = (x^2-1)^{\frac{m}{2}} \frac{d^m P_n(x)}{dx^m} \quad (\text{A5})$$

and

$$Q_n^m(x) = (-1)^m (x^2-1)^{\frac{m}{2}} \frac{d^m Q_n(x)}{dx^m}. \quad (\text{A6})$$

This definition of Q_n^m differs by a factor $(-1)^m$ from that adopted by Wait (1982, p. 58).

T_n^m denotes the Ferrers' associated Legendre function of the first kind, defined by MacRobert (1947, p. 126):

$$T_n^m(x) = (-1)^m (1-x^2)^{\frac{m}{2}} \frac{d^m P_n(x)}{dx^m}, \quad |x| < 1. \quad (\text{A7})$$

Considering the boundary conditions at discontinuities in conductivity:

- i. the potential function V is continuous at interface of two media;
- ii. the normal flow of electrical current is continuous across interface of two media.

According to these conditions, we have: at $\eta = \eta_0$,

$$AP(\eta_0) + BQ(\eta_0) = A'P(\eta_0) + B'Q(\eta_0) \quad (\text{A8})$$

$$\frac{1}{\rho} [AP'(\eta_0) + BQ'(\eta_0)] = \frac{1}{\rho_1} [A'P'(\eta_0) + B'Q'(\eta_0)] \quad (\text{A9})$$

and at $\eta = \eta_1$,

$$A'P(\eta_1) + B'Q(\eta_1) = CP(\eta_1) \quad (\text{A10})$$

$$\frac{1}{\rho_1} [A'P'(\eta_1) + B'Q'(\eta_1)] = \frac{C}{\rho_2} P'(\eta_1) \quad (\text{A11})$$

where subscripts and superscripts have been omitted for convenience.

From the equations (A8)-(A11), we solved for the coefficients A', B', B and C as follows:

$$A' = \rho_1 A [P(\eta_0)Q'(\eta_0) - P'(\eta_0)Q(\eta_0)] \quad (A12)$$

$$[\rho_2 P(\eta_1)Q'(\eta_1) - \rho_1 P'(\eta_1)Q(\eta_1)]/F$$

$$B' = \rho_1 A (\rho_1 - \rho_2) [P(\eta_0)Q'(\eta_0) - P'(\eta_0)Q(\eta_0)] P(\eta_1) P'(\eta_1) / F \quad (A13)$$

$$B = A [(\rho - \rho_1)(\rho_2 P(\eta_1)Q'(\eta_1) - \rho_1 P'(\eta_1)Q(\eta_1)) P(\eta_0) P'(\eta_0) \quad (A14)$$

$$+ (\rho_1 - \rho_2)(\rho P(\eta_0)Q'(\eta_0) - \rho_1 P'(\eta_0)Q(\eta_0)) P(\eta_1) P'(\eta_1)] / F$$

and

$$C = \rho_1 \rho_2 A [P(\eta_0)Q'(\eta_0) - P'(\eta_0)Q(\eta_0)] \quad (A15)$$

$$[P(\eta_1)Q'(\eta_1) - P'(\eta_1)Q(\eta_1)] / F$$

where

$$F = [\rho_1 P(\eta_0)Q'(\eta_0) - \rho P'(\eta_0)Q(\eta_0)] [\rho_2 P(\eta_1)Q'(\eta_1) \quad (A16)$$

$$- \rho_1 P'(\eta_1)Q(\eta_1)] + (\rho_1 - \rho_2)(\rho_1 - \rho) P(\eta_1) P'(\eta_1) Q(\eta_0) Q'(\eta_0)$$

Potential problems in oblate spheroidal coordinates (u, δ, ϕ) , as shown in Figure 3.1 (b), can be handled as a straightforward transformation. The preceding formulae for the potentials of the prolate spheroid are applicable if η is replaced by corresponding iu , where $u=u_0$ and $u=u_1$ define the surfaces of the oblate spheroid and the core (Wait, 1982).

APPENDIX B
A MODIFIED METHOD OF IMAGE
FOR BOREHOLE RESISTIVITY

(after Fullagar, 1993 a)

There are three cases when the current source and receiver are in subsurface: both are outside the spheroid; one of them is outside the spheroid and another is inside the spheroid; and both are inside the spheroid (Fig. B.1).

Consider the first case, both current and receiver are outside the sphere (Fig. B.2). With the conventional image method, the net potential at P is given by

$$V = V_R + V_I \quad (\text{B1})$$

where V_I is the potential due to the image source C' acting on the image sphere and V_R is from excitation of the real sphere by the original source.

When we reverse the locations of receiver and source, as shown in Figure B.2 (b), the total potential at P is

$$U = U_R + U_I \quad (\text{B2})$$

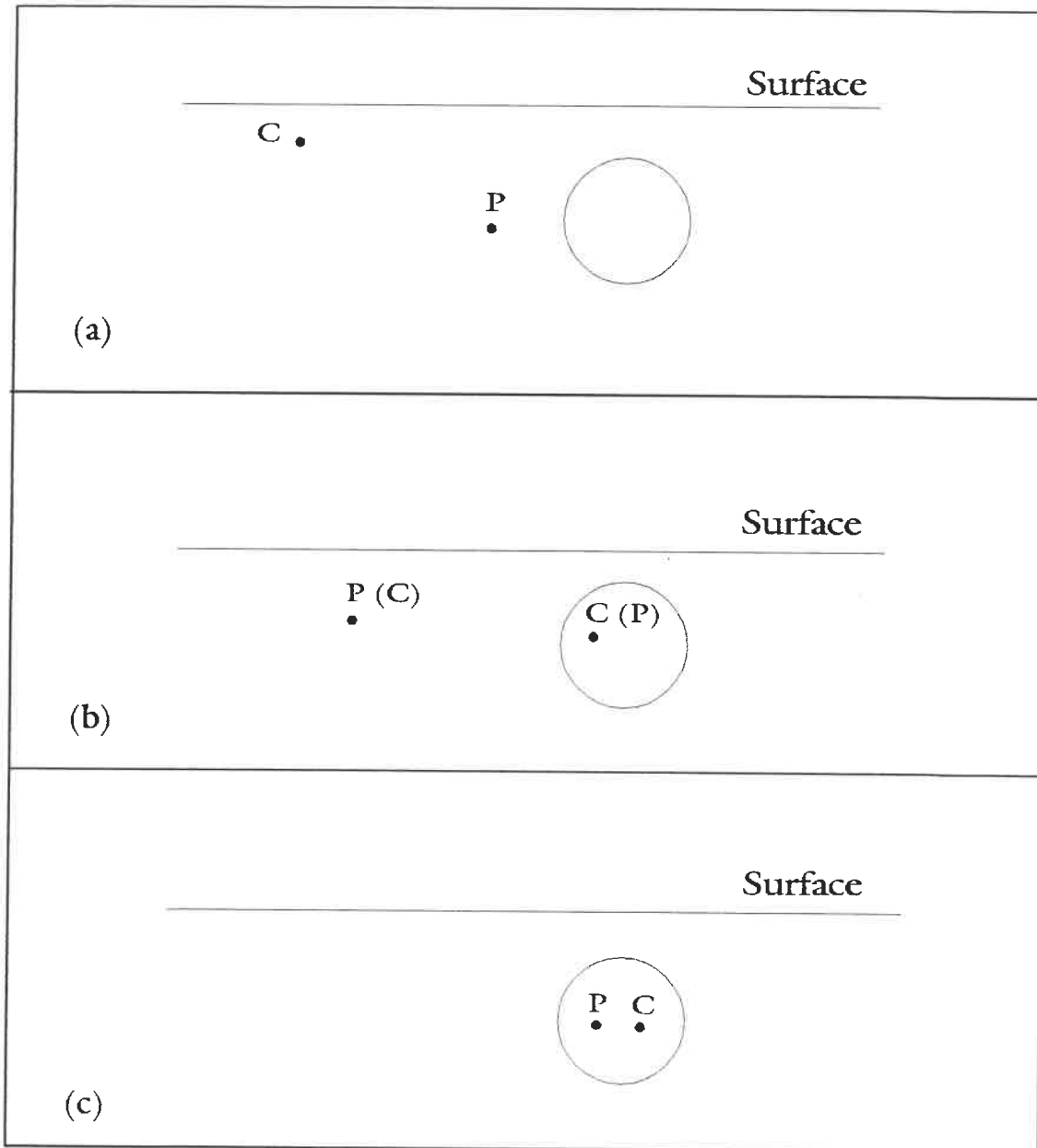


Figure B.1: Three cases when current source C and receiver P are in subsurface; (a) both C and P are outside the sphere; (b) either C or P is inside the sphere and another is outside; (c) both C and P are inside the sphere.

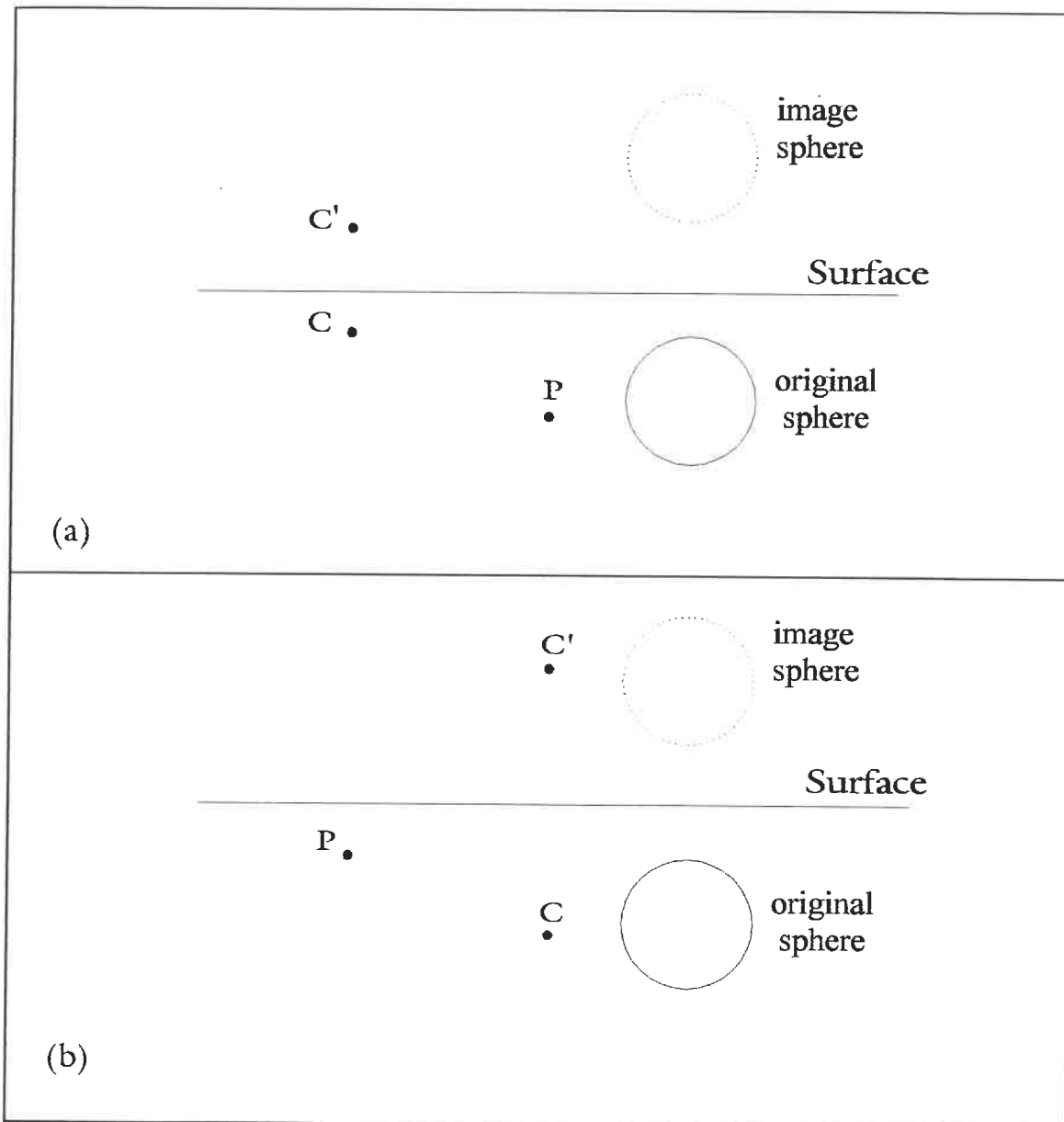


Figure B.2: The image method and reciprocity, when both current source and receiver are outside the sphere; (a) potential at P is the sum of two contributions, one is from the image source C' acting on the image sphere and another is from excitation of the real sphere by the original source C ; (b) reciprocal of the experiment of (a), the locations of source C and receiver P are reversed.

where U_I is the potential due to the image source C' acting on the image sphere and U_R is from the true source C acting on the real sphere.

Comparing (B1) with (B2), according to the "Principle of Reciprocity", we know:

$$U_R = V_R \quad (\text{B3})$$

However, in general,

$$U_I \neq V_I \quad (\text{B4})$$

and hence $U \neq V$. From this example, we see that even though the conventional image method satisfies the requirement of no current normal to the free surface, it violates the Principle of Reciprocity.

This problem can be overcome, in a strictly formal fashion, by adopting the following estimate

$$\bar{V} = \frac{1}{2} (V+U) = V_R + \frac{1}{2} V_I + \frac{1}{2} U_I \quad (\text{B5})$$

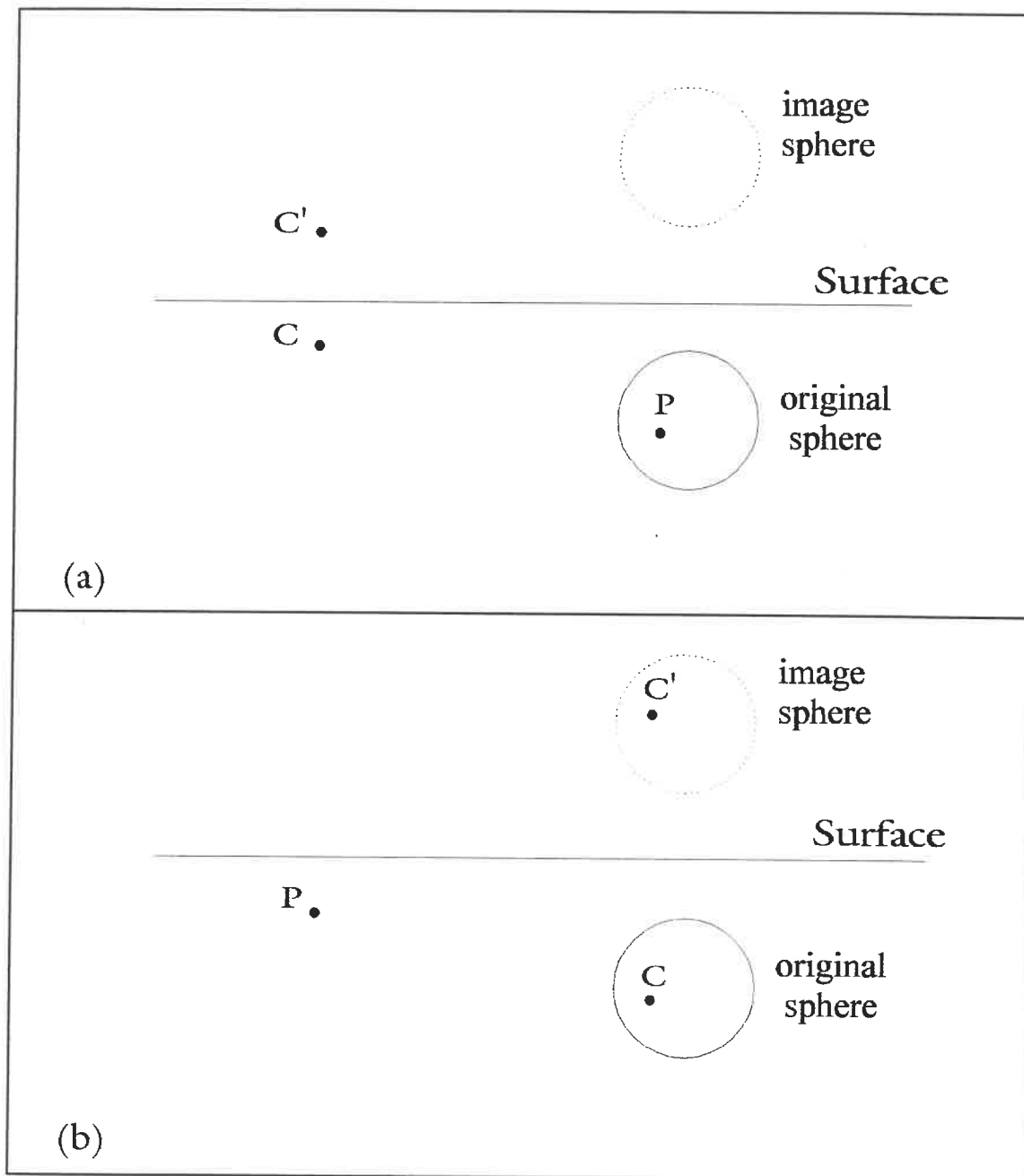


Figure B.3: The receiver is inside the sphere, (a) in the image model, receiver is outside the sphere, it is not consistent with the true geometry; (b) if we change positions of C and P , then C and its image C' are always inside the sphere.

The potential \tilde{V} is approximate too, but in general it is a superior approximation to the true half-space voltage than the potential V obtained by the conventional image method.

In the second case, either the current source is inside the sphere and the voltage electrode is outside the sphere, or vice versa, as shown in Figure B.3 (a). If we use the conventional image method, then the receiver is outside the image sphere. That is not consistent with the true geometry and it can produce a big error. To overcome this problem, we have to treat the internal receiver as a current source, (interchanging the positions of receiver and current source), as shown in Figure B.3 (b). The Principle of Reciprocity permits us to make this change. Now, when we use the image method, the current source is always in the sphere and the voltage electrode outside. This is consistent with the real geometry.

The third case is when both current source and receiver are inside the sphere. In this case (Fig. B.1 c), the use of the image method is not appropriate, because the image model will always have the receiver outside the sphere.

From the discussion above, it is evident that in the three different cases we use a different method. When both current and receiver are outside the sphere, we use the formula (B5) to approximate the response of the sphere in half-space; when the receiver

alone is inside the sphere, we firstly interchange its position with the current source, then compute the response of the image of the modified (reciprocal) model; if the current source alone is inside the body, the conventional method of image is employed; for the case when both current and receiver are inside the sphere, no image contribution is calculated. We use the name "modified image method" to represent this approach.

ÉCOLE POLYTECHNIQUE DE MONTRÉAL



3 9334 00236704 1